OUKA
The University of Osaka
Institutional Knowledge Archive

Title	Quantum Dynamics and Computation with D-Wave Machine
Author(s)	池田, 一毅
Citation	大阪大学, 2020, 博士論文
Version Type	VoR
URL	https://doi.org/10.18910/76364
rights	
Note	

The University of Osaka Institutional Knowledge Archive : OUKA

https://ir.library.osaka-u.ac.jp/

The University of Osaka

PhD Thesis

Quantum Dynamics and Computation with D-Wave Machine

Kazuki Ikeda

Particle Physics Theory Group, Department of Physics, Osaka University, Toyonaka, Osaka 560-0043, Japan

E-mail: kazuki7131@gmail.com

Abstract: Recent advances in quantum computing and quantum information have clarified the potential of the technology to accelerate a lot of principal science and engineering applications, including high energy physics, condensed matter physics, quantum chemistry and data science. As such, there is a growing demand to expand the testability and the programmability of quantum devices. In this thesis we explore quantum dynamics of several models that are used for quantum annealing and study applications of quantum annealing with D-Wave quantum annealer. Especially we consider quantum phase transitions that occur while quantum annealing from a vew point of quantum chaos and quantum scrambling. In addition we offer a new model for which non-stoquastic dynamics can turn a first-order phase transition into a second-order phase transition. Moreover we formulate the nurse scheduling problem as a quadratic unconstrained binary optimization (QUBO) problem and solve it with D-Wave 2000Q. Furthermore supperconducting qubits can be also applied to quantum simulation and useful to reproduce any exotic complex quantum behaviour. One of the famous example is the fractal energy structure of electrons. We investigate fractal energy spectrum of electrons on a lattice with a single point defect. This novel property should be confirmed experimentally with qubits or real material.

Contents

Overview, Summary and Remarks toward Future Directions

What I have done in this thesis

In Sec.2.2 and 2.3, **we investigate phase transitions of the p-spin model by the out-of-time-order correlator (OTOC)**. We show that phase transitions that happen in the process of quantum annealing and reverse annealing are diagnozed via OTOCs. In Sec. 2.4 **we created a Majorana fermion model which shows first-order or second-order phase transitions in the process of quantum annealing.** We draw the phase diagram by the spin-coherent state and confirm them by studying the Gibbs free energy. **As a result, non-stoquastic quantum annealing can turn first-order phase transitions into second-order phase transitions.** This is a new model which exhibits such phenomena. In this context, to our best knowledge, **this is the first model consisting of Majorana fermions, whereas the conventional models consist of simple spins.** Moreover, **we also study the phase transitions with OTOCs and confirm that they indeed change behavior around the critical points.** In Sec.3 **we address the nurse scheduling problem (NSP) with the D-Wave quantum annealer** at Oak Ridge National Laboratory. We formulated the problem with Ising spins, implemented with the 2000Q and analyze its performance, in comparison with simulated annealing and reverse annealing. In Sec.4 **we explore the fractal energy spectrum of Bloch electrons on several lattice with defects**. We show that linear spectra associated with localized current appear in all energy gaps. In

appendix A, **base on the Langlands program, we summarize the uniform theory of duality that is crucial for topological matter, topological quantum computation, Ising model, high energy physics, and mathematical physics.**

Introduction, Summary and Future Directions

This thesis consists of the following parts. Part I is based on [1–3]. Part II is based on [4, 5] and Appendix A is based on [6–8]. Part I includes a review on adiabatic quantum computation, a study on phase transition in terms of quantum chaos, and an application to a combinatorial optimization problem by means of D-Wave 2000Q, the current version of the D-Wave quantum annealer. The main achievements of this part are as follows. It is known that quantum phase transitions occur in the process of quantum annealing. And by a lot of examples, the order of phase transition and computational efficiency are closely related with each other. Moreover quantum computation starts with a non-entangled state and evolves into some entangled states, due to many body interactions and the dynamical delocalization of quantum information over an entire system's degrees of freedom, which is usually refereed to as information scrambling. It is common to diagnose scrambling by observing the time evolution of single qubit Pauli operators. In addition, scrambling makes a system chaotic, and early time exponential growth in the out-of-time-order correlator (OTOC) is believed to be a sign of quantum chaos. In this way, quantum phase transitions are relevant to quantum chaos and scrambling. We aim at establishing a method to clarify those relations by OTOCs. We succeeded in diagnosing first-order and second-order phase transitions by taking the time average of the OTOCs which change behavior around the corresponding critical point. Our method is powerful enough to detect phase transitions associated with quantum annealing and reverse annealing. Using the p-spin model in Sec.2.2, we also find that that the chaos/integrable transition occurs in the process of quantum annealing. Those results suggest that information scrambling and quantum chaos are crucial to phase transitions and shed light on the computational efficiency of quantum annealing in terms of quantum chaos. In Sec. 2.4, we provide a novel Majorana fermion model and study phase transitions in multiple ways. This model can be also efficiently solvable when non-stoquastic terms is used for quantum annealing. Namely, first-order phase tansitions can be avoided if anti-ferromagnetic interactions are implemented. Especially we confirm that the time average of the OTOC can diagnose quantum phase transitions. As an application of quantum annealing, we analyze performance of D-Wave 2000Q in Sec. 3. Especially we formulate the nurse scheduling problem (NSP), which is an NP-hard problem, with Ising spins and program the quantum device. The NSP consists of several hard constrains which must be satisfied and soft constraints which is preferred to be satisfied. It is in general a hard task to

implement those constrains in the Ising formulation. We compare the probability to obtaining the optimized solution by D-Wave 2000Q with that by classical method. Although the current version of the quantum annealer is not always better than classical computers, the Hamiltonian we created there can be generalized to other scheduling problems and is useful for quantum annealing with any updated devise in future which may be superior to classical computers.

Part II addresses energy spectra of electrons on two dimensional systems in magnetic flux. This model has been widely studied theoretically and experimentally. More recently, by means of a chain of nine superconducting qubits, a novel technique for directly resolving the energy levels of interacting photons was implemented [9], where the Hofstadter butterfly is reproduced with photons in Google's quantum chip. In this way, quantum computing technology opens up new directions of material research. Our study in this part is a natural extension of their study, hence it could be a new benchmark for a large scale quantum devise. This setup is commonly used for a study on the quantum Hall effect and has many relevant physics including high energy physics and mathematical physics (see Appendix A for the detail). Especially the quantum Hall system is important as the most basic example of the symmetry protected phase which is practically used to establish robust quantum computation. It is widely known that the energy spectra exhibit the fractal nature, called the Hofstadter butterfly. Hofstadter's problem is usually considered on a system without defects, whereas the problem on a system with defects is less studied. Since realistic material has a lot of defects and impurities, it is natural to investigate the problem on the defect systems. If a system has a defect, there exist localized states which generate current. We first report that the linearly aligned energy spectra associated with the localized current appear in energy gaps of all generations of the fractal butterflies. The localized length is proportional to inverse square of the given flux, hence numerical results agree with the standard description of quantum mechanics.

Appendix A describes the relation between the Langlands program and the quantum Hall effect, which is the most basic examples of the symmetry protected topological phase and is applied to topological computation. Roughly speaking, it is all about the duality, including strong/weak duality and electric/magnetic duality, from a viewpoint of modern mathematics. The essence of such duality is also crucial for quantum computation, in particular for topological quantum error correction. For example, a surface code state on a given graph is dual (transformed by the Hadamard operator) to another surface code on the dual graph. This procedure corresponds to the quantum version of Fourier transformation and can be understood by the duality of the two dimensional Ising model. For the Langlands program, the duality is formally described by the correspondence of L-functions. In terms of physics, the partition functions can be thought as the counterpart to the L-functions. Indeed, the S-duality (or electric/magnetic duality) claims the correspondence of the partition functions. The duality of the Ising model explicitly shows the correspondence

of the partition functions by the Fourier transformation of the Boltzmann weight. Although we focus on quantum annealing in this work, physics of the Ising model and quantum Hall effect should be closely related with each other in many sense, which implies the existence of a fundamental mathematical theory. Our perspective based the Langlands program would be a part of that.

A quantum computer consists of a many particle system, thereby allows us to study more about the advanced properties of materials and molecules, and also to explore fundamental physics. Quantum field theory (QFT) is a powerful tool to address countably or uncountably many degrees of freedom. Indeed it has had a major impact in condensed matter, cosmology, high energy physics and even pure mathematics. The question whether QFTs can be efficiently simulated by quantum computers was raised by Feynman [10]. According to Deutsch [11], the quantum version of Church-Turing thesis [12, 13] states that "Every finitely realizable physical system can be perfectly simulated by a universal model computing machine operating by finite means". Here a finitely realizable physical system includes any experimentally testable physical object. Usually a quantum computer works on a graph consisting of a fixed number of particles. Quantum algorithms which simulate the dynamics of quantum lattice systems with a fixed number of particles have been considered by many authors [14–16]. Although theories on a connected space and a discrete space look very different, some QFT on a connected space can be well approximated by quantum mechanics on a discrete system. For instance, scalar field theory can be precisely approximated with finitely many qubits by discretization of space via a lattice [17]. Moreover scattering in scalar field theory is also known to be BQP complete [18]. Those references imply that quantum algorithms are nice technological substitutes for QFT on a connected space. So this motivates us to consider QFT from a viewpoint of quantum computation. However, from a viewpoint of QFT, it is believed that a theory on a fixed-particle-number Hilbert space is not powerful to describe high energy physics including cosmology and quantum gravity. From those point of view, adiabatic quantum computation (AQC) is a powerful way to simulate physical process, at least as an effective theory, and should be applied to various topics on natural science including molecular dynamics and quantum chemistry. Moreover quantum annealing is also useful to explore Boltzmann machine learning [19], which is a foundation of the modern deep learning technology, and is a promising quantum computational technology. Any problem in the world should be somehow related with physics, which is founded by quantum physics. Therefore, recent advances in quantum technology motivate us to consider any problem from a view point of physics.

Part I
Quantum Dynamics and Computation

1 Review on Quantum Annealing

1.1 Preliminaries

We first formulate quantum field theoretical computation on a lattice. In the standard physics literature, particles are generally classified into two categories: bosonic or fermionic. Bosons are particles that obey the Bose-Einstein statistics, can occupy the same state simultaneously and are symmetric under exchange of particle labels[1]. On the other hand, fermions obey the Fermi-Dirac statistics, cannot occupy the same state simultaneously and are anti-symmetric under exchange of particle labels[2]. When it comes to coding, fermionic operators are not good since they produce negative signs, which trigger coding errors. Bosonic operators can solve this problem, but they occupy the same state simultaneously, hence there exist some inactive particles that consume memory. Therefore, a simple question may come to our mind: is there any particles that cannot occupy the same state simultaneously and are symmetric under exchange of particle labels? A simple way to construct such particles is as follows. Let $a^\dagger$ and a be the 0-dimensional fermionic creation and annihilation operators whose representations are

$$a = \begin{pmatrix} 0 & 1 \\ 0 & 0 \end{pmatrix} \quad a^\dagger = \begin{pmatrix} 0 & 0 \\ 1 & 0 \end{pmatrix}. \tag{1.1}$$

Then $a^\dagger + a$ corresponds to the Pauli X operator and $[a, a^\dagger]$ corresponds to the Pauli Z operator. Let a_i and $a_i^\dagger$ be the annihilation and creation operators acting on the Hilbert space of i-th particle:

$$a_i := 1 \otimes \cdots \otimes 1 \otimes a \otimes 1 \otimes \cdots \otimes 1 \tag{1.2}$$

$$a_i^\dagger := 1 \otimes \cdots \otimes 1 \otimes a^\dagger \otimes 1 \otimes \cdots \otimes 1, \tag{1.3}$$

which obey $[a_j, a_i^\dagger] = Z_i \delta_{ij}$, $[a_i^\dagger, a_j^\dagger] = [a_i, a_j] = 0$ and $a_i^\dagger a_i^\dagger = a_i a_i = 0$ for all i, j. Note that $\{a_i, a_j^\dagger\} \neq \delta_{ij}$ for different i, j. We denote by $n_i = a_i^\dagger a_i$ the number operator. So a general state in a system with size L is a superposition of

$$|n_1 \cdots n_L\rangle \tag{1.4}$$

[1] $[a_i, a_j^\dagger] = \delta_{ij}, [a_i, a_j] = [a_i^\dagger, a_j^\dagger] = 0$ for bosons

[2] $\{a_i, a_j^\dagger\} = \delta_{ij}, \{a_i, a_j\} = \{a_i^\dagger, a_j^\dagger\} = 0$ for fermions

and the vacuum state is $|\emptyset\rangle = |0\cdots 0\rangle$ which vanishes $a_i |\emptyset\rangle = 0$ by any a_i. A particle $a_i^\dagger |\emptyset\rangle = |1_i\rangle$ created at i disappears when $a_i^\dagger$ acts on the same state again due to $a_i^{\dagger 2} = 0$. Regarding a two particle state $|1_i, 1_j\rangle = a_i^\dagger a_j^\dagger |\emptyset\rangle$, one cannot tell one particle from another because of the commutation relation $a_i^\dagger a_j^\dagger = a_j^\dagger a_i^\dagger$ at different sites ($i \neq j$). Therefore the creation and annihilation operators describe particles which cannot occupy the same position simultaneously and particles labels are indistinguishable. A common interpretation of those operators is that $a_i, a_i^\dagger$ annihilates/creates the z-spin at i, respectively. One may wonder if multiple fermions can be addressed with $a_i, a_i^\dagger$, but any operation can be reconstructed by them as we discuss below.

1.2 Universality

Universality of quantum computation can be described in two ways. In a strong sense it means one can obtain any unitary operation, and in a weak sense it means one can get any desired probability distribution. Since wave functions are not physical observables, the latter is adequate for practical use. We first show our model is as powerful as universal computation in the following sense.

Theorem 1.1. Let $\{x_i\}_{i=1}^M$ and $\{x'_j\}_{j=1}^N$ be coordinates of M and N particles on a discrete system. Any operator $\mathcal{O}$ on a discrete system can be written with $a_x, a_x^\dagger$ in such a way that

$$\mathcal{O} = \sum_{M=0,N=0} \sum_{x_i, x'_j} A_{MN}(x_1, \cdots, x_M, x'_1, \cdots, x'_N) a_{x_1}^\dagger \cdots a_{x_M}^\dagger a_{x'_1} \cdots a_{x'_N}. \tag{1.5}$$

Proof. Proof can be done by induction. Let $|\psi_{x_1 \cdots x_M}\rangle = \prod_{i=1}^M a_{x_i}^\dagger |\emptyset\rangle$ be a M-particle state. The zero particle state corresponds to the vacuum $|\psi_0\rangle = |\emptyset\rangle$. Clearly it is always possible to assign $\langle\emptyset| \mathcal{O} |\emptyset\rangle$ with any value, by choosing some A_{00}. Suppose the same things are true for matrix elements $\langle\psi_{x_1 \cdots \cdots x_M}| \mathcal{O} |\psi_{x'_1 \cdots \cdots x'_N}\rangle$ of all M and N particle states satisfying $M < K, N \leq L$ or $M \leq K, N < L$. Then we obtain

$$\begin{aligned} \langle\psi_{x_1 \cdots x_K}| \mathcal{O} |\psi_{x'_1 \cdots x'_L}\rangle =& L!K! A_{KL}(x_1, \cdots, x_K, x'_1, \cdots, x'_L) \\ &+ \text{terms with } A_{MN} \text{ for } M < K, N \leq L \text{ or } M \leq K, N < L. \end{aligned} \tag{1.6}$$

By choosing appropriate A_{KL}, one can assign the right hand side with any desired value. Therefore, with an appropriate set of coefficients $\{A_{MN}\}$, any operation $\mathcal{O}$ can be approximated by some combinations of creation and annihilation operators.

Thanks to this theorem, one can realize any Hamiltonian thereby approximate any result of quantum computation. More simply, it is also possible to construct a universal gate set. For example, the CNOT operator acting on different i, j cites can be represented by

$$\begin{aligned} \text{CNOT} =& \frac{1}{2}(1 + [a_i, a_i^\dagger]) + \frac{1}{2}(1 - [a_i, a_i^\dagger])(a_j + a_j^\dagger) \\ =& 1 - n_i + n_i(a_j + a_j^\dagger) \end{aligned} \tag{1.7}$$

Since any n-qubit unitary gate can be well simulated by CNOT and single qubit gates, we can create a universal gate set by $\{a_i, a_i^\dagger\}$. Any unitary operator can be created by some algebraic operation to a defined over $\mathbb{C}$ and, in this sense, a is the primary operator of quantum computation.

In what follows we give another representation of universal computation with $\{a_i, a_i^\dagger\}$. To this end, we begin with several operators [20]:

1. $H_{\text{init}} = H_{\text{clock init}} + H_{\text{input}} + H_{\text{clock}}$
2. $H_{\text{final}} = H_{\text{prop}} + H_{\text{input}} + H_{\text{clock}}$
3. $H_{\text{prop}} = \frac{1}{2}\sum_{\tau=1}^{L} H_\tau$

And consider the total Hamiltonian defined by

$$H(t) = (1-t)H_{\text{init}} + tH_{\text{final}}, \quad t \in [0,1]. \tag{1.8}$$

The clock Hamiltonian H_{clock}

$$H_{\text{clock}} = \sum_{\tau=1}^{L-1} |0_\tau 1_{\tau+1}\rangle_c \langle 0_\tau 1_{\tau+1}| \tag{1.9}$$

has the correct clock state as its ground state. Here $|0_\tau 1_{\tau+1}\rangle_c$ denotes Feynman's clock register [21]. The clock register can be more simply written as $|\tau\rangle\langle\tau-1| = |1_{\tau-1}1_\tau 0_{\tau+1}\rangle_c \langle 1_{\tau-1}0_\tau 0_{\tau+1}|$, for example. Since the initial clock state is 0 at $\tau = 0$,

$$H_{\text{clock init}} = |1_1\rangle_c \langle 1_1| \tag{1.10}$$

assigns 0 to the correct initial state, otherwise 1. Moreover, at the initial time,

$$H_{\text{input}} = \sum_{i=1}^{N} |1_i\rangle\langle 1_i| \otimes |0_1\rangle_c \langle 0_1| \tag{1.11}$$

gives 0 if all qubits used for computation are 0, otherwise 1. So the ground states of H_{init} has 0 as the corresponding eigenvalue. A family of unitary operations $\{U_\tau\}_{\tau=1}^L$ can be accommodated into $\{H_\tau\}_{\tau=1}^L$ in such a way that

$$\begin{aligned}
H_1 =& 1 \otimes |0_1 0_2\rangle_c \langle 0_1 0_2| - U_1 \otimes |1_1 0_2\rangle_c \langle 0_1 0_2| - U_1^\dagger \otimes |0_1 0_2\rangle_c \langle 1_1 0_2| + 1 \otimes |1_1 0_2\rangle_c \langle 1_1 0_2| \\
H_\tau =& 1 \otimes |1_{\tau-1} 0_l 0_{\tau+1}\rangle_c \langle 1_{\tau-1} 0_\tau 0_{\tau+1}| - U_\tau \otimes |1_{\tau-1} 1_\tau 0_{\tau+1}\rangle_c \langle 1_{\tau-1} 0_\tau 0_{\tau+1}| \\
& - U_\tau^\dagger \otimes |1_{\tau-1} 0_\tau 0_{\tau+1}\rangle_c \langle 1_{\tau-1} 1_\tau 0_{\tau+1}| + 1 \otimes |1_{\tau-1} 1_\tau 0_{\tau+1}\rangle_c \langle 1_{\tau-1} 1_\tau 0_{\tau+1}| \\
H_L =& 1 \otimes |1_{L-1} 0_L\rangle_c \langle 1_{L-1} 0_L| - U_L \otimes |1_{L-1} 1_L\rangle_c \langle 1_{L-1} 0_L| \\
& - U_L^\dagger \otimes |1_{L-1} 0_L\rangle_c \langle 1_{L-1} 1_L| + 1 \otimes |1_{L-1} 1_L\rangle_c \langle 1_{L-1} 1_L|
\end{aligned} \tag{1.12}$$

Now we consider the representation by $\{a_i, a_i^\dagger\}$. It is easy to see that

$$H_{\text{clock}} \Leftrightarrow \sum_{\tau=1}^{L-1}(1-n_\tau)n_{\tau+1} \tag{1.13}$$

is 1 if and only if it acts on $|0_\tau 1_{\tau+1}\rangle_c$. And we find

$$H_{\text{clock init}} \Leftrightarrow n_1 \tag{1.14}$$

returns 1 if and only if it acts on $|1_1\rangle_c$. Moreover the input Hamiltonian corresponds to

$$H_{\text{input}} \Leftrightarrow \sum_{i=1}^{N} n_i \otimes (1-n_1), \tag{1.15}$$

where n_i acts on logical qubits and $1-n_1$ acts on the clock state. As mentioned previously, any unitary operator U_i can be reconstructed by CNOT and single qubit operators. So each gate operation is, for example,

$$\begin{aligned} H_\tau \Leftrightarrow & 1 \otimes n_{\tau-1}(1-n_\tau)(1-n_{\tau+1}) - U_\tau \otimes n_{\tau-1}a_\tau^\dagger(1-n_{\tau+1}) \\ & - U_\tau^\dagger \otimes n_{\tau-1}a_\tau(1-n_{\tau+1}) + 1 \otimes n_{\tau-1}n_\tau(1-n_{\tau+1}). \end{aligned} \tag{1.16}$$

In summary, we find that it is possible to do universal computation by $\{a_i, a_i^\dagger\}$. To implement the universal adiabatic quantum computation, we want to seek for the simplest Hamiltonian. It is known that the 5-local Hamiltonian above can be well approximated by the following QMA-complete 2-local Hamiltonian [22]

$$H = \sum_i h_{zi}Z_i + \sum_i h_{xi}X_i + \sum_{ij} J_{ij}Z_iZ_j + \sum_{ij}\Gamma_{ij}X_iX_j \tag{1.17}$$

$$= \sum_i h_{zi}[a_i, a_i^\dagger] + \sum_i h_{xi}(a_i + a_i^\dagger) + \sum_{ij} J_{ij}[a_i, a_i^\dagger][a_j, a_j^\dagger] + \sum_{ij}\Gamma_{ij}(a_i + a_i^\dagger)(a_j + a_j^\dagger). \tag{1.18}$$

Instead of using eigenvalues $s_i \in \{-1, +1\}$ of the spin Z_i operator, we may use variables in $\{0, 1\}$, that are the eigenvalues of $\frac{1-Z_i}{2} = n_i$ operators. Then the corresponding representation of the Hamiltonian is

$$H = \sum_i h_{zi}n_i + \sum_i h_{xi}X_i + \sum_{ij} J_{ij}n_in_j + \sum_{ij}\Gamma_{ij}X_iX_j. \tag{1.19}$$

Remark 1.2. Another important way of quantum field theoretical universal computation is called matchgate [23]. Free fermions play a crucial role. A standard representation of the fermionic creation $b_j^\dagger$ and annihilation b_j operators is given by the Jordan-Wigner representation [24]

$$b_j = Z_1Z_2\cdots Z_{j-1}a_j \qquad b_j^\dagger = Z_1Z_2\cdots Z_{j-1}a_j^\dagger, \tag{1.20}$$

They obey $\{b_i, b_j^\dagger\} = \delta_{ij}$ and $\{b_i, b_j\} = 0$. And Majorana fermions are represented by

$$c_{2k-1} = b_k + b_k^\dagger \qquad c_{2k} = -i(b_k - b_k^\dagger), \tag{1.21}$$

which satisfy $\{c_\mu, c_\nu\} = 2\delta_{\mu,\nu}$.

1.3 Quantum Supremacy and Complexity

The question "Is a quantum computer faster than any classical computer?" is affirmatively solved when "BQP$\neq$ BPP" is proved. To state more clearly, we prepare some concepts. In what follows we consider decision problems, that can be solved by "Yes (1)" or "No (0)". Then any problem x is expressed by a bit string $x \in \{0,1\}^*$ and a language L is defined by a subset of the set of all bit strings $\{0,1\}^*$. For example, the problem to decide whether x is even or odd is solved by the set of even numbers $L = \{0, 10, 100, 110, 1000, 1010, 1100, 1110, \cdots\}$. If x is even, $x \in L$. We call x is accepted (rejected) when a machine outputs 1 (0), respectively.

The standard classes of classical problems are P,NP and BPP. We call a language L is in P, if there is a polynomial time deterministic Turing machine which accepts x if $x \in L$ and rejects x if $x \notin L$. And we call a Language L is in NP (Non-deterministic Polynomial Time), if there is a polynomial time probabilistic Turing machine whose acceptance probability of x is greater than 0 if $x \in L$ and is equal to 0 if $x \notin L$. Finally we call a language L is in BPP (Bounded-error Probabilistic Polynomial Time) if there is a polynomial time probabilistic Turing machine whose acceptance probability of x is greater than or equal to $2/3$ if $x \in L$ and is smaller than or equal to $1/3$ if $x \notin L$. By definition, P $\subset$ BPP is clear but BPP $\subset$ P is an unsolved problem in computer science. A problems is BQP-hard if it is at least as hard as the hardest problems in BQP. A problem which is both BQP-hard and contained in BQP is called BQP-complete. The class BQP is the quantum version of BPP. In the strict sense, BQP$\neq$ BPP is unsolved, but there are some problems that a quantum computer could solve more efficiently than any classical computer. One of them is to sample a given probability distribution D. It is known that if a classical computer is able to solve this problem for any D in a polynomial time, then the Polynomial Hierarchy is broken (computer scientists believe this never happens). At least for this problem, even a non-universal quantum computer could perform better than any classical computer and more recently some evidences have been reported [25]. We may call the superiority of non-universal quantum computers over classical computers as quantum supremacy.

1.4 Combinatorial Optimization Problem

Combinatorial optimization is all about finding an optimal object from a finite set of objects. A lot of combinatorial optimization problems are NP-complete or NP-hard, and are widely studied from a perspective of computational complexity theory.

One of the most famous examples of combinatorial optimization problems is the traveling salesman problem (TSP), which is NP-hard. An algorithm to find the solution of TSP in a polynomial time is not known. As an example we formulate the TSP in the AQC formalism. Let a salesman visit cities $i = 1, \cdots N$ step by step only one time. Let D_{ij} be the distance between i, j, hence it is symmetric $D_{ij} = D_{ji}$.

Then the H_0 term which respects those constraints is given by

$$H_0 = \sum_{t=1}^{N-1} \sum_{ij} D_{ij} n_{i,t+1} n_{j,t} + \sum_{t=1}^{N} \lambda_1(t) \left(\sum_{i}^{N} n_{i,t} - 1 \right) + \sum_{i=1}^{N} \lambda_2(i) \left(\sum_{t}^{N} n_{i,t} - 1 \right), \tag{1.22}$$

where $\lambda_1(t)$ and $\lambda_2(i)$ are Lagrange multipliers. We redefine the operators by $n_{i,t} = n_{i+N(t-1)}$ and label the problem by N^2 indexes. An eigenstate $|\psi\rangle$ satisfying the equality constraints of H_0 looks like

$$|\psi\rangle = \prod_{t=1}^{N} a^{\dagger}_{i_t+N(t-1)} |\emptyset\rangle, \quad \{i_t\}_t \subset \{1, 2, \cdots, N\} \tag{1.23}$$

and has the corresponding eigenvalue

$$\sum_{t=1}^{N-1} D_{i_{t+1} i_t}. \tag{1.24}$$

Therefore the ground state of H_0 is the solution of the TSP. Many of generic classical combinatorial optimization problems are solvable with some $H_0 = H_0(n)$. It is straightforward to translate Ising formulation of NP problems [26] into ours. Regarding quantum speedup by quantum annealing, the glued-trees problem [27] is the only example known to date [28]. And it requires further studies to show the efficiency of quantum annealing

1.5 Relevant Classical Methods

Here we shortly summarize some relevant classical methods. We will use simulated annealing in Sec.3 to compare results with D-Wave 2000Q. Quantum annealing is a quantum version of simulated annealing (SA) [29], which is an algorithm to find the optimal solution by thermal fluctuation and transitions. Here we briefly explain SA based on the Markov chain Monte Carlo by the Metropolis method. Let σ be a set of Ising spins and $P_t(\sigma)$ be the probability at time t. The Markov chain is defined by the dynamics of $P_t(\sigma)$ in such a way that

$$P_{t+1}(\sigma') = \sum_{\sigma} P(\sigma'|\sigma) P_t(\sigma), \tag{1.25}$$

where $P(\sigma'|\sigma)$ is a certain probability amplitude. For the Metropolis method, it is defined by

$$P(\sigma'|\sigma) = \min\{1, \exp(-(E(\sigma') - E(\sigma))/T)\}, \tag{1.26}$$

where T is temperature and σ' differs from σ by a single spin. σ' is updated as follows. In general σ is written as $\sigma = (\sigma_1, \cdots, \sigma_N)$. Then σ' is defined by a single spin flip at some i: $\sigma'_i = -\sigma_i, \sigma'_j = \sigma_j$. If $\Delta = E(\sigma') - E(\sigma) < 0$, then

we accept $\sigma_i' = -\sigma_i$. If $\Delta E > 0$ we generate a number $r \in [0,1]$ randomly and accept $-\sigma_i'$ if $r < \exp(-\Delta E/T)$, otherwise accept $\sigma_i' = \sigma_i$. If this process is repeated for sufficiently long times, the probability distribution converges into the Gibbs-Boltzmann distribution $P(\sigma) = \exp(-E(\sigma)/T)/Z$. The way to find the lowest energy solution by gradually decreasing temperature T is called SA.

Quantum Monte Carlo is also a widely used classical algorithm to simulate quantum many body system. The Hamiltonian $H = H_1 + H_2$ accommodates non-commutative terms $[H_1, H_2] \neq 0$ in general, hence it is hard to replace quantum spins by classical spins. The Suzuki-Trotter formula [30, 31]

$$e^{H_1+H_2} = \lim_{n\to\infty} \left(e^{H_1/n} e^{H_2/n}\right)^n \tag{1.27}$$

or n products $e^{H_1/n}e^{H_2/n} \cdots e^{H_1/n}e^{H_2/n}$ is commonly used for replacing the quantum spins into classical spins, by inserting $1 = \sum_{\sigma_z} |\sigma_{z,i}\rangle \langle\sigma_{z,i}|$ between $e^{H_1/n}$ and $e^{H_2/n}$. As a result, all spins are replaced by σ_z, which allows us to perform the classical Monte Carlo.

1.6 Programming D-Wave 2000Q

The physical hardware graph associated with the D-Wave 2000Q is a fixed sparse graph $G = (V, E)$, called the Chimera graph, consisting of a 16×16 array of 4-vertex. Each unit cell accommodates 8 qubits, hence there are 2048 qubits and 6016 couplers. Fig. 1 presents the working graph of the D-Wave 2000Q located at Oak Ridge National Laboratory.

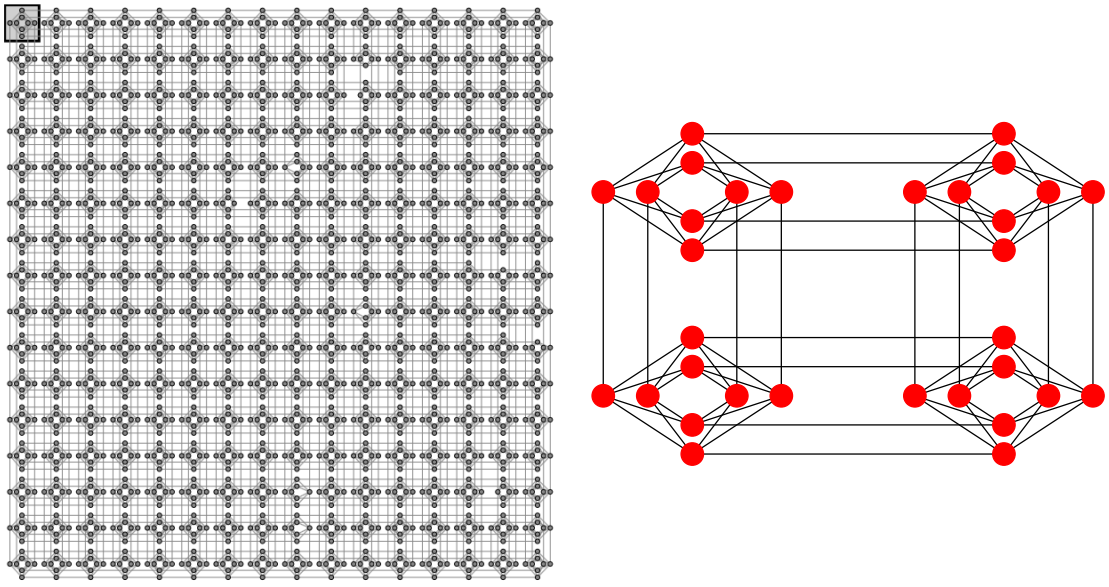

Figure 1. Chimera graph associated with the D-Wave 2000Q.

An optimization problem can be solved by embedding the corresponding Hamiltonian which should be written by Ising spins into the chimera graph. Physical couplings among qubits on the graph represent the matrix components.

Qubits evolve according to a predetermined schedule, in which states get close to some eigenstates of the target Hamiltonian. In the standard usage of the D-Wave 2000Q, functions used for annealing grow or decrease quadratically with time. In the conventional system, the default annealing time is set to $20\mu s$.

2 Phase Transition, Energy Gaps and OTOC

2.1 Phase Transitions and Energy Gaps

The general form of adiabatic quantum computation that we study here is given by the Hamiltonian

$$H(s) = sH_0 + (1-s)H_1, \qquad s \in [0,1] \tag{2.1}$$

where H_0 is a target Hamiltonian and H_1 is an initial Hamiltonian. They should not commute $[H_0, H_1] \neq 0$. The transverse magnetic field

$$H_1 = -\sum_i^N X_i \tag{2.2}$$

is widely used for the initial term [32, 33]. It is believed that adding a stoquastic Hamiltonian is not helpful for quantum speedup and there are some known examples of non-stoquastic terms that make problems efficiently solvable by adiabatic quantum computation [34] (AQC restricted to stoquastic Hamiltonians becomes universal when non-standard computational bases are used [35]). We say a Hamiltonian is stoquastic if all off-diagonal matrix elements in the standard basis are real and non-positive, otherwise it is non-stoquastic [36], which in general hard to simulate by quantum Monte Carlo due to the negative sign problem. We add the following antiferromagnetic interactions

$$H_{\mathrm{AF}} = +N\left(\frac{1}{N}\sum_i^N X_i\right)^2 \tag{2.3}$$

as a non-stoquastic term in such a way that

$$H(s,\lambda) = s(\lambda H_0 + (1-\lambda)H_{\mathrm{AF}}) + (1-s)H_1. \tag{2.4}$$

The initial Hamiltonian should be $H(0,\lambda) = H_1$ with any λ and the final Hamiltonian should be $H(1,1) = H_0$. In many cases, a phase transition occurs in the annealing process, some of which adversely affect the performance of annealing machines. Therefore it is crucial to clarify the properties of phase transitions. Since

$X_i |+\rangle_i = |+\rangle_i$, at the initial stage of annealing ($s = 0$), the ground state $|\psi_0\rangle$ of H_1 is a super position of all possible 2^N states with the equal probability weight

$$\begin{aligned} |\psi_0\rangle &= \bigotimes_i^N |+\rangle_i \\ &= \frac{1}{\sqrt{2^N}}(|\uparrow\uparrow\cdots\uparrow\rangle + |\uparrow\uparrow\cdots\uparrow\downarrow\rangle + \cdots + |\downarrow\downarrow\cdots\downarrow\rangle) \end{aligned} \tag{2.5}$$

We call this phase as quantum paramagnetic (QP) phase. The ground state of H_0 is not necessary a PQ phase, hence a phase transition occurs in general. The first-order (second-order) phase transitions are defined by the discontinuity (continuity) of a given order parameter, respectively.

To evaluate the required computational time, we refer to the adiabatic theorem. According to the adiabatic theorem, the computational time t_* that is needed to efficiently obtain the ground state is proportional to the inverse square of the minimal energy gap Δ between the ground state and the first excited state ($t_* \sim \frac{1}{\Delta^2}$). We want to stay in the ground state throughout. So computation should be done slowly around the point where the energy gap becomes minimum. The smaller Δ becomes, the slower we need to run our algorithm to avoid excitation. If a level crossing happens ($\Delta = 0$), then we most likely leave the ground state. For a large N, Δ is proportional to either N^{-a} ($a > 0$) or e^{-bN} ($b > 0$). (In the limit of $N \to \infty$, Δ goes to 0.) And by a lot of examples, it is known that Δ decays polynomially if a phase transition is second-order [37, 38], whereas Δ decays exponentially if it is first-order (although there are some exceptions [39–41]). Therefore, the problem on system with second-order phase transition is efficiently solved. It is known that when a non-stoquastic Hamiltonian is used, the first-order phase transitions can be avoided. The following Majorana fermion model (2.17) and the p-spin model is such an example. In the fixed time slice at the end of computation, it looks like that quantum annealing uses quantum tunneling to find a global minimum state. A role of quantum tunneling in the efficiency of quantum annealing is summarized in [42].

2.2 Spin Model and OTOC

In this section, we study quantum phase transitions from the viewpoint of quantum chaos. In particular, we would like to distinguish/characterize the different phases of the system in terms of their chaotic properties. We first consider the p-spin model as a target Hamiltonian of quantum annealing. As we change the parameter s from 0 to 1, this system displays a quantum phase transition from a disordered QP phase to an ordered F phase. Naively, we expect the ordered F phase to be less chaotic than the disordered QP phase. Various phenomena are involved in quantum phase transitions due to non-trivial many body interactions. Quantum chaos or information scrambling is one of the standard examples that occur because of strong correlations among

quantum states. It is believed that Out-of-Time-Order Correlators (OTOCs) [43–45], which are experimentally measurable [46–48], reflect some aspects of quantum chaos, information scrambling [49] and symmetry of the system. A process of symmetry breaking associated with the quantum phase transitions should be detected by an OTOC. So in this work, we aim at diagnosing quantum phase transitions of the quantum annealing process by means of OTOCs. The relation between the second-order phase transition and the time average of OTOCs is reported [50–52], but not proven in general and should be confirmed by some other examples. For example, less is known about the relation between the order of phase transition and the behavior of the OTOC. To our best knowledge this is the first work in the following two senses: (1) relating both of first-order and second-order phase transitions with the dynamics of OTOCs, (2) applying OTOCs to a study on quantum annealing or adiabatic quantum computing, (3) diagnosing PTs with multiple combinations of operators for the OTOCs and (4) and the Hamiltonians we employed are non-stoquastic, which means it is hard to simulate the models efficiently by the Monte Carlo method due to negative sign problem. Some stoquastic models are studied elsewhere [53–55]. We would like to understand the chaotic behavior of the system in terms of OTOCs of the form

$$F(t) = \langle W(t)VW(t)V\rangle, \tag{2.6}$$

where V and W are Hermitian and unitary local operators. In chaotic many-body systems, one expects $F(t)$ to vanish a late times for almost any choice of operators V and W.

The late-time vanishing of OTOCs is tied to the idea of scrambling of quantum information, which takes place in chaotic systems. Using the Baker-Campbell-Hausdorff (BCH) formula, we can write the Heisenberg operator as

$$W(t) = e^{iHt}We^{-iHt} = W + it\,[H,W] + \frac{(it)^2}{2!}[H,[H,W]] + \cdots . \tag{2.7}$$

At $t = 0$, the operator only involves the local degrees of freedom associated with W. Under time evolution, higher order terms in the BCH become important, and $W(t)$ becomes more and more complicated as it starts to act non-trivially in an increasing number of degrees of freedom. In other words, the operator $W(t)$ grows with time, and the initially local information gets scrambled into a non-local form.

The scrambling of the operator $W(t)$ can be probed by considering its commutator with some other, local operator, V. To avoid phase cancellations, one usually defines the double commutator

$$C(t) = \langle |[W(t),V]|^2\rangle, \tag{2.8}$$

which starts at zero and grows as $W(t)$ scrambles with an increasing number of degrees of freedom. After the so-called 'scrambling time', the operator $W(t)$ is scrambled with essentially all the degrees of freedom of the system, and $C(t)$ saturates to a constant value, which equals to $2\,\langle VV\rangle\langle WW\rangle$.

The double commutator is closely related to OTOCs. For unitary V and W, the double commutator can be written as $C(t) = 2(1 - \mathrm{Re}[F(t)])$. Hence, the saturation of the double commutator after the scrambling time implies the vanishing of OTOCs. For an intuitive explanation (in the context of spin chains) of why the vanishing of OTOCs implies chaos, we refer to [56]. See also section 3 of [57].

In contrast, in non-chaotic systems, one expects a non-universal behavior of the OTOCs, which in general depends on the choice of the operators V and W. Moreover, the absence of thermalization in integrable systems is expected to lead to an oscillatory behavior of OTOCs.

The way $F(t)$ approaches to zero is particularly simple in systems that display some sort of classical limit (e.g. quantum mechanical systems that have a well-defined $\hbar \to 0$ limit or large-N systems). In those cases, in an appropriate time window, the double commutator grows exponentially, i.e., $C(t) \sim e^{\lambda_L t}$, which is reminiscent of the divergence in the distance between initially nearby trajectories in the phase space of classically chaotic systems. In those cases, one can define a quantum Lyapunov exponent λ_L characterizing the onset of chaos in the system. By contrast, in standard spin chains models with local interactions $F(t)$ does not have any sort of exponential behavior with time [58, 59], even for systems that are know to be strongly chaotic by other more conventional criteria for quantum chaos. This prevents the definition of a quantum Lyapunov exponent for those systems. The time scale at which the OTOC saturates to a constant value is called the scrambling time t_*, which scales as $t_* \sim \log N_{\mathrm{dof}}$, where N_{dof} is the number of degrees of freedom per site. For a spin chain one have $t_* \sim \mathcal{O}(1)$, which leaves no room for an exponential growth [58, 59]. (see, however, [60]). Despite the absence of exponential behavior, one usually expects to distinguish chaotic and integrable systems by the late-time saturation value of the OTOCs, as discussed above.

In finite-size systems, OTOCs do not decay exactly to zero at late times. In fact, it has been shown that the residual late-time value of OTOCs provide useful insights into the chaotic dynamics [56]. For energy-conserving chaotic spin chains, for example, the late-time value of the OTOCs scale as an inverse polynomial in the system size [56]. Here, since we are dealing with spin chains with a relatively small number of sites ($N \sim 8$), we expect to observe those finite-size effects in the late time behavior of OTOCs (see Fig.2).

In this section we consider the p-spin model

$$H_0 = -N \left(\frac{1}{N} \sum_{i=1}^{N} Z_i \right)^p \tag{2.9}$$

and the total Hamiltonian

$$H(s, \lambda) = s(\lambda H_0 + (1 - \lambda) H_{\mathrm{AF}}) + (1 - s) H_1. \tag{2.10}$$

Note that H_0 conserves the total spin and the z-spin : $[H_0, S^2] = 0, [H_0, S^z] = 0$. The ground state of H_0 is degenerated if p is even. So we consider cases where p is odd. Then the ground state of H_0 consists of all up spins $|\uparrow\uparrow\cdots\uparrow\rangle$. Hence the initial QP phase moves into the ferromagnetic phase. The corresponding order parameter is $m_z = \langle \frac{1}{N}\sum_i^N Z_i \rangle$. Without the antiferromagnetic interactions ($\lambda = 1$), it is known that this model costs exponentially long time to obtain the ground state of H_0 due to a first-order phase transition [61]. It is known that the first-order phase transition can be avoided by the antiferromagnetic interactions, hence the problem is efficiently solvable [34, 62]. A rapid increase in the entropy at the critical value of phase transition implies that phase transitions have a crucial effect on the propagation of quantum information in the quantum many body system.

We study the phase transitions from a viewpoint of quantum chaos. Especially we use the following OTOC

$$F_{\rm gs}(t) = \langle \phi_0 | \, W(t)^\dagger V^\dagger W(t) V \, | \phi_0 \rangle \, , \tag{2.11}$$

where V and W are Hermitian and unitary local operators and $|\phi_0\rangle$ is the ground state of the total Hamiltonian $H = H(s, \lambda)$. We first consider $W = V$ cases and work on $V \neq W$ cases later.

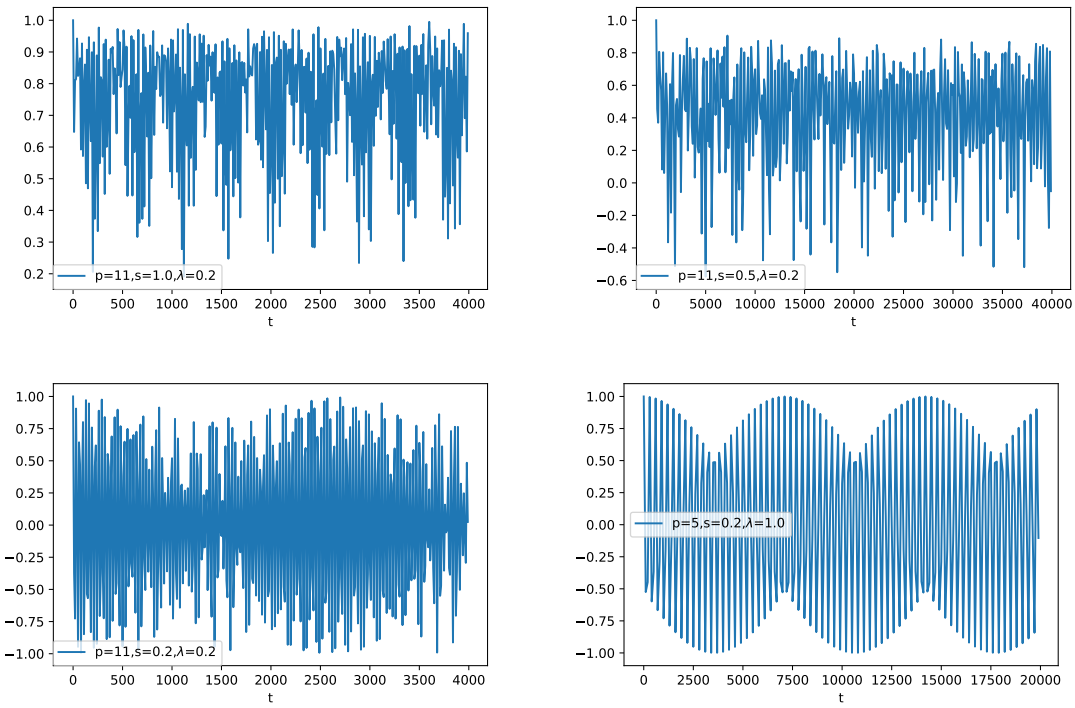

Figure 2. Tine dependence of OTOC $F_{\rm gs}(t)$ with $V = Z_i$ in the F phase ($(s, \lambda) = (1, 0.2), (0.5, 0.2)$) and in the QP phase ($(s, \lambda) = (0.2, 0.2), (0.0, \star)$). The OTOC oscillates around 0 in the QP phase, whereas it behaves non-trivially in the F phase.

Fig.2 indicates that once enough time passes, the average of $F_{\rm gs}(t)$ goes to some non-zero values in the F phase and zero in the QP phase. Those facts explain why the time-average of $F_{\rm gs}(t)$

$$\tilde{F}_{\rm gs} = \lim_{T\to\infty} \frac{1}{T} \int_0^T F_{\rm gs}(t) dt \tag{2.12}$$

can diagnose phase transition. Indeed, $\tilde{F}_{\rm gs}$ stays around 0 in the QP phase and converge into a certain non-zero value in the F phase. Note that, for a chaotic system, we expect $\tilde{F}_{\rm gs} = 0$, while for a non-chaotic system we generically expect $\tilde{F}_{\rm gs} \neq 0$. In this work we consider $W = V$ and we use both local operators, $V = Z_i$, and non-local operators, $V = S^z = \frac{1}{N}\sum_i^N Z_i$. We find that $\tilde{F}_{\rm gs}$ can efficiently diagnose the quantum phase transition. Fig. 3 shows that, in the QP phase $\tilde{F}_{\rm gs} = 0$, while in the F phase $\tilde{F}_{\rm gs}$ takes a non-zero value that increases with s. The critical points of the second-order phase transitions obey the formula $s = \frac{1}{3-2\lambda}$ and those of the first-order phase transitions are numerically estimated in [62]. If the temporal fluctuation of the OTOC is small, its expectation value should be almost equal to the long time average of the OTOC.

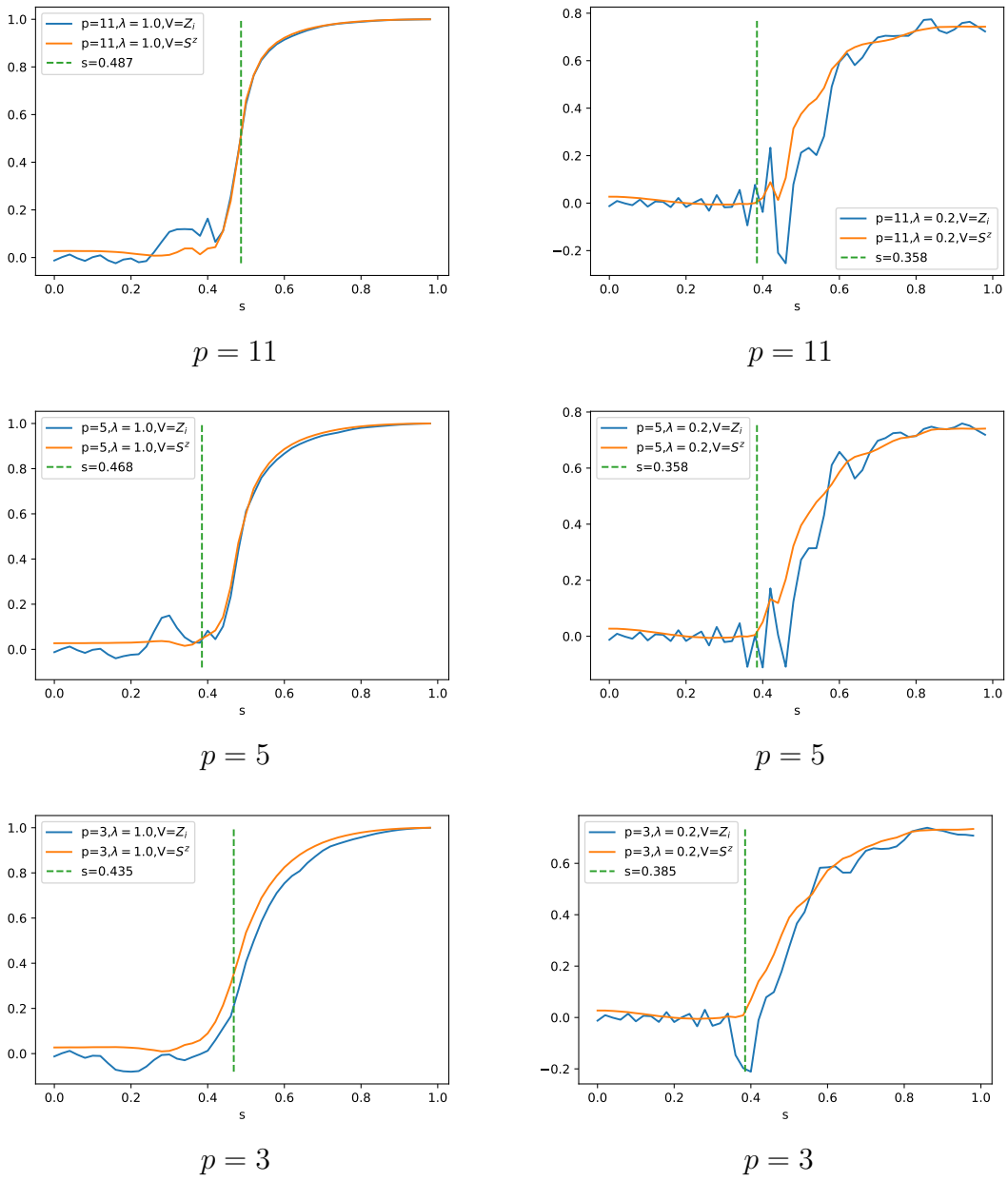

$p = 11$ $p = 11$

$p = 5$ $p = 5$

$p = 3$ $p = 3$

Figure 3. s dependence of $\tilde{F}_{\rm gs}$ with the local operator $W = V = Z_i$ and the non-local operator $V = S^z$ on the $N = 8$ system. Phase transitions occur at the corresponding critical points (first-order for $(p, \lambda) = (11, 1.0), (5, 1.0), (3, 1.0), (3, 0.2)$ and second-order for $(p, \lambda) = (11, 0.2), (5, 0.2)$. Critical points are as estimated in [62].

We show that our method is not limited to a particular choice of operators. Behavior of $\tilde{F}_{\rm gs}$ with $W = V = X_i, S^x = \frac{1}{N}\sum_{i=1}^{N} X_i$ and mixed cases $(W, V) = (Y_i, X_i), (X_i, Z_i)$ is exhibited in Fig.4. In both cases, $\tilde{F}_{\rm gs}$ changes behavior around the critical points. Especially, it is remarkable that phase transitions are detected even when different combinations of operators are used for W and V. (The $W = V = Z_i$

case is reported elsewhere.)

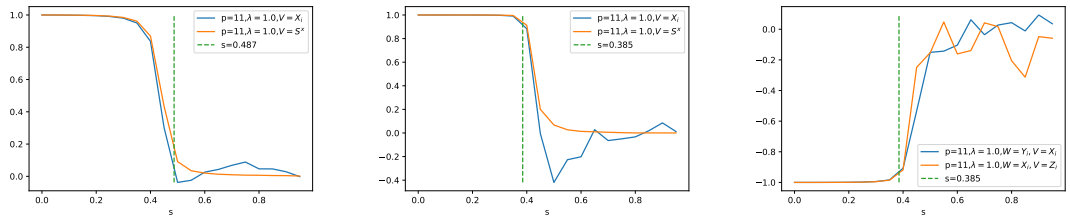

Figure 4. s dependence of $\tilde{F}_{\rm gs}$ with $W = V = X_i, S^x$ and mixed cases $(W, V) = (Y_i, X_i), (X_i, Z_i)$. Phase transitions occur at the corresponding critical points.

Now let us choose operators acting on different sites. Dynamical delocalization of operators is usually referred to as quantum scrambling. Here we use one-body operators acting on two different sites. The support of an operator gets larger and larger as it grows, and after some sufficiently large time, their supports may overlap. Fig.5 show the long time average of the OTOC at $\lambda = 1.0$ with different V, W. Qualitatively they show the same behavior in the QP phase. For the case with $\lambda = 1.0$, it turns around the critical point and increases to 1 in the F phase.

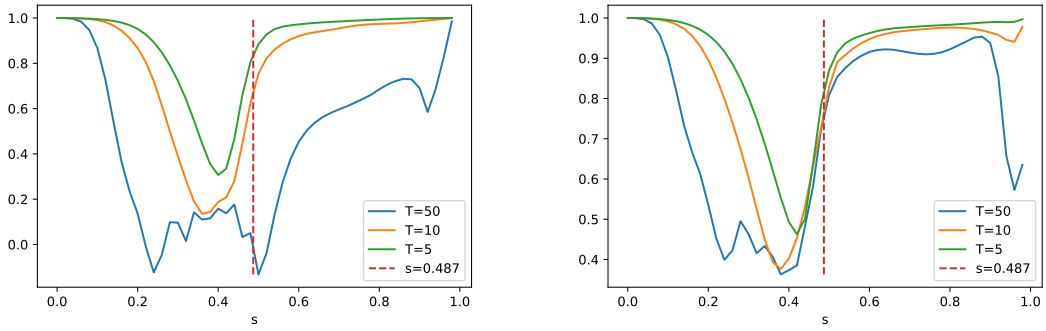

Figure 5. Time average of the OTOC $\frac{1}{T}\int_0^T \langle W(t)VW(t)V\rangle dt$ for $N = 8$ and $\lambda = 1.0$ [Left] $V = Z_N$ and $W = Z_1$ [Right] $V = Z_N, W = X_1$

We compare the results with correlation functions $\langle W(t)V\rangle^2$. Fig.6 presents $\frac{1}{T}\int_0^T \langle W(t)V\rangle^2 dt$. We find that behavior of OTOCs is more sensitive to a choice of operators.

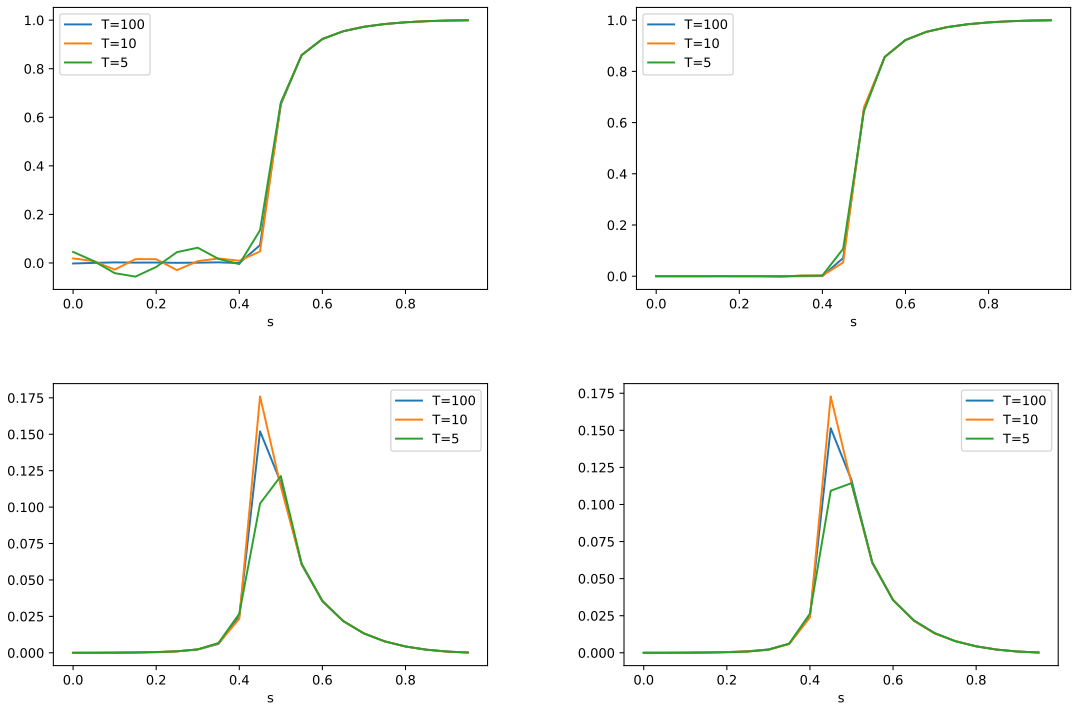

Figure 6. Plots of $\frac{1}{T}\int_0^T \langle W(t)V\rangle^2 dt$ at $\lambda = 1$ and $N = 8$ [Upper-Left] $V = W = Z_1$ [Upper-Right] $V = Z_N$ and $W = Z_1$ [Lower-Left] $V = Z_N$ and $W = X_1$ [Lower-Right] $V = Z_1$ and $W = X_1$

One might notice that we compute the expectation value in (2.6) in the ground state of the system, while one usually considers the thermal expectation value in such calculations. The reason behind this choice is the fact that the phase transition is related to the physics of the ground state of the system. Moreover, it has been shown that with such a choice, the OTOC is dominated by a contribution F_{gs} coming from the ground state of the system, while the contribution F_{ex} from excited states is sub-dominant [50]

$$F(t \to \infty) = F_{gs}(t \to \infty) + F_{ex}(t \to \infty)\,, \quad \text{with } F_{ex}(t \to \infty) \ll 1. \tag{2.13}$$

To figure out the state-dependence on the time average of the OTOC, we show in Fig.7 the behavior of $\tilde{F}_{\text{1st-ex}} = \lim_{T\to\infty} \frac{1}{T}\int_0^T \langle\psi_1| V(t)VV(t)V |\psi_1\rangle\, dt$ with the first excited state $|\psi_1\rangle$. In comparison with previous results, it is clear that the relation $|\tilde{F}_{\text{gs}}| \gg |\tilde{F}_{\text{1st-ex}}|$ is held for any s larger than each critical value and contributions from the excited state are negligible.

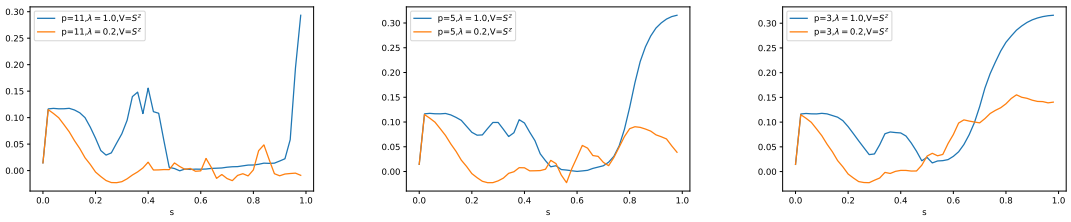

Figure 7. s dependence of $\tilde{F}_{\text{1st-ex}}$ with $V = S^z$.

2.3 Reverse Annealing and OTOC

We study relation between the reverse annealing and quantum chaos. Reverse annealing is a way to find a better classical solution than a given initial solution by starting from an appropriate classical state and gradually increasing and the decreasing the transverse magnetic field [63]. The current D-Wave quantum annealer, D-Wave 2000Q, implements reverse annealing and the performance has been studied for various cases [2, 64, 65]. Some studies on the efficiency of reverse annealing are provided theoretically [66] and numerically [67], where it is shown that, at least for the p-spin model, reverse annealing can turn first-order phase transition into second-order phase transition by choosing an appropriate process. The Hamiltonian of reverse annealing is

$$H(s,\lambda) = sH_0 + (1-s)(1-\lambda)H_{\text{init}} + \Gamma(1-s)\lambda H_1, \tag{2.14}$$

where s, λ both take values in [0,1], Γ tunes the strength of the transverse magnetic field, and H_{init} is the initialization term

$$H_{\text{init}} = -\sum_{i=1}^{N} \epsilon_i Z_i, \tag{2.15}$$

where $\epsilon_i \in \{-1, 1\}$ is the ith component of the given classical initial state. Due to high spacial symmetry of the p-spin model, without loosing generality we can assign ϵ_i so that

$$\epsilon_i = \begin{cases} +1 & \text{for } i \leq N-n \\ -1 & \text{for } i > N-n, \end{cases} \tag{2.16}$$

where $n \in \{0, 1, \cdots, N\}$. Then $c = 1 - \frac{n}{N} \in [0, 1]$ is the probability for ϵ_i to be $+1$ and the initial magnetization is $2c - 1$. A large c implies the solution is close to the ground state of H_0. If c is closer to 1, the transition is second-order, otherwise first-order. In what follows we use the local operator with $W = V = Z_i$, since we have confirmed the non-local cases show the same properties. s dependence of $\tilde{F}$ is exhibited in Fig.8. According to [67], the p-spin model experiences phase transitions by reverse annealing. And our results are consistent with their report. Similar to the previous cases, $\tilde{F}$ behaves differently around the critical points. The smaller c

becomes, the larger the critical s becomes. This property is clearly shown in the figure: The smaller c becomes, the slower $\tilde{F}$ approaches to 1. For any case of p, we find $\tilde{F}$ shows qualitatively the same behavior. Especially the curves of $\tilde{F}$ converge into 1 at the the same speed after the critical points, regardless of p and c. Moreover, Figs. 8,9 and 10 show that the bigger Γ becomes, the bigger the critical points s becomes, which is also consistent with [67].

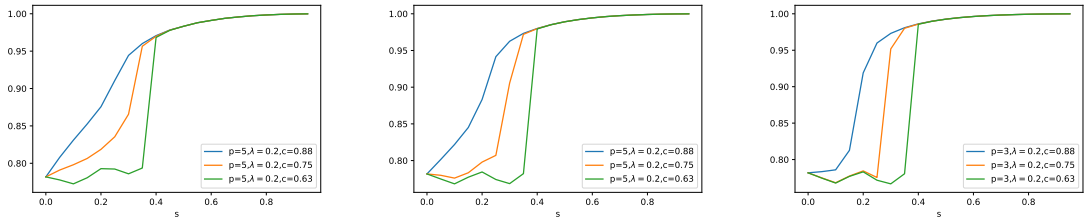

Figure 8. s dependence of $\tilde{F}_{\rm gs}$ for $p = 3, 5, 11$ with $N = 8, \Gamma = 1$.

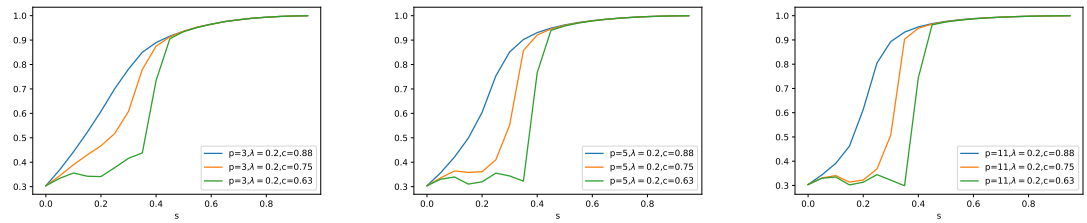

Figure 9. s dependence of $\tilde{F}_{\rm gs}$ for $p = 3, 5, 11$ with $N = 8, \Gamma = 2$.

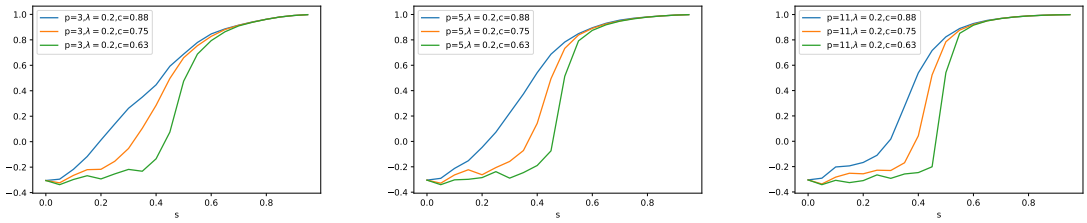

Figure 10. s dependence of $\tilde{F}_{\rm gs}$ for $p = 3, 5, 11$ with $N = 8, \Gamma = 5$.

2.4 Phase Transition of Majorana Chain Model and OTOC

So far we have investigated cases where target Hamiltonian consists of only classical spins. We next consider a case where a target Hamiltonian has complex couplings among Majorana fermions [3]. We will show this model has both first-order and second-order phase transitions. A model we are interested in has the Hamiltonian of Majorana fermions

$$H_0 = i \sum_{k=1}^{N-p} c_{2(k+p)-1} c_{2k} + c_{2(k+p)} c_{2k-1}, \tag{2.17}$$

where p is an integer and c_i is defined by the Jordan-Wigner formulation (1.21)

$$\begin{aligned} c_{2k-1} &= Z_1 \cdots Z_{k-1} X_k \\ c_{2k} &= Z_1 \cdots Z_{k-1} Y_k. \end{aligned} \tag{2.18}$$

Let $|\theta, \phi\rangle$ be the spin coherent state

$$|\theta, \phi\rangle = \bigotimes_i^N |\theta, \phi\rangle_i \tag{2.19}$$

where $|\theta, \phi\rangle_i = \cos(\theta/2)\,|0\rangle_i + e^{i\phi}\sin(\theta/2)\,|1\rangle_i$ with $\theta \in [0, \pi], \phi \in [0, 2\pi]$. Using ${}_i\langle\theta, \phi|\, X_i\, |\theta, \phi\rangle_i = \sin\theta\cos\phi$, we find

$$\begin{aligned} \langle\theta, \phi|\, H_1\, |\theta, \phi\rangle &= -N\sin\theta\cos\phi \\ \langle\theta, \phi|\, H_2\, |\theta, \phi\rangle &= \frac{1}{N}\sum_i^N h_{ii} + \frac{\sin^2\theta\cos^2\phi}{N}\sum_{i\neq j} h_{ij} \end{aligned} \tag{2.20}$$

The semi-classical potential $V(s, \lambda, \theta, \phi)$ is then defined by

$$V(s, \lambda, \theta, \phi) = \lim_{N\to\infty} \frac{1}{N}\langle\theta, \phi|\, H(s, \lambda)\, |\theta, \phi\rangle\,. \tag{2.21}$$

In what follows we address cases where $\langle\theta, \phi|\, H_0\, |\theta, \phi\rangle$ is independent of ϕ. Then it is easy to see that $V(s, \lambda, \theta, 0) \leq V(s, \lambda, \theta, \phi)$ for any $(s, \lambda, \theta, \phi)$. So $\phi = 0$ gives a ground state. We define $\theta_{\min}$ by $V(s, \lambda, \theta_{\min}, \phi) \leq V(s, \lambda, \theta, \phi)$ for all θ. The first-order phase transition occurs when V is discontinuous with respect to $\theta_{\min}$. Starting $s = 0, \lambda = 1$, the ground state is initially located at $\theta = \pi/2$ and $\phi = 0$, hence a second-order phase transition occurs when they satisfy

$$\left.\frac{\partial^2 V}{\partial\theta^2}\right|_{\theta=\frac{\pi}{2},\phi=0} = 0 \tag{2.22}$$

Then we obtain the potential

$$V = s\lambda\cos^{p-1}\theta\sin^2\theta - (1-s)\sin\theta\cos\phi + \frac{s(1-\lambda)\sin^2\theta\cos^2\phi}{N^2}\sum_{i\neq j} h_{ij}, \tag{2.23}$$

by using the forms

$$\begin{aligned} \langle\theta, \phi|\, c_{2(k+p)-1}c_{2k}\, |\theta, \phi\rangle &= -i\cos^{p-1}\theta\sin^2\theta\cos^2\phi \\ \langle\theta, \phi|\, c_{2(k+p)}c_{2k-1}\, |\theta, \phi\rangle &= -i\cos^{p-1}\theta\sin^2\theta\sin^2\phi. \end{aligned} \tag{2.24}$$

Then the condition of the second-order phase transitions is independent of p

$$\lim_{N\to\infty}(1-s) - 2s(1-\lambda)\frac{1}{N^2}\sum_{i\neq j} h_{ij} = 0. \tag{2.25}$$

In what follows we set $h_{ij} = 1$. This model experiences various phase transitions (Fig. 11). For a large λ, it is a first-order as shown in the left of Fig.12. There are no second-order phase transitions on the dashed line. For medium $\lambda \sim 0.4$, a first-order phase transition occurs after a second-order phase transition. For a small λ, a first-order phase transition is avoided. One can directly confirm some quantum effects by studying the trace distance between $|\theta_{\min}, 0\rangle$ and the ground state of H. So we can conclude that the non-stoquastic term plays a crucial role to avoid a first-order phase transition, which leads to quantum speedup. For a fist-order phase transition, even p is important. One can confirm that a phase transition is second order if p is odd.

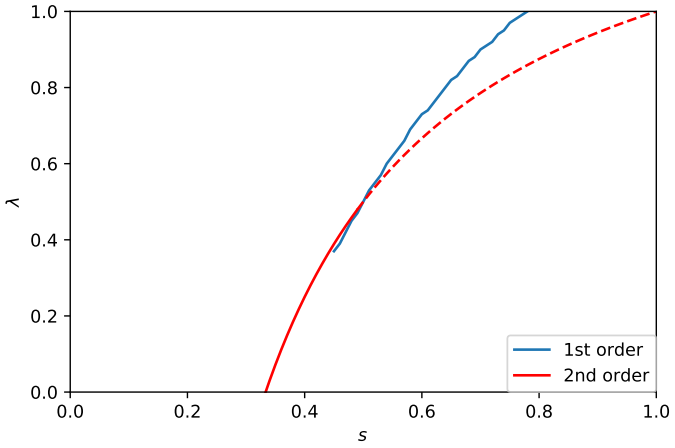

Figure 11. Phase diagram of the $p = 6$ case.

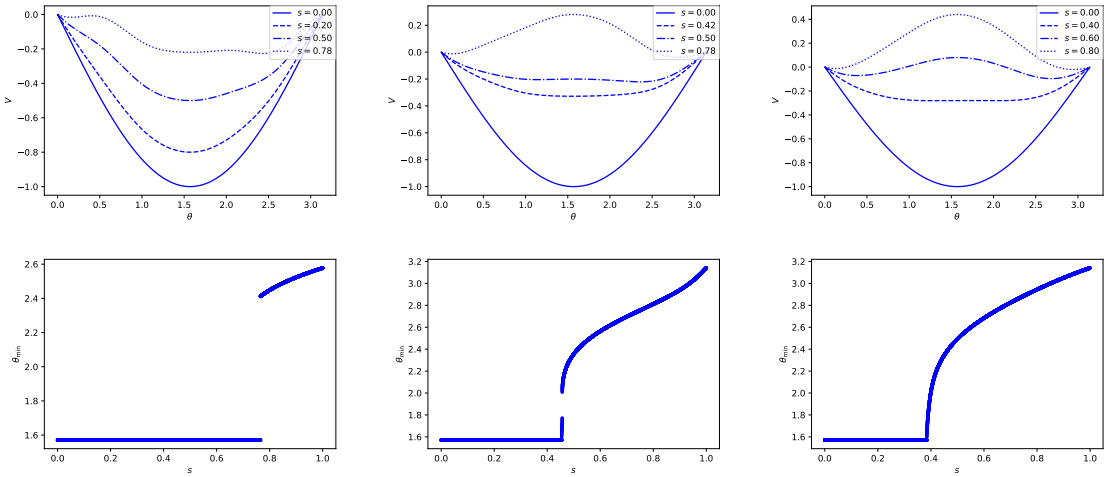

Figure 12. $p = 6$ [Left] $\lambda = 1.0$ [Middle] $\lambda = 0.4$ [Right] $\lambda = 0.2$

Although the previous study is based on a semi-classical method, we can provide additional evidences based on statistical physics. Fig.13 is the derivative of the Gibbs free energy $F = -\beta \ln Z$ with respect to s. In the $\lambda = 0.8$ case, $\frac{\partial F}{\partial s}$ become discontinuous around the critical point. The abrupt change around $s = 0.5$ in the left figure show it is a first-order phase transition, which is consistent with the Fig.11, and continuous but rapid change at $s = 0.3$ implies it is a second-order phase transition.

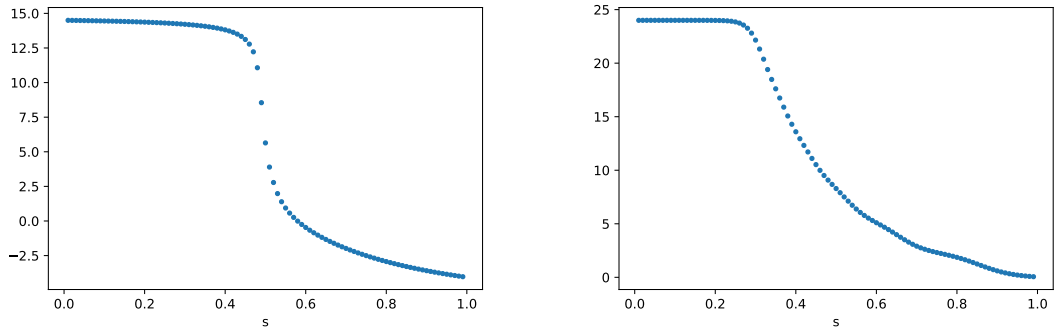

Figure 13. Derivative of the Gibbs free energy at $\lambda = 0.55$ (left), 0.0 (right) and $\beta = 20$

To relate quantum phase transitions with quantum scrambling, we again consider the OTOC. We study the phase transitions from a viewpoint of quantum chaos. Especially we use the following OTOC of the form

$$F_{\rm gs}(t) = \langle \phi_0 |\, c_i(t)^\dagger c_i^\dagger c_i(t) c_i \,| \phi_0 \rangle \,, \tag{2.26}$$

where $|\phi_0\rangle$ is the ground state of the total Hamiltonian $H = H(s, \lambda)$. Fig.14 indicates that once enough time passes, the average of $\tilde{F}_{\rm gs}(t)$ goes to zero in the QP phase and to some non-zero value in a different phase.

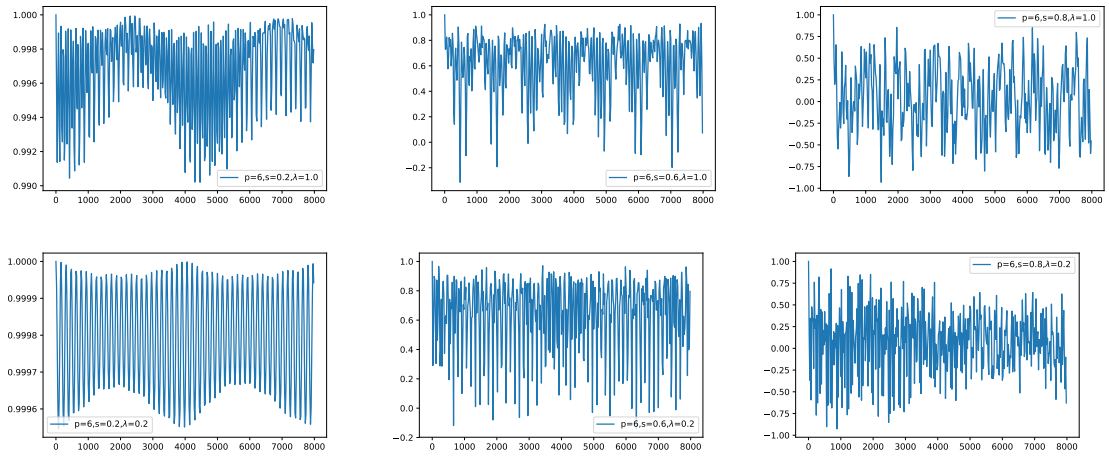

Figure 14. Long time behaviour of the OTOC [Upper] $\lambda = 1.0$ and $s = 0.2, 0.6, 1.0$ [Lower] $\lambda = 0.2$ and $s = 0.2, 0.6, 1.0$

By considering the time-average of the OTOC

$$\tilde{F}_{\text{gs}} = \lim_{T\to\infty} \frac{1}{T} \int_0^T F_{\text{gs}}(t)dt, \tag{2.27}$$

we again confirm that $\tilde{F}_{\text{gs}}$ diagnose phase transitions (Fig.15). $\tilde{F}_{\text{gs}}$ changes the behavior abruptly around the corresponding critical point. Though the order parameter of this not straightforward, we can use the OTOC to study phase transitions.

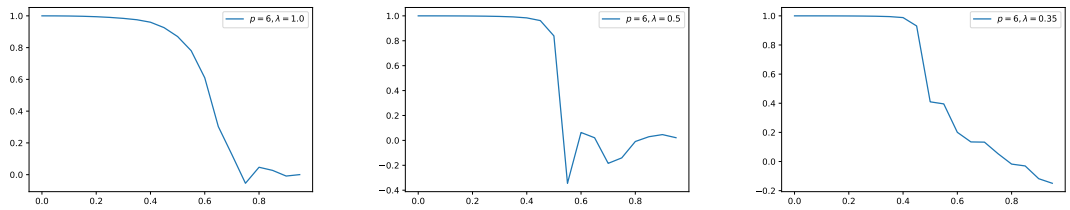

Figure 15. Plots of $\tilde{F}_{\text{gs}}$ at $\lambda = 1.0, 0.5, 0.35$. The horizontal axis is s.

2.5 Short Summary and Remarks on Future Directions

In this work we related quantum chaos to phase transitions associated with quantum annealing and reverse annealing for the p-spin model in Sec.2.2, 2.3 and a Majorana chain model in Sec.2.4. In particular, we have shown that the average value of OTOCs (avgOTOCs) changes behavior around the quantum critical point, diagnosing the corresponding phase transition. In the case of quantum annealing (QA), the system's ground state is initially in a quantum paramagnetic (QP) phase ($s = 0$). As we increase the value of s, the system's displays a quantum phase transition to a different phase. We observed that the average value of the OTOC is zero in the QP phase, and it starts to grow around the quantum critical point, saturating a constant value as s approaches 1.

In chaotic systems, one expects the OTOC to vanish at late-times for almost any operators V and W. In contrast, for an integrable system, one expects a non-universal behavior, i.e., the OTOC depends on the operators V and W, and its saturation value will not, in general, be zero, except maybe for some specific operators. The above results suggest that the system is chaotic in the QP phase, and becomes integrable in the F phase when the target is the p-spin model. However the OTOC is clearly non-zero in the QP phase, although it oscillates around zero. In the F phase, the system also display an oscillatory behavior, but in this case the average value is positive. Therefore, even though the OTOC is not zero for the QP phase, this phase is, in some sense, more chaotic than the F phase, at least from the point of view of the average value of OTOCs. We observed that the avgOTOCs have qualitatively the same behavior across either first order or second order phase transitions. In particular, the avgOTOCs does not have a discontinuous behavior in first order

phase transitions, as it happens in the case of order parameters. This shows that avgOTOCs cannot be thought of as order parameters of QPTs, as suggested in [53]. In the case of reverse QA, the p-model also displays quantum phase transitions, as shown in [67]. In this case, the avgOTOC shows qualitatively the same behavior as in the case of QA, although there are some quantitative differences. In the beggining of the reverse annealing schedule, at $s = 0$, the system already displays a non-zero value of the avgOTOC, which then increases as we increase the values of s.

Regarding the Majorana chain model we have investigated interactions among Majorana fermions and it may be a good toy model for a future quantum annealer which allows one to address complicated couplings among physical qubits. This new model confirms the efficiency of the anti-ferromagnetic XX interactions for quantum annealing. To our best knowledge, this is the first model with a complex coupling in which a first-order phase transition can be avoided by the effect of non-stoquastic quantum annealing. In addition, the aveOTOCs successfully diagnose phase transitions.

By a number of examples we have established a way to diagnose phase transitions with OTOCs. Especially, we succeeded in detecting quantum phase transitions on not necessarily chaotic systems. It will require a further study to clarify relations between quantum phase transitions and quantum chaos. We leave it open to investigate the possibility of telling first-order phase transitions from second-order phase transitions with OTOCs.

3 Application of Quantum Annealing to Nurse Scheduling Problem

3.1 Preliminaries

Among non-deterministic polynomial time (NP)-hard problems, timetabling or rostering problems represent a number of practically important examples. For example, in operations research, the nurse scheduling problem (NSP) arises when finding the optimal schedule for a set of available nurses over a fixed timetable of shifts. Solutions to NSP are required to respect hard constraints, such as days off and minimum availability, as well as soft constraints, such as minimum shift assignments, for each nurse. Examples of NSP are often cast as linear or quadratic programming problems, depending on the nature of the constraints, but they may also be formulated in terms of unconstrained optimization and solved using search methods, including tabu search. Complexity of NSP is summarized in [68]. Practical solutions of NSP for an Italian hospital are studied with variable neighborhood search in [69]. NSP has been explored by various algorithm, such as coordinate descent [70] and a neighborhood-search algorithm [71]. A summary of several algorithm and solutions of NSP is given in [72]

Quantum annealing (QA) is a metaheuristic method for solving combinatorial optimization problems derived from the principles of quantum mechanics [32]. QA operates by driving the Hamiltonian dynamics of an initial quantum state to a sought-after final state that represents the minimum energy configuration of an encoded optimization problem [20]. In the limit that the dynamics are strictly adiabatic and the Hamiltonian sufficiently complex, this coincides with the universal model of adiabatic quantum computing [73, 74]. In practice, however, the adiabatic condition is rarely obtained and the guarantee that the true solution will be recovered is lost. Instead, these quasi-adiabatic dynamics yield the sought-after final state with some non-unit probability and it remains open as to when such behavior can provide a computational advantage [20, 35].

We demonstrate the use of QA to solve NSP and we evaluate its efficiency and accuracy for this problem from empirical results. Our approach uses the commercial quantum annealer available from D-Wave Systems to implement several hard constraints. The D-Wave 2000Q is a commercially available quantum annealing device based on superconducting flux qubits designed to solve quadratic unconstrained binary optimization (QUBO) [75]. It uses the principles of QA operating in the presence of a transverse-Ising Hamiltonian by encoding the problem into a sparsely connected graph expressing the hardware interactions. By reducing NSP to QUBO form and then embedding this problem into the D-Wave processor, we use QA to recover candidate solutions for different problem instances.

Previous applications of QA to unconstrained optimization span a broad variety of topics [76–83], while some efforts have investigated closely related timetabling problems, such as the job-shop problem [84]. The distinguishing features of NSP include the multiple hard constraints, which make the problem difficult to address for con ventional numerical solvers [85]. Equally challenging is the effort to recover approximately optimal solutions, which may fail to find the true minimum with some parameterized tolerance.

Our interest lies in casting NSP as a combinatorial optimization problem in order to validate the capabilities of QA. This may be seen as a first step toward developing quantum-enhanced solvers for other scheduling problems as well. However, the question as to whether QA satisfies the question of quantum computational advantages cannot be addressed here. In addition to limitations on the existing hardware, in both capacity and control [86], there is poor theoretical understanding of the computational power for QA generally. Prior analyses have suggested that NSP and other classical combinatorial optimization problems belong to the complexity class stoqAQC, for which the relationship to the uniquely quantum complexity class BQP is not yet established [20]. These so-called stoquastic problems may be solved efficiently by strictly classical methods, but this is also unknown [35]. However, there is a clear potential for quantum advantage for non-stoquastic problems, which do not correspond to NSP or other combinatorial optimization problems [87].

Our presentation is organized as follows. Sec. 3 defines NSP formally in terms of the hard and soft constraints considered here; Sec. 3.3 introduces QA specialized to the D-Wave 2000Q in terms of a transverse Ising Hamiltonian that encodes an NSP instance. Results from evaluating various problem instances on the 2000Q processor are summarized in Sec. 3.5, and the influence of reverse annealing to improve these results are discussed. Lastly, we conclude in Sec. 3.8 with comments for future work.

3.2 Nurse Scheduling Problem

Several alternative definitions for NSP exist, yet its fundamental concepts can be summarized as follows. NSP is a problem to create a rotating roster of nurses working at a hospital while respecting constraints on their availability and level of effort. In the simplest example of a two-shift system, a schedule assigns nurses to the day duty and night duty shifts of the roster. We will apply two hard constraints to this example that enforce a minimum number of nurses assigned to each shift while also ensuring a minimal period of rest between shifts for each nurse. We refer to these as shift constraints and nurse constraints, respectively.

Shift constraints require that a sufficient number of nurses be assigned to each shift. However, the necessary number may depend on the experience of the assigned nurses, as more experienced nurses may be capable of performing more work during their shift. Nurses usually work as part of a group with each in charge of multiple jobs. Hence it is important to allocate the minimum number of nurses needed to cover all the jobs during a shift. In addition, sometimes it would be also required to distribute jobs to nurses evenly. By contrast, nurse constraints represent the need to satisfy the appropriate working condition for each nurse. This includes time between shifts to get enough rest as well as days off and scheduled vacations. We will apply the following constraints to our instance of NSP:

1. Upper and lower limit of the number of breaks.
2. The number of nurses in duty for each shift slot.
3. Upper and lower limit of time interval between two days of duty.

According to [68], imposing a hard shift constraint and balanced rosters condition becomes NP-complete. The Hamiltonian (3.7) that we use below accommodates those constraints, hence our setup can be useful to solve problems. In what follow, we impose simplified constraints for a benchmark analysis of D-Wave 2000Q.

3.3 Quantum Annealing with the D-Wave 2000Q

The D-Wave 2000Q is based on quantum annealing, which is a derivative of adiabatic quantum optimization. The latter is based on the time-dependent Schrodinger equation

$$i\hbar\frac{\partial\psi(t)}{\partial t} = H(t)\psi(t) \tag{3.1}$$

where $\psi(t)$ denotes the quantum mechanical wave function of an underlying physical system and $H(t)$ is the time-dependent Hamiltonian that drives the dynamics. A generic form of this Hamiltonian is

$$H(t) = A(t)H_0 + B(t)H_1, \tag{3.2}$$

with $t \in [0, T]$ and T the final evolution time. The schedules $A(t), B(t)$ are monotonic and satisfy $A(0) = 1, B(0) = 0$ and $A(T) = 0, B(T) = 1$. Therefore, the quantum state $\psi(0)$ evolves under an interpolation from H_0 to H_1 in order to prepare the final state $\psi(T)$. Assuming the initial state is an eigenstate of H_0, then the adiabatic theorem promises that the quantum state will remain an instantaneous eigenstate of $H(t)$ provided the dynamics evolve sufficiently slow. The latter condition may be enforced by choice of the annealing time T or the schedules. That is, we may select the final Hamiltonian H_1 to represent a computational problem in which the eigenstates encode a well-defined solution. More precisely, we will focus on the case in which the ground state encodes the computational solution.

Let s_i^x, s_i^z be Pauli spin operators at sites. The D-Wave 2000Q implements an initial Hamiltonian expressed as

$$H_0 = -\sum_{i \in V} s_i^x, \tag{3.3}$$

where V is a set of spin sites, and a final Hamiltonian that takes the Ising spin model form

$$H_1 = \sum_{i \in V} J_{ij} s_i^z s_j^z + \sum_{i \in V} h_i s_i^z, \tag{3.4}$$

where J_{ij} describe the interaction between sites i, j and h_i are the weights of the linear terms. The resulting time-dependent Hamiltonian corresponds to the well-known transverse field Ising model which is used widely in statistical physics to describe complex spin systems. Finding the ground state of the Ising model itself is known to be NP-Hard and, therefore, this Hamiltonian is capable of expressing a broad variety of combinatorial optimization problems including, as we show below, NSP. By contrast, the ground state of H_0 is easy to deduce.

Notwithstanding the premise of adiabatic quantum optimization, the technical challenges of reliably preparing a quantum physical system in a pure, zero-temperature quantum state prevent these ideals from being realized in practice. Rather, the behavior of the 2000Q is better approximated by a mixed quantum state evolving as an open system. In addition to the limits on controllability, there is more general concern that knowing the optimal annealing schedule and duration require a priori information about the solution itself. Therefore, quantum annealing is most often treated as a heuristic that may be applied with good accuracy in certain situations.

In our examples below, we interface with the quantum annealer by providing a logical representation of the Ising spin model H_1 to be solved. Additional steps address the transformation of the logical input into a physical representation which can be embedded into the hardware [88]. This step, known as minor embedding, depends strongly on the connectivity of the vertex set V and the sparsity of the chimera layout [89, 90]. Consequently, additional auxillary spin variables may be introduced during embedding to ensure logical connections are satisfied [91]. In addition, the ability to express the logical parameters, $J_{i,j}$ and h_i, is limited by the dynamic range of the hardware control.

The 2000Q offers a variety of controls for modifying the annealing time and schedules that determine the quantum dynamics leading to solution. Forward annealing corresponds to the process of driving the quantum system from the initial Hamiltonian H_0 to the final Hamiltonian H_1 and then performing measurements. We use forward annealing to compute the outcome of a given problem instance and we repeat this process many times to estimate the frequency with which computed solutions are observed. Reverse annealing builds on the result of a forward anneal by first initializing the processor to a previously computed result and then reversing the Hamiltonian dynamics to anneal backward. This process reintroduces the transverse field and potentially prepares a new, intermediate quantum state. The process is then completed by annealing forward in time to the final Hamiltonian. We investigate the relative accuracy of both forward and reverse annealing to solve instances of NSP.

3.4 Ising Model Formulation of NSP

A common approach to casting combinatorial optimization as an Ising model is to first express the problem as unconstrained optimization and, more specifically, as quadratic unconstrained binary optimization (QUBO) [26]. The QUBO form offers a direct mapping into the Ising model using a simple change of variable from binary to bipolar representation. We take this approach to formulate NSP as a QUBO problem with respect to minimization and then transform to the equivalent Ising model.

Consider a set of N nurses labeled as $n = 1, \ldots, N$ and a schedule consisting of D working days labelled as $d = 1, \ldots, D$. Using the binary variable $q_{n,d} \in \{0, 1\}$, let $q_{n,d} = 1$ specify the assignment of nurse n to day d. We then consider specific instances of the shift and nurse constraints discussed above. For the hard shift constraint, we require that the schedule must ensure at least 1 nurse is assigned each working each day. For the hard nurse constraint, the schedule must ensure no nurse works two or more consecutive days, while the soft nurse constraint requires that all nurses should have approximately even work schedules.

We construct objective functions that correspond to each shift and nurse constraint and then use the sum of these terms to express the QUBO form. We introduce

composite indices $i(n,d)$ and $j(n,d)$ as functions of the nurse n and the day d. We construct the hard nurse constraint by introducing a symmetric, real-valued matrix J such that $J_{i(n,d),j(n,d+1)} = a$ and zero otherwise. The positive correlation constant a enforces the nurse constraint by penalizing a schedule for nurse n to work two consecutive days. The resulting objective function is quadratic, i.e., $J_{i,j}q_iq_j$, and takes its minimal when the hard nurse constraint is satisfied. Note that the nurse constraint can be modified by changing the entries of the matrix J.

We express the hard shift constraint in terms of the required workforce $W(d)$ needed on each day d and the level of effort $E(n)$ available from each nurse n. We seek an equality solution for this constraint by introducing a quadratic function that penalizes schedules with too many or too few nurses assigned. We take a similar approach for the soft nurse constraint by introducing a quadratic penalty for failing to account for nurse preferences in the work schedule. We use $F(n)$ to specify the number of work days that each nurse wishes to be scheduled and $G(n,d)$ to define a the preference for nurse n to work on day d.

As a simplified example of the soft nurse constraint, we decompose the preference function into the product $G(n,d) = h_1(n)h_2(d)$, in such a way that

$$h_1(n) = \begin{cases} 3 & \text{busy} \\ 2 & \text{moderate} \\ 1 & \text{idle,} \end{cases} \tag{3.5}$$

In addition, they can also have options whether they may work on weekend/night or not by tuning $h_2(d)$:

$$h_2(d) = \begin{cases} 2 & \text{weekend or night} \\ 1 & \text{weekday,} \end{cases} \tag{3.6}$$

The formulation can be more sophisticated by including three-shift systems, distinction
of weekdays and weekends regarding burden, or day-off request with priority (see appendix). We simply require the minimum duty days $F(n)$ for all nurses n are equal to or greater than $[D/N]$, where $[x]$ ($x \in \mathbb{R}$) means the integer part of x.

Composing these individual terms into a single objective function yields the QUBO form

$$\begin{aligned} H_1(q) = &\sum_{n,n'}^{N}\sum_{d,d'}^{D} J_{i(n,d),j(n',d')}q_{i(n,d)}q_{j(n',d')} \\ &+ \lambda\sum_{d}^{D}\left(\sum_{n}^{N} E(n)q_{i(n,d)} - W(d)\right)^2 + \gamma\sum_{n}^{N}\left(\sum_{d}^{D} h_1(n)h_2(d)q_{i(n,d)} - F(n)\right)^2 \end{aligned} \tag{3.7}$$

where the positive real-valued numbers λ and γ tune the relative significance of each term. The objective function has its minimum when all the constraints are satisfied and takes on a positive value otherwise. We will assume that the functions $E(n), F(n)$ and $W(d)$ are integer-valued functions of n or d but this is not required. We will require the minimum duty days $F(n)$ for all nurses n are equal to or greater than $[D/N]$, where $[x]$ $(x \in \mathbb{R})$ means the integer part of x.

We next transform the QUBO expression in Eq. (3.7) into an equivalent Ising spin model. This requires changing from the binary variables q_i to the bipolar spin variable $s_i = 2q_i - 1$. The resulting quadratic terms are then collected to match the form of the Ising spin model in Eq. (3.4). Notably, the connectivity between spin sites is determined by the relatively sparse nurse constraints J and $F(n)$ as well as the shift constraints set by $E(n)$, $W(d)$, and $G(n, d)$.

3.5 Results

Using the Ising model for NSP, we solve this combinatorial optimization problem with the D-Wave 2000Q. Our implementations use the randomized embedding algorithm based on work by Cai, Macready and Roy and implemented in the D-Wave software toolchain [92]. We first discuss results obtained using forward annealing and then with reverse annealing. For our studies, we fix the annealing time for a single sample to 20 μs and we collect 1000 samples per problem instance to estimate the solution frequency. We present results for $N = 3$ and 4 nurses and $D = 5 - 14$ days. Throughout our study, we fix the parameters $\gamma = 0.3$ and $\lambda = 1.3$, and for the soft nurse constraints, we use the simplest example with $h_1(n) = 1$, $h_2(d) = 1$, $E(n) = 1$, $W(d) = 1$ and the penalty $a = 7/2$. The results of simulated annealing show that ground states were found well when those vales of a, γ and λ were used (see Fig.17).

A graphical representation of the computed schedules are shown in Fig. 16 of two solutions obtained from forward annealing for an instance with $N = 3$ and $D = 4$. The schedule in Fig. 16(a) satisfies all the constraints of this NSP instance, whereas the result in Fig. 16(b) does not satisfy the nurse constraint that every nurse has an assignment. Consequently, solution (a) minimizes the energy of the Ising spin model, i.e., it represents a ground state, while the result in (b) is necessarily higher due to the penalty term. Similar results are obtained for all the instances tested here, and in the following, we present statistical estimates for the frequency with which the computed schedules satisfy all the constraints. Of course, the ground state may be degenerate and multiple satisfying schedules are possible.

3.6 Forward Annealing

We first consider the quality of solutions obtained by forward annealing. Figure 17 presents the probability of finding a ground state with D-Wave 2000Q (left) and simulated annealing (right) for the case of $N = 3$ and 4 over a schedule of D days. While there is significant probability to recover completely satisfying solutions for smaller

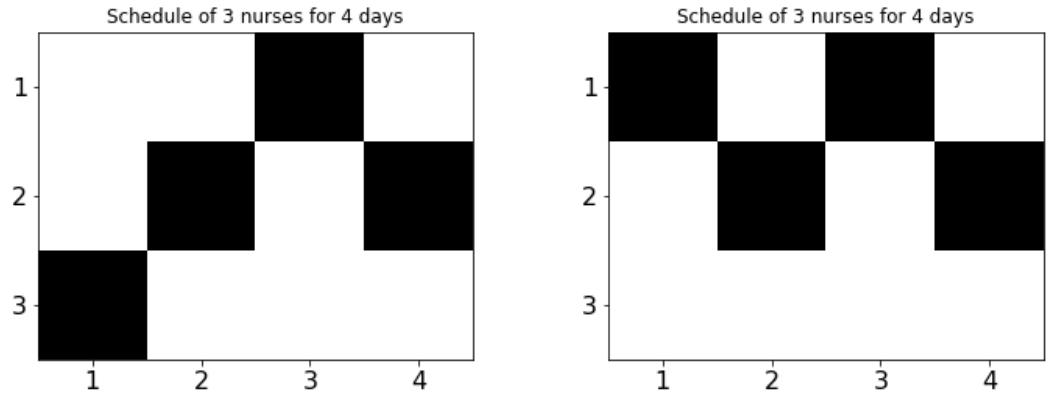

(a) (b)

Figure 16. Graphical examples of the computed shift schedules for the case of $N = 3$ nurses for $D = 4$ days. A black square indicates that a nurse is scheduled to work. The horizontal axes labels the days and the vertical axes labels the nurses. (a) Represents a schedule that satisfies all the constraints, while (b) represents a schedule that fails to satisfy the soft nurse constraint of every nurse being assigned some days of work.

schedules, we observe that the probability to satisfy all constraints falls below our sampling level for larger schedules. In particular, we did not observe completely satisfying solutions from D-Wave 2000Q for $N = 4, D = 10, 11, 12, 13, 14$, whereas some ground states were obtained with D-Wave 2000Q for $N = 3, D = 11, 12, 13, 14$ and for $N = 4, D = 9$. Regarding the results by simulated annealing, we observed ground states for all (N, D). Comparing those results, we may say simulated annealing has a considerable advantage.

We next evaluate the deviation of computed solutions from the completely satisfying solution using the Hamming distance. For these calculations, we express the schedules as ordered binary vectors of size ND and we sum the elements of their inner product to calculate the number of position in which they agree. Subtracting this number from ND yields the Hamming distance, which measure the number of position in which the vectors disagree. In particular, a value of zero indicates exact agreement between the computed schedule and the observed ground state solution. Figure 18 plots the Hamming distance between consecutive solutions obtained by means of the D-wave processor. It is apparent from these statistics that the average Hamming distance is well below the maximum value if ND but significantly greater than 0 for all forward annealing solutions. We will present a comparison with reverse annealing solutions in the next section.

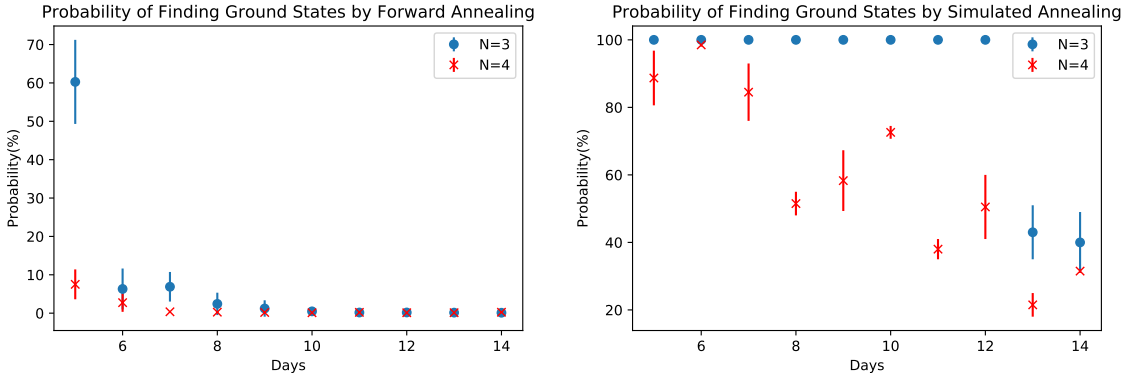

Figure 17. The probability of finding a ground state of the Hamiltonian by using D-Wave 2000Q (left) and simulate annealing (right) for (blue) $N = 3$ and (red) $N = 4$ with respect to the number of days D in the schedule. Each error bar is generated by the standard deviation (1000 samples for 10 shots).

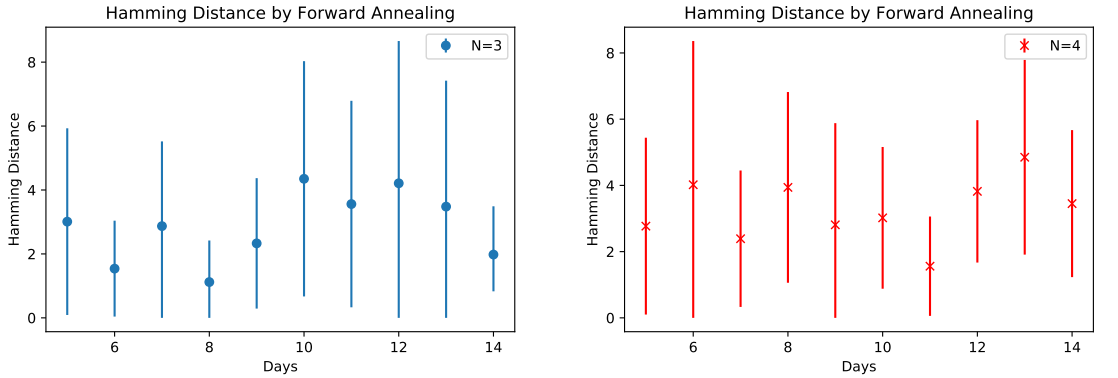

Figure 18. The Hamming distance between consecutive forward annealing solutions with respect to number of schedule days for (blue) $N = 3$ nurses and (red) $N = 4$ nurses. Error bars are based on the standard deviation.

3.7 Reverse Annealing

Reverse annealing is a way to find a better classical solution than a given initial solution by starting from an appropriate classical state and gradually increasing and the decreasing the transverse magnetic field [63]. Some studies on the efficiency of reverse annealing are provided theoretically [66] and numerically [67], where it is shown that, at least for the p-spin model, reverse annealing can turn first-order phase transition into second-order phase transition by choosing an appropriate process. The reverse annealing implemented by D-Wave 2000Q is called iterated reverse annealing, which is based on the Hamiltonian

$$H(t) = s(t)H_0 + (1 - s(t))H_1, \tag{3.8}$$

where H_1 is the transverse magnetic field and $s(t)$ is a convex function such that $s(0) = s(\tau) = 1$, where τ is the annealing time of a single cycle. Computation starts with an eigenstate of H_0 and try to find better solution by iterating many times. So if the procedure is iterated for n times, then the total computational time is $n\tau$.

We study the performance of reverse annealing when using the schedules computed by forward annealing. Reverse annealing implemented in D-Wave 2000Q is a heuristic methods to improve the frequency with which a computed solution satisfies the problem constraints. The procedure basically consists of the following three steps: (1) evolving the Hamiltonian $H(T)$ to an intermediate value $H(sT)$ where $s \in [0, 1]$, (2) pausing the evolution for a hold period h_t, and then (3) evolving from $H(sT)$ to $H(T)$. The first step begins from a candidate solution and prepares an intermediate computational state of the quantum annealer, while the pause period enables the intermediate computational states to non-adiabatically mix with nearby instantaneous eigenstates due to the applied transverse field. The final step yields to potentially new computed solution state.

An example of a reverse annealing schedule used in our study is shown in Fig. 19. The schedule reverses to $s = 0.6$ at time $2\mu s$, holds for $h_t = 10\mu s$ and then anneals forward at $12\mu s$ to end at $14\mu s$. Though there are various choices of the target s and hold time h_t, we have found the heuristic to work for our problem instances when $s \in [0.6, 0.8]$ and $h_t \in \{10, 50, 100\mu s\}$.

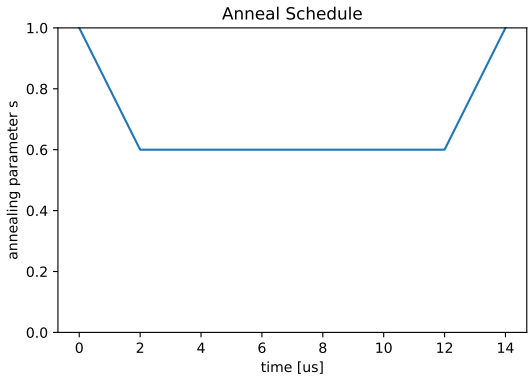

Figure 19. A reverse annealing schedule used in our study plotted with respect to the evolution of the dimensionless parameter s.

We apply reverse annealing to two different sets of forward annealing solutions. The first use of reverse annealing processes randomly chosen samples from the distribution of forward annealing solution reported in the previous section. Using the schedule shown in Fig. 19, we show in Fig. 20 that the probability of finding a completely satisfying solution of the NSP instance decreases and, in some cases, vanishes. The probabilities for $N = 4, D = 11, 12, 13, 14$ are exactly zero. While it is noted that solutions for $N = 3, D = 13$ and $N = 4, D = 10$ were successfully improved

by reverse annealing, the average success rate decreased. By this methodology, the probability of finding ground states is highly related to the frequency distribution of forward annealing, since initial inputs of reverse annealing are randomly chosen. Comparing Fig. 20 with the probability of forward annealing given in Fig. 17, we see that the accuracy is not always improved by reverse annealing. This is understood as follows. When accuracy is improved by reverse annealing, this is because the relatively many forward annealing solutions which are close to ground states are obtained and those solutions are frequently picked up as initial inputs of reverse annealing.

We examine the corresponding Hamming distance between consecutive solutions computed with reverse annealing in Fig. 21, which shows the mean Hamming distance and their standard deviation. Comparing Fig.21 with Fig.18, we notice that overall reverse annealing decrease the mean and the standard deviation of the Hamming distance becomes close to 0, which implies that reverse annealing successfully refined solutions and grouped them together.

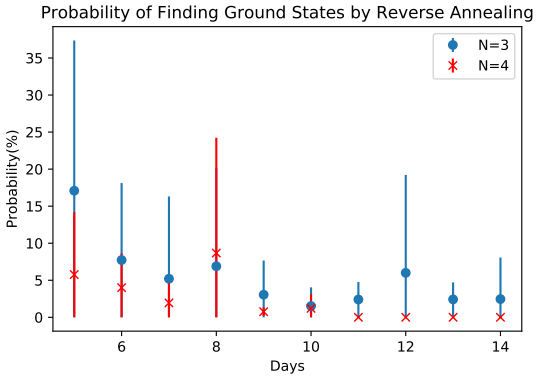

Figure 20. Probability of finding the ground states of the NSP Hamiltonian by reverse annealing. Each error bar is generated by the standard deviation (1000 samples for10 shots)

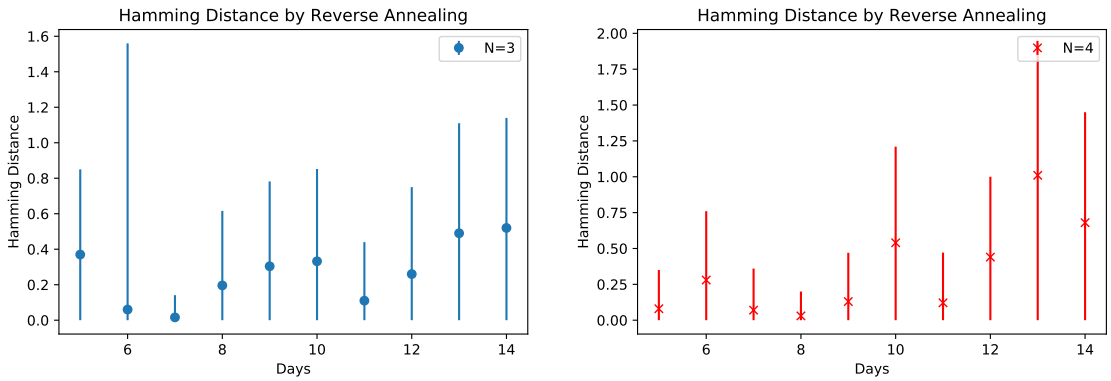

Figure 21. Hamming distance between consecutive reverse annealing solutions. Error bars are based on the standard deviation.

We now discuss application of reverse annealing to the low-lying energy states of the forward annealing solution distribution. These states represent the best solutions obtained from forward annealing and, therefore, may be the most likely to be effected by the process. This approach can be useful to estimate the essential effect of reverse annealing, since it is natural to ask whether reverse annealing works well when an initial state already close to the true ground state.

We used the lowest energy solution from each forward annealing distribution as the initial state of reverse annealing. Figure 22 presents the probability of finding a solution that completely satisfies the constraints of the NSP instance from reverse annealing with these initial states. In a process of analyzing data, we noticed that even if a satisfying solution is used as the initial input, it is not guaranteed that computed solution will be the same state. There are many local minima and reverse annealing may get trapped in such local minima depending on the schedule parameters. We find that the accuracy is close to 100% when the ground state is used for an input, otherwise the probability decreases. Figure 22 is based on different lowest energy states, some of which are ground states, of forward annealing.

Some ground states were successfully obtained by reverse annealing even though the initial input was not a ground state. This shows that it is possible to improve solution quality by reverse annealing for the case of using the low-lying energy states as input. However for the $N = 4$ case, ground states were not observed for $D = 10, 11, 12, 13, 14$. Figures 23 show the mean Hamming distance and the standard deviation for these results. Both statistics are greatly reduced compared to the forward annealing results as expected from the improved accuracy.

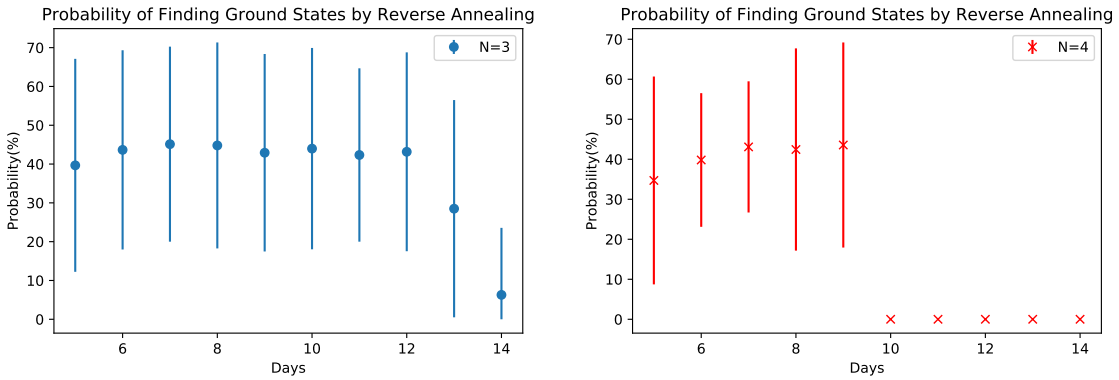

Figure 22. Probability of finding the ground states of the NSP Hamiltonian by reverse annealing. Error bars are based on the standard deviation (1000 samples for10 shots)

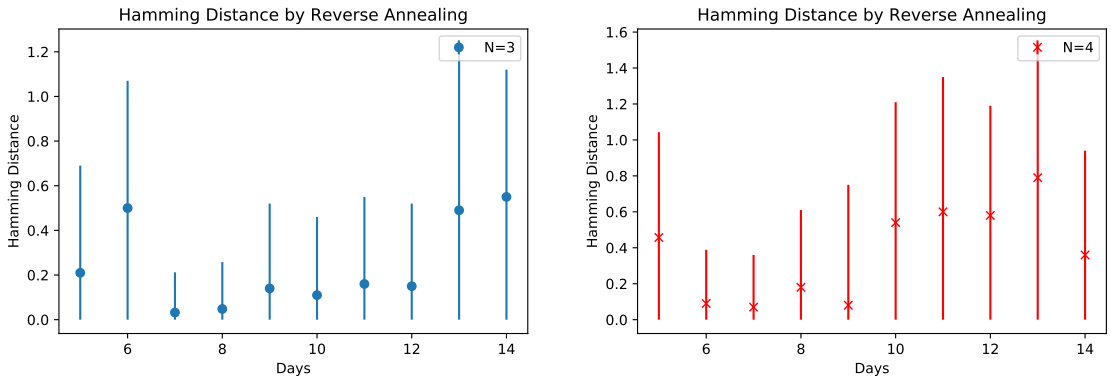

Figure 23. The Hamming distance of consecutive reverse annealing solutions. Error bars are based on the standard deviation.

3.8 Short Summary and Discussion

We have presented a formulation of the nurse scheduling problem (NSP) as an Ising spin Hamiltonian that can be solved using quantum annealing with the commercially available quantum processor. Our approach casts the constraint satisfaction problem into QUBO form and then translates directly to the Ising model. We estimate the frequency for satisfying all constraints using a variety of quantum annealing techniques performed on the D-Wave 2000Q quantum annealer. Our results demonstrate that for a fixed sample size and fixed annealing duration T the probability of successfully matching all constraints decays with increasing size of the schedule D and increasing size of the roster N. Reverse annealing methods do improve the probability of success but not uniformly.

This is an encouraging sign that the quantum annealer is suited to solve a complementary set of practical problems but we do not address the question of performance relative to conventional solver method, since here we aim at giving some benchmark analysis on an application of D-Wave 2000Q to a simple NSP. Current realization of quatnum annealers are insufficient in capacity to explore realistic sizes of N and D. However, it may prove possible to decompose larger problems into a set of smaller optimization problems that could then be solved [93]. For example, we have tested an open-source software package called *qbsolv*, which is based on a variant of tabu search. We found that qbsolv was capable of find satisfying solutions to NSP instances of size $(N, D) = (4, 160)$ using the same parameters used in this work (see the figure in the next page).

Though quantum computation is in an early stage, the approach we have presented may be extended to more general scheduling problems, and anticipate several future directions to improve this methodology. While we have confirmed that reverse annealing can be useful to obtain ground state solutions, it is unclear the necessary parameters to ensure this improvement and further empirical investigations are war-

ranted. In general, reverse annealing depends on several schedule variables and it is natural to try to investigate more on their dependence on those parameters. While our study has been limited to the schedule shown in Fig.19, different schedule parameters may influence the results. An example of such a study is given in [94]. Our work is a first step toward solving scheduling problems with a quantum annealer. In addition, a way of accommodating the hard constraints should be improved. Though simulate annealing can find solutions which satisfy both soft and hard constraints quite nicely, we cannot deny the possibility that the hard constrains were not treated well due to quantum tunneling. This problem in addition to noise of the processor would be responsible for the low probability of finding ground states. This requires further investigation (see [95] for example). There would be various ways to extend and generalize our method on the NSP to different scheduling problems.

Part II
The Hofstadter problem

4 Hofstadter problem with Defects

4.1 Preliminaries

The energy spectra of Bloch electrons moving in two dimensional square lattice under a uniform magnetic field exhibit a fractal structure, called the Hofstadter butterfly [96]. The Hofstadter problem is one of the most widely known research subjects not only in condensed matter physics [97, 98] but also in mathematics [6–8] and quantum geometry [99, 100]. More recently some direct experimental method to confirm a fractal butterfly was proposed by applying quantum computational technology to this research field [9]. The fractal nature of the energy spectra on a lattice without a defect has been widely studied, whereas less is know for cases with defects and impurities [5, 101, 102]. Since real material has more or less defects, it is natural to pursue this problem on a defect system. We previously investigated the Hofstadter problem on a small unit cell with multiple defects and impurities [5], and implied the existence of *in-gap states*. To explore more on the spectra and associated physics, we work on systems with a point defect in a large unit cell of a square lattice and a honeycomb lattice. In this section, we show the linear energy spectra (see. Figs.24 and 25) associated with localized current of the state around the defect, and these states exist in each energy gap of Hofstadter butterfly and the linear energy spectra of these states are retained in even a high magnetic region.

4.2 Hofstadter Butterfly

We pursue the Hofstadter problem on a finite square/honeycomb lattice with boundaries and a point defect to consider realistic situation. We prepare the finite 24×24 square/hexagonal lattices with a single defect at the center of the system. Graphene is a standard example of a honeycomb lattice system and exhibits the QHE [103, 104]. The tight-binding Hamiltonian of our problem is given by

$$\hat{H} = -t \sum_{\substack{\langle m,n \rangle \\ m,n \neq d}} \mathrm{e}^{i\theta_{mn}} c_m^\dagger c_n, \tag{4.1}$$

where $t > 0$ is the nearest neighbor hopping energy, $\langle \cdot, \cdot \rangle$ represents the nearest neighbor sites, d is the site of a defect, and $\theta_{mn} = -2\pi \int_n^m \vec{A} \cdot d\vec{\ell}$, called the Peierls phase[105]. When we solve the eigenvalues of this Hamiltonian while varying magnetic flux $\phi/\phi_0 = p/q$ over rational values with co-prime integers p, q, we would have a fractal energy spectrum, that is Hofstadter's butterfly with defect states. In considering the periodic lattice case, the magnetic Bloch condition [106] is imposed. For

example,in a square lattice case,

$$\psi(\vec{r} + qL\hat{x}) = e^{ik_x qL} e^{-i2\pi eBqLy} \psi(\vec{r}) \tag{4.2}$$

$$\psi(\vec{r} + L\hat{y}) \qquad = e^{ik_y L} \psi(\vec{r}), \tag{4.3}$$

where L is the size of unit cell.

Quantum Hall conductance, which is a topological invariant quantity, is obtained by means of Widom-Středa formula [107, 108] as well as the TKNN formula [109]:

$$\sigma = -e\frac{\partial N}{\partial B}, \tag{4.4}$$

where N is the 2-dim electron density and we let the speed of light c is 1. We obtain the Hall conductance σ for our lattice with a single defect and showed the results in Fig.24 and Fig.25. The local electric current J_{nm} which runs from m to n is given by

$$J_{nm} = -i2\pi\frac{et}{h}(e^{i\theta_{mn}}\psi_n^*\psi_m - h.c.), \tag{4.5}$$

where e is positive. As we show in Figs.34-39, the electric current runs around the defect if the lattice has a defect. Energy associated with localized electric current is given by the well-known formula

$$E = -\vec{m} \cdot \vec{B}, \tag{4.6}$$

where $\vec{m}$ is the magnetic moment $\vec{m} = J \cdot \vec{S}$ and $\vec{S}$ is the oriented area surrounded by the electric current J. In what follows from our numerical method, the energy spectra which originate from the magnetic moment appear in energy band gaps of fractal energy spectra of the Hofstadter problem. We explain the result in the succeeding paragraphs.

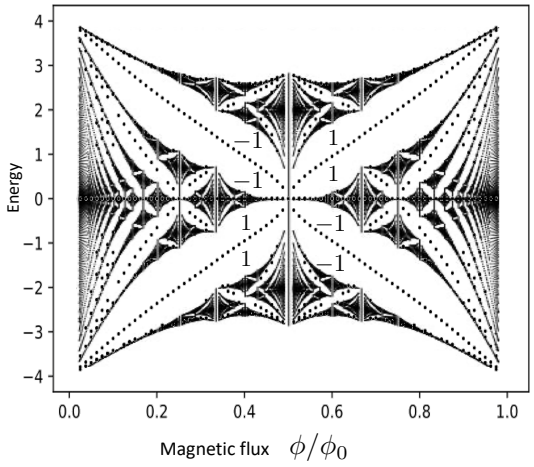

Figure 24. The energy spectra of in-gap states in a square lattice. The numbers in the energy gaps are the Hall conductance.

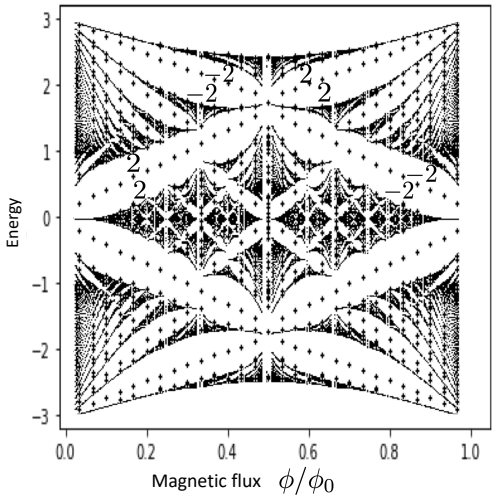

Figure 25. The energy spectra of in-gap states in a honeycomb lattice.

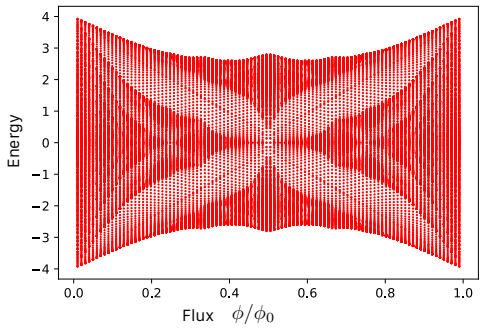

Figure 26. Hofstadter butterfly on a square lattice with boundaries and a defect.

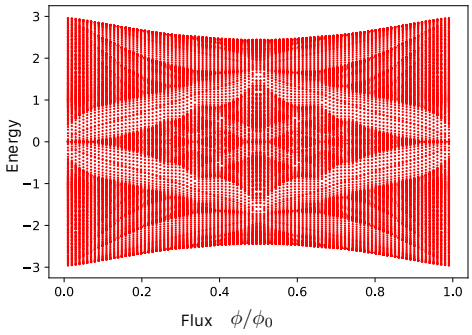

Figure 27. Hofstadter butterfly in a honeycomb lattice with a defect.

4.3 Results and Analysis

Our key finding is that the linear energy spectra associated with the localized states appear as well as the original Hofstadter butterflies (see Fig.24 and Fig.25).

Now we show that these linear spectra have the following properties. (a) They exist in all energy gaps, and the linearity is retained in even high magnetic region. (b) They do not carry Hall conductance. (c) The state on the linear spectrum is localized around the defect. (d) The linearity originates from the magnetic moment.

First of all, to check the properties (a) and (b), we confirm the linear energy spectra by removing the edge-localized states (see Fig.24 and Fig.25). The number in each gap in Fig.24 and Fig.25 represents the Hall conductance which is derived from the formula (4.4). From these numerical results, we can confirm the property (a). This is why we call the linear energy spectra *in-gap states*. Moreover, we can also show the property (b), and this is consistent with the well-known fact that the localized states do not carry Hall conductance.

Next, we show the property (c). Figs.28-30 show the density of states, which correspond to the positive-energy in-gap states in the largest wing of the fractal butterfly under uniform magnetic fluxes (1-a) $\phi = 1/6$, (1-b) $\phi = 1/5$ and (1-c) $\phi = 3/4$, respectively in the square lattice. Moreover Figs.31-33 show that in the honeycomb lattice case. The radius of the each circle in Figs.28-33 represents the probability amplitude at each site. From Figs.28-33, we can conclude that the property (c) is true in a wide magnetic region in not only a square lattice but also a honeycomb lattice.

Now let us explain why the energy of in-gap state is linear, the property (d). Namely we show the gradient of energy with respect to magnetic flux corresponds to that evaluated by formula (4.5) and (4.6). The electric current around the defect in the same situation is shown in Fig.34 $\phi = 1/6$, Fig.35 $\phi = 1/5$ and Fig.36 $\phi = 3/4$ in the square lattice. Figs. 37-39 also show that in the honeycomb lattice case. The relations between magnetic moment and the gradient of energy with respect to magnetic flux are exhibited in Table 1. The magnetic moment is calculated with the formulae (4.5) and (4.6) for both of the square lattice and the honeycomb lattice. As a result, the magnetic moment matches the gradient with a high degree of accuracy.

Note that the properties (a)-(d) are satisfied in the irrational magnetic fluxes.

From these results, we conclude that the linear energy spectra in all energy gaps are created by the current running around the single vacancy defect in all monolayer lattices.

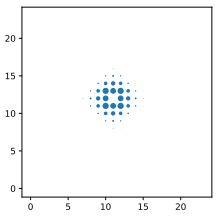

Figure 28. The density of defect-localized states at $\phi/\phi_0 = 1/6$ in a square lattice.

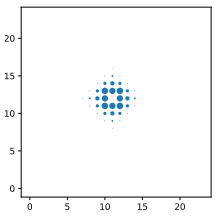

Figure 29. The density of defect-localized states at $\phi/\phi_0 = 1/5$ in a square lattice.

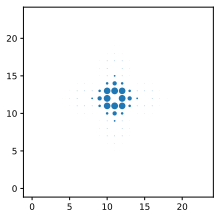

Figure 30. The density of defect-localized states at $\phi/\phi_0 = 3/4$ in a square lattice.

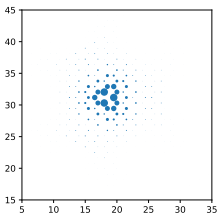

Figure 31. The density of defect-localized states at $\phi/\phi_0 = 1/6$ in a honeycomb lattice.

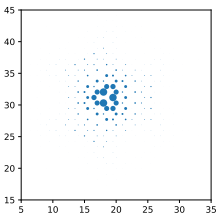

Figure 32. The density of defect-localized states at $\phi/\phi_0 = 1/5$ in a honeycomb lattice.

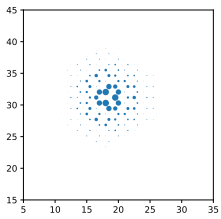

Figure 33. The density of defect-localized states at $\phi/\phi_0 = 5/12$ in a honeycomb lattice.

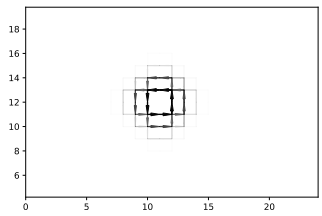

Figure 34. The localized current at $\phi/\phi_0 = 1/6$ in a square lattice.

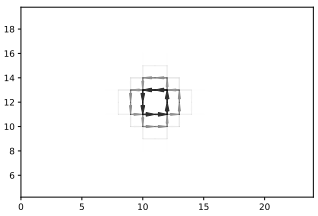

Figure 35. The localized current at $\phi/\phi_0 = 1/5$ in a square lattice.

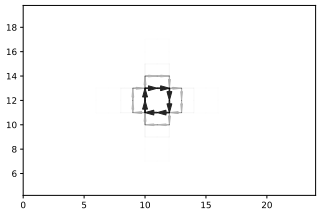

Figure 36. The localized current at $\phi/\phi_0 = 3/4$ in a square lattice. The direction of the current is opposite unlike other cases.

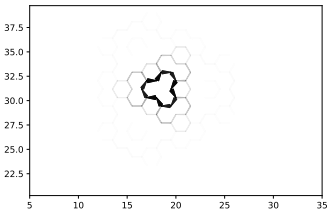

Figure 37. The localized current at $\phi/\phi_0 = 1/6$ in a honeycomb lattice.

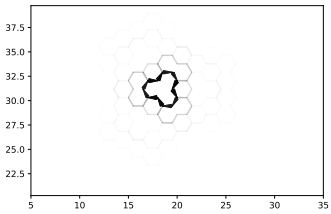

Figure 38. The localized current at $\phi/\phi_0 = 1/5$ in a honeycomb lattice.

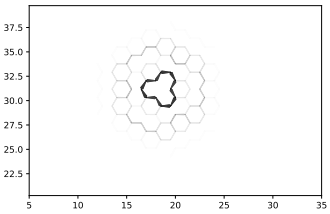

Figure 39. The localized current at $\phi/\phi_0 = 5/12$ in a honeycomb lattice.

Table 1. The comparison between the gradient and magnetic moment

lattice	ϕ/ϕ_0	magnetic moment	gradient	accuracy(%)
square	1/6	-7.4918	-7.7294	96.9
	1/5	-7.3595	-7.3936	99.5
	3/4	7.02782	7.0290	99.8
honeycomb	1/6	7.1862	7.9401	97.9
	1/5	8.2702	8.3319	99.3
	5/12	7.4795	7.9401	94.2

Finally, we give comments on the localization length of the in-gap states. As shown in the Figs.28-33, the wave functions extend as the magnetic flux decreases. This comes from the fact the localization length ξ is proportional to $1/\sqrt{B_{\text{eff}}}$, where B_{eff} is the effective magnetic field. Figs.40 and 41 show the wave function of in-gap states associated with the dominant gaps in the first generation of butterflies in a square lattice. The length ξ are 4.02 at $\phi/\phi_0 = 1/20$ and 6.47 at $\phi/\phi_0 = 1/80$.

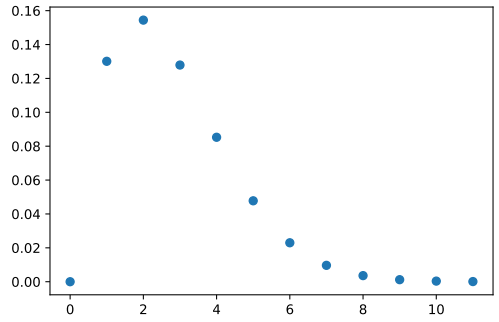

Figure 40. The in-gap state in the main gap at $\phi/\phi_0 = 1/20$. The localization length ξ is 4.02.

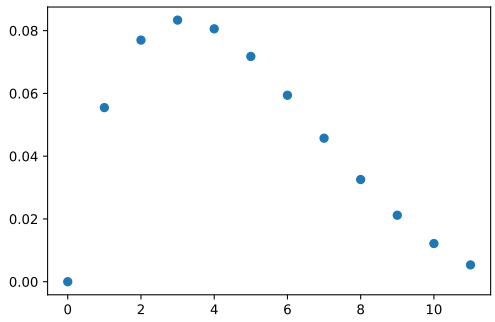

Figure 41. The in-gap state in the main gap at $\phi/\phi_0 = 1/80$. The localization length ξ is 6.47.

4.4 Discussion and Conclusion

In this section, we first report that energy spectra associated with localized state, *in-gap states*, around a point defect are explicitly detectable as a solution of the Hofstadter problem. And the energy spectra of these states which originated from the localized electric currents appear in all energy band gaps. Moreover, these states do not contribute to Hall conductance. We predict the similar story can be true to another lattice model. In addition, the case where the tight-binding Hamiltonian has the second nearest neighbor interactions is an open problem. Furthermore investigating the problem in bilayer graphene systems with defects will be also interesting.

It is known that several bilayer graphene systems, including twisted one, also exhibit the fractal energy spectra [110, 111].

Another interesting research direction can be found in terms of quantum geometry or high energy physics. There are several studies which linked the high energy physics and Hofstadter butterfly [99, 100], yet formal formulation on lattice systems with defects has not been known. Furthermore, working on the relation between in-gap states and the plateau is interesting.

From a view point of experimental study, it will be rather easier to verify our prediction in this article since the energy spectra of in-gap states exist even at the low magnetic field limit $B \to 0$, as shown in Figs.24 and 25. Though there are many reports which pursued fractal energy spectra of the Hofstadter problem, its direct observation would require an inaccessibly high magnetic field. Therefore it is a formidable task to find a butterfly structure by a direct method and indeed many experimental works provided evidences in various indirect approaches [112, 113]. Our novel findings shed a new light on this research field directly or indirectly, since it dose not require such an experimental setup with high magnetic field to verify our results experimentally.

A Quantum Hall Effect and Langlands Program

A.1 Preliminaries

This ancilla part is based on [6–8]. We aim at giving a comprehensive viewpoint for the mathematical foundation of the quantum Hall effect, whose properties are crucial for condensed matter physics, high energy physics and quantum computation. Duality is ubiquitous in modern physics. It provides a succinct description of key connections among apparently different phenomena and unveil a series of titillating stories. They are often referred to electric/magnetic duality, strong/weak duality or high/low duality. These dualities are closely linked in a "duality web", yet formal modeling has been illusive, thereby it will be natural to seek for an underling theoretical framework. Langlands program [114] is a mathematical coherent conjecture that offers a compelling and captivating story to connect a wide variety of mathematical concepts in terms of duality [115–119]. It is also related to high energy physics [120–122]. We aim at applying it to topological physics, which leads to enhance our knowledge on the "duality web". Topological invariance is a central concept in modern physics. Especially the quantum Hall effect [123–126] has led to a number of both theoretical and experimental studies of the problem. In this article we exploits the Langlands program to offer an unified description of 2d integer and fractional quantum Hall effect (IQHE and FQHE). Consequently it elicits a part of uncanny insights into various cardinal principles of physics and also sheds light on salutary applications of topological physics (e.g. topological quantum computation).

Traditionally the IQHE $\sigma_{xy} = \frac{e^2}{h} n$ $(n \in \mathbb{Z})$ has been explained by the Kubo formula [107–109, 127] and the Anderson localization model [128, 129]. The FQHE has been explained by the Laughlin theory [130] and composite particle models [131–133].

Ramanujan's finding on automorphic forms is crucial to modern number theory. Around 1916, he calculated the expansion coefficients a_n of the following infinite series.

$$q \prod_{n=1}^{\infty} (1-q^n)^2 (1-q^{11n})^2 = \sum_{n=1} a_n q^n. \tag{A.1}$$

About 40 years later, Eichker proved that there is a profound correspondence between the automorphic form above and the elliptic curve defined on $\mathbb{Q}$

$$y^2 + y = x^3 - x. \tag{A.2}$$

Astonishingly, for $b_p = p + 1 - \#$ (points of (A.2) mod p), the equation

$$a_p = b_p \tag{A.3}$$

is true for any prime p. It is the Langlands program [114] that connects these dualities from general viewpoints of mathematics. In the Langlands program, the correspondence between automorphic forms and elliptic curves are all about the correspondence between the eigenvalues of Hecke operators and Frobenius operators, namely a_p and b_p are eigenvalues of Hecke and Frobenius operators respectively. The Langlands program can be interpreted geometrically [134–136], and the geometric Langlands correspondence foresees many nontrivial aspects of gauge theories. From a perspective of geometry, in a simple case, this is achieved by considering a gauge theory on a Riemann surface, and a Hecke operator modifies the given principle bundle at a singular point so that the 1st Chern-number jumps at the singularity, as a vortex or a monopole operator do, and a Frobenius operator is analogous to a holomony operator, like a Wilson loop [120, 137, 138].

The aim of this article is to endow it with physical meaning. In a seminal piece of research made by A. Kapustin and E. Witten [120], they predict the electric magnetic duality and mirror symmetry are intimately related to the geometric Langlands correspondence. While there are many relevant works [138–141], what would follow in view of non supersymmetric physics had not been known. In this work, we address the quantum Hall effect and enjoy the panoptic picture of the quantum Hall effect drawn as a natural consequence of the Langlands program. One can seek a cue from the Langlands/GNO dual group to understand the connection with the quantum Hall effect and the geometric Langlands duality. In electric-magnetic duality, Dirac monopoles and Dirac's quantization condition explain the dual group ${}^L G$ of a general Lie group G from a perspective of physics [142]. The quantization condition of the Hall conductance is understand in a similar manner.

A.2 General Setup

Throughout this article we consider the IQHE on Laughlin's type of geometry [124], namely a square lattice in the uniform magnetic flux ϕ perpendicular to the system which has a period $L_y \in \mathbb{Z}$ in the y direction. We assume ϕ is rational P/Q, where P and Q are mutually prime integers, then the Hall conductance σ_{xy} is quantized and there are Q energy bands. To consider energy bands, we prefer to work on a generic tight-binding Hamiltonian

$$H = \sum_{m,n} \left(c^\dagger_{m+1,n} c_{m,n} e^{i\theta^x_{m,n}} + c^\dagger_{m,n+1} c_{m,n} e^{i\theta^y_{m,n}} + h.c. \right), \tag{A.4}$$

where $c_{m,n}$ ($c^\dagger_{m,n}$) is the annihilation (creation) operator at (m,n) site. If we choose the Landau gauge $(\theta^x_{m,n}, \theta^y_{m,n}) = (0, 2\pi m\phi)$, the Schrödinger equation (Harper equation) becomes

$$\Psi_{m+1,n} + \Psi_{m-1,n} + e^{i2\pi m\phi}\Psi_{m,n+1} + e^{-i2\pi m\phi}\Psi_{m,n-1} = E\Psi_{m,n}. \tag{A.5}$$

We write $\Psi_{m,n} = e^{ik_y n}\psi_m(k_y)$ $(0 \le k_y \le 2\pi)$ since the system is periodic in the y direction. Under the assumption that L_y is sufficiently large, the wave number $k_y = 2\pi l/L_y$ $(l \in \mathbb{Z})$ is usually regarded as a continuous parameter. Moreover the system has a period Q in the x direction because of the rational flux $\phi = P/Q$, therefore Bloch's theorem allows us to write the wave function as $\psi_m(k_y) = e^{i2\pi m k_x} u_m(k_x, k_y)$ $(0 \le k_x \le 2\pi/Q)$, where u_m is periodic $u_{m+Q} = u_m$. In view of the wavenumber space or the Brillouin zone, the system has two periods $2\pi/Q$ and 2π in the k_x and k_y directions respectively, hence we identify the BZ with a torus T^2_{BZ} by gluing its boundary. There are Q-energy bands[3] and each of them is a $U(1)$-bundle on T^2_{BZ}. A $U(1)$-connection for the j-th bundle is given by the Berry connection $A^j = -i\sum_{m=1}^{Q}({u^j_m}^\dagger \partial_{k_x} u^j_m dk_x + {u^j_m}^\dagger \partial_{k_y} u^j_m dk_y)$, where u^j_m is the Bloch function for the j-th energy band and normalized $|u^j|^2 = \sum_{m=1}^{Q} {u^j_m}^\dagger u^j_m = 1$.

A.3 Hall Conductance

One of the reasons for the quantized Hall conductance σ_{xy} can described by the Chern numbers of the fiber bundles. Let σ^j_{xy} be the Hall conductance of the j-th energy band. The well-known formula

$$\sigma^j_{xy} = \frac{e^2}{h} \int_{T^2_{BZ}} \frac{d^2k}{2\pi} \left(\frac{\partial A^j_y}{\partial k_x} - \frac{\partial A^j_x}{\partial k_y} \right) \tag{A.6}$$

tells that the Hall conductance is given by the Chern number of the j-th $U(1)$-bundle $\mathcal{L}^j$. If the Berry connection a^j is holomorphic on entire T^2_{BZ}, then the Stokes theorem

[3] One should be careful not to confuse the band and site indexes. Their total numbers are the same.

implies $\sigma^j_{xy} = 0$. So for σ^j_{xy} being nontrivial, a^j must have a singular point on T^2_{BZ}. At such a point, the Bloch function $u^j(k)$ vanishes and the Chern number corresponds to vorticity of the function [143, 144]. If there exist many singular points, σ^j_{xy} is given by the total vorticity. This viewpoint is important for the Langlands correspondence, especially for the Hecke modifications of bundles.

Let us generalize the statement above. Suppose the Fermi energy E_F lies in the M-th gap, and we write M states of bands below E_F by $u = (u^1, \cdots, u^M)$. This multiplet forms a $U(M)$-bundle $\mathcal{E}$ over T^2_{BZ}, whose Berry connection is given by $A = -i\mathrm{Tr}(u^\dagger du)$. Then the Hall conductance σ_{xy} is given by the Chern number $c(\mathcal{E}) = \frac{1}{2\pi}\int_{T^2_{BZ}} \mathrm{Tr}(dA)$. The famous TKNN formula [109] tells that the total Hall conductance σ_{xy} is given by the sum of Chern numbers $c(\mathcal{L}_j) = \frac{1}{2\pi}\int_{T^2_{BZ}} dA^j$ associated with all energy bands below E_F:

$$\sigma_{xy} = \frac{e^2}{h}\sum_{j=1}^{M} c(\mathcal{L}_j). \tag{A.7}$$

A.4 Geometric Langlands Correspondence

The geometric Langlands correspondence is a branch of the Langlands program. There are a lot of surveys and the conjecture is partly proven [134–136]. The $GL_1 = \mathbb{C}^\times$ case[4] is the simplest and established. We will focus on this case for a while. A readable introduction is [137] whose part II will help us greatly. Let X be a compact Riemann surface. We consider a holonomy representation $\rho : \pi_1(X) \to GL_1$. A famous mathematical theorem[5] guaranties a bijection between the set $\mathrm{Loc}_1(X)$ of isomorphism classes of flat GL_1-bundles on X and the set of conjugacy classes of the holomony representations. Hence, one can attach a flat connection for a given representation ρ. (This is the same trick we define a Wilson loop.) An element of $\mathrm{Loc}_1(X)$ is called a local system. Let T^2_{BZ} be the 2d toric Brillouin Zone. We denote by $\mathbb{C}^m_{T^2_{BZ}} = T^2_{BZ} \times \mathbb{C}^m$ the constant sheaf whose fibre is $\mathbb{C}^m$. A sheaf $\mathcal{L}$ of $\mathbb{C}_{T^2_{BZ}}$-module is called a rank m local system if every point $p \in T^2_{BZ}$ has an open neighbor U on which $\mathcal{L}|_U$ is isomorphic to $\mathbb{C}^m_{T^2_{BZ}}$. For any $p \in T^2_{BZ}$, the category $\mathrm{Loc}(T^2_{BZ})$ of local systems and the category $\mathrm{Rep}(\pi_1(T^2_{BZ}, p))$ of finite dimensional representations of $\pi_1(T^2_{BZ}, p)$ are equivalent. Such a functor ρ is given as follows. Let $[\gamma] \in \pi_1(T^2_{BZ}, p)$ be a loop. Parallel translation of sections along γ defines a monodromy representation $\rho(\mathcal{L}, p) : \pi_1(T^2_{BZ}, p) \to GL_m(\mathbb{C})$. A functor defined by the monodromy representation gives an equivalence of categories

$$\rho : \mathrm{Loc}(T^2_{BZ}) \to \mathrm{Rep}(\pi_1(T^2_{BZ}, p)) \tag{A.8}$$

[4]The compactification of $GL_1 = \mathbb{C}^\times = \mathbb{C} \setminus \{0\}$ is $U(1)$.

[5]This is true for any smooth manifold M and any representation $\rho : \pi_1(M) \to G$, where G is an arbitrary Lie group.

Moreover the category $\mathrm{Conn}(T^2_{BZ})$ of integrable connections on T^2_{BZ} is equivalent to $\mathrm{Loc}(T^2_{BZ})$. Let $\mathcal{E} = (\mathcal{E}, \nabla)$ be a rank m integrable connection on T^2_{BZ}. For a given $\mathcal{E}$, horizontal sections form the subsheaf $\mathcal{E}^\nabla = \{A \in \mathcal{E} : \nabla A = 0\}$. Then the functor

$$\begin{aligned} E : \mathrm{Conn}(T^2_{BZ}) &\to \mathrm{Loc}(T^2_{BZ}) \\ \mathcal{E} &\mapsto \mathcal{E}^\nabla \end{aligned} \tag{A.9}$$

yields an equivalence of categories. Let $G = GL_m(\mathbb{C})$ and $\mathrm{Bun}_m(T^2_{BZ})$ be the moduli stack of rank m bundles on T^2_{BZ}. The n-th Hecke correspondence $\mathcal{H}_n$ is the moduli space of $(\mathcal{M}, \mathcal{M}', p)$, where sections of $\mathcal{M}' \in \mathrm{Bun}_m$ are that of $\mathcal{M} \in \mathrm{Bun}_m$ having a pole of order n at p. Let $h^\to(\mathcal{M}, \mathcal{M}', p) = \mathcal{M}'$, $h^\leftarrow(\mathcal{M}, \mathcal{M}', p) = \mathcal{M}$ and $\mathrm{supp}(\mathcal{M}, \mathcal{M}', p) = p$. The fiber $(h^\to)^{-1}(\mathcal{M}')$ of $\mathcal{H}_{n,p} = \mathrm{supp}^{-1}(p)$ is isomorphic to the Grassmannian $Gr(n, m)$. The geometric Langlands conjecture says that to $\mathcal{E}$ we can associate a $\mathcal{D}$-module $\mathcal{F}_\mathcal{E}$ on Bun_m, which is a Hecke eigensheaf of a given $\mathcal{E}$. For simplicity we wonsider $G = GL_1(\mathbb{C})$ or its compactification $G_c = U(1)$. Then Bun_1 is the Picard variety

$$\begin{aligned} \mathrm{Pic} &= \bigsqcup_{d=0} \mathrm{Pic}_d \\ \mathrm{Pic}_d &= \left\{ \mathcal{L} \in \mathrm{Pic} : d = \int_{T^2_{BZ}} c_1(\mathcal{L}) \right\}. \end{aligned} \tag{A.10}$$

A rank 1 local system Loc_1 is a pair $\mathcal{E} = (\mathcal{L}, \nabla)$ of a holomorphic line bundle and a flat connection. There is a natural map sending $\mathcal{E}$ to $\mathcal{L} \in \mathrm{Pic}_0$. Laumon [117] and Rothstein [145] established the geometric Langlands correspondence by applying the Fourier-Mukai transformation [146]: Loc_1 is transfered to Pic_0. In this case $h^{\to *}(\mathcal{F})$ is the Hecke modification of a $\mathcal{D}$-module $\mathcal{F}$. The operation $h^\to : T^2_{BZ} \times \mathrm{Pic} \to \mathrm{Pic}$ maps a holomorphic line bundle $\mathcal{L}$ as $(p, \mathcal{L}) \to \mathcal{L}' = \mathcal{L}(p)$, by which $c_1(\mathcal{L}') = c_1(\mathcal{L}) + 1$. One can consider a more general modification of $\mathcal{L}$ to $\mathcal{L}'$ at N-tuple of points $(x_i), i = 1, \cdots, N$ so that $c(\mathcal{L}') = c(\mathcal{L}) + N$.

What the geometric Langlands correspondence expects is that for a given flat GL_1-bundle $\mathcal{E}$ on X, there exist a unique $\mathcal{D}$-module $\mathcal{F}_\mathcal{E}$ on $\mathrm{Pic}(X)$ associated with the modification h_x. This correspondence is proven by P. Deligne. The general conjecture of the Langlands correspondence for a Lie group G can be stated as follows. We denote by ${}^LG$ the Langlands dual group of G. If $G = GL_1$, then its dual is isomorphic to GL_1. The set $\mathrm{Loc}_{{}^LG}(X)$ of local systems is again identified with the set of conjugacy classes of representations $\rho : \pi_1(X) \to {}^LG$. And $\mathrm{Pic}(X)$ is generalized to the moduli stack $\mathrm{Bun}_G(X)$ of principle G-bundles on X. So the geometric Langlands correspondence implies that for a given flat ${}^LG$-bundle $\mathcal{E}$ on X, there is a unique $\mathcal{D}$-module $\mathcal{F}_\mathcal{E}$, called a Hecke eigensheaf, defined on $\mathrm{Bun}_G(X)$ associated with the Hecke modification.

The tight-binding Hamiltonian of the IQHE in fractional magnetic flux $\phi = a/b$ can be written by the quantum group $U_q(sl_2)$, where $q = e^{2\pi i a/b}$ with coprime

integers a, b [147]. The strong/weak duality $(\phi, U_q(sl_2)) \leftrightarrow (1/\phi, U_{L_q}(sl_2))$ can explain the fractal energy spectra, called the Hofstadter problem [96]. Here $U_{L_q}(sl_2)$ is the Langlands dual quantum group. There is a relation $\nu_L = \phi\nu_B$ between the tight-binding band filling factor $\nu_B = t\phi + s$ with $s, t \in \mathbb{Z}$ and the Landau level filling factor $\nu_L = t(1/\phi) + s$. Hence The strong/weak duality is $(s, t) \leftrightarrow (t, s)$ [148]. The Widom-Středa formula $\sigma_{xy} = -\frac{e^2}{h}\frac{\partial \nu_B}{\partial \phi}$ gives $(\phi, \sigma_{xy} = -\frac{e^2}{h}t)$ and $(1/\phi, \sigma_{xy} = -\frac{e^2}{h}s)$. More precisely, the strong/weak duality is a duality between momentum space in the flux ϕ to the real space in $1/\phi$. In this sense, the duality is also based on a picture of the Fourier transformation.

A.5 Hecke Eigensheaf

In this section we give a physical explanation about Hecke eigensheaves. The sections 4.3∼4.5 in [137] will be helpful for more information. For this purpose, we physically interpret a sheaf. We are interested in a sheaf $\mathcal{S} = (\mathcal{S}, \pi, B)$ whose fiber $\mathcal{S}_p = \pi^{-1}(p)$, $p \in B$ is a vector space. The dimension of fibers may differ at points. A standard example is the skyscraper sheaf $\mathcal{O}(x)$, which is a sheaf supported at a single point $x \in B$. How will they come into play in our story? First of all, sections of our sheaf are wave functions and the base space is the Riemann (complex energy) surface [144, 149]. Now we are ready to explain Hecke eigensheavs. Note that only one-dimensional momentum k_y is a good quantum number. So one can define the only one-dimensional Berry connection A_{k_y}. Hence we may regard it as a flat connection[6] on T^2_{BZ}, by setting $A_{k_x} = 0$. A Hecke eigensheaf on $\mathrm{Pic}^0(X) = \left\{\mathcal{L} \in \mathrm{Pic}(X) : 0 = \int_X \mathcal{L}\right\}$ is a $\mathcal{D}$-module of such flat connections. Of course this is not the whole story. Actual energy bands are "wavy" as shown with pictures in [144, 149], and the wavy parts possess nontrivial Chern numbers. This is the mechanism of Hecke modifications $\mathcal{L} \to \mathcal{L}(x) = \mathcal{L} \otimes \mathcal{O}(x)$, $x \in T^2_{BZ}$.

Moreover the existence of plateaus can be described by Hecke eigensheaves as shown in the figure below. If there exist impurity potentials in the system, wave functions localize around the potentials (in the real space). This phenomenon is called the Anderson localization [128]. As a result, each of the Landau levels becomes wide. However, the localized wave functions do not carry non trivial Chern numbers and only the extended wave function living in the original Landau level contributes to the Hall conductance [124]. This is why the Hall conductance has plateaus. In the language of the geometric Langlands correspondence, this can be explained by saying that the Berry connections associated with those localized wave functions are flat, and hence they form a $\mathcal{D}$-module.

[6] This flat connection, which is a Berry connection of $U(1)$-bundle, is a different one we used for a Wilson loop $W : \pi_1(T^2_{BZ}) \to^L U(1)$.

A.6 Duality, Hecke operator, and K-theoretic view

Algebraically, a vortex operator for G is defined by a homomorphism $\varrho : U(1) \to G$, which is classified by highest weights of the dual group ${}^LG$ up to conjugation. We write it in the most general way as $\varrho : e^{i\alpha} \to \mathrm{diag}(e^{im_1\alpha}, \cdots, e^{im_M\alpha})$, where ${}^Lw = (m_1, \cdots, m_M)$ is an M-plet of integers with $m_1 \geq \cdots \geq m_M$, which is a highest weight of ${}^LG = U(M)$. As we have already seen, we obtain decomposition of the $U(M)$-bundle $\mathcal{E}$ into the sum of line bundles $\oplus_{i=1}^M \mathcal{L}_i$. Let k_i be a singular point of $\mathcal{L}_i$. The vortex operator $V({}^Lw)$ acts on $\mathcal{L}_j$ as $V({}^Lw) : \mathcal{L}_i \to \mathcal{L}_j \otimes \mathcal{O}(k_j)^{m_j}$, where m_j is vorticity at k_j. In other words, it changes the Chern number $c(\mathcal{L}_j)$ by m_j. The total Hall conductance σ_{xy} is the total Chern numbers of this system $\sigma_{xy} = \sum_{j=1}^M \sigma_{xy}^j$, which is the total vorticity of the system, in other words.

By the way, the classification of vortex operators or Hecke operators is exactly the same as that of effective Hamiltonians. So far we have neglected contribution from conduction bands, and from now we suppose there are N conduction bands and M valence bands. So this system has $U(M+N)$ gauge group in general. Then effective Hamiltonians of the quantum Hall system is classified by the Grassmannian $Gr_{M,M+N} = U(M+N)/U(M) \times U(N)$ from the K-theoretic perspectives [150]. In terms of the geometric Langlands correspondence, the Hecke operators are classified as follows. Let $\mathcal{M}, \mathcal{M}' \in \mathrm{Bun}_G$ be principle $G = U(M+N)$ bundles on a Riemann surface X such that $\mathcal{M} \subset \mathcal{M}'$ and $\mathcal{M}'/\mathcal{M} \simeq \mathcal{O}(x)^M$, where $x \in X$. As discussed, the Hecke operators modify the G-bundle $\mathcal{M}$ to $\mathcal{M}'$ at this singular point x, and it is known the space of such modifications is parametrized by points in $Gr_{M,M+N}$. (One may discover extra value in mathematical explanations [137] or in physical explanations [120, 138]).

A.7 Hofstadter's Butterfly and Langlands Duality of Quantum Groups

Now we see that the Langlnads/S-duality also enhance our understanding on a different aspect of the quantum Hall effect. As we discussed, ν is equivalent to the ratio of the number of electrons n_e and flux quanta ϕ per placket. If $\nu = 1/k$ there are k flux quanta per electron. We identify it with $\phi = k$ and $n_e = 1$. The integer quantum Hall effect $\nu = k$ case can be regarded as $(\phi, n_e) = (1/k, 1)$. The duality $(\nu, \phi) \to (1/\nu, 1/\phi)$ is crucial for the duality in Hofstadter's butterfly. On the q-parameter level, it states the duality between theories with q and ${}^Lq$. As a well-known subject, the Hamiltonian (A.4) of the integer quantum Hall effect can be written by use of the quantum group $\mathcal{U}_q(sl_2)$ [147] and the Langlands duality of the quantum group endows with novel perspective on its fractal energy spectrum structure, known as Hofstadter's butterfly [96].

It is known that this fractal spectrum is generated by the maps

$$\begin{aligned} &(\phi, E) \to (\phi + 1, E) \\ &(\phi, E) \to (1/\phi, f(E)), \end{aligned} \tag{A.11}$$

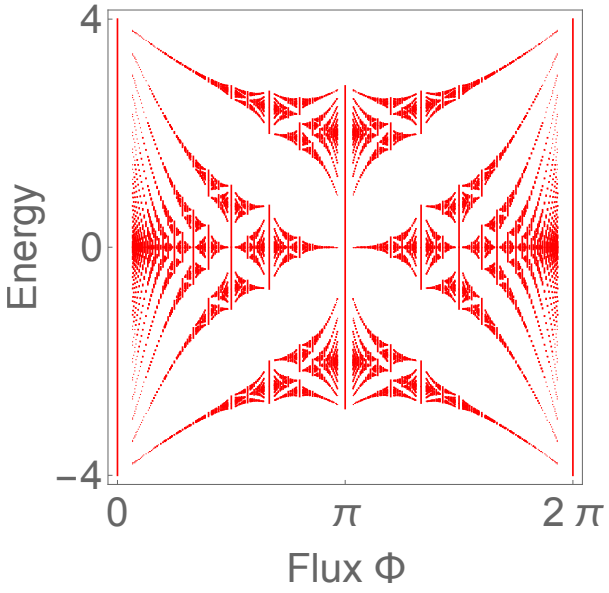

Figure 42. Fractal energy spectrum, called Hofstadter's butterfly

where f is a some function. In [99], this duality is described by a quantum geometric viewpoint and they relate the butterfly with the energy spectrum of relativistic Toda lattice. Tough the duality works for general ϕ, we consider rational $\phi = P/Q$ to consider the butterfly (P and Q are co-prime). Now, our q-parameter is $q = \exp(i2\pi\phi)$. The duality is understood by the formula

$$P_\phi(E) = P_{1/\phi}(\widetilde{E}), \quad \widetilde{E} = f(E). \tag{A.12}$$

A generic tight binding Hamiltonian we are interested in is

$$H = \sum_{m,n} \left(c^\dagger_{m+1,n} c_{m,n} e^{iA^x_{m,n}} + R^2 c^\dagger_{m,n+1} c_{m,n} e^{iA^y_{m,n}} + h.c. \right), \tag{A.13}$$

where $c_{m,n}$ ($c^\dagger_{m,n}$) is the annihilation (creation) operator at (m,n) site. When we choose the Landau gauge $A^x_{m,n} = 0, A^y_{m,n} = 2\pi m\phi$, it can be written as

$$H = T_x + T_x^\dagger + R^2(T_y + T_y^\dagger), \tag{A.14}$$

where we choose a Q-dimensional representation ρ_Q of $\mathcal{U}_q(sl_2) = \{K^{\pm 1}, X^\pm\}$ with $q = e^{i2\pi P/Q}$ so that

$$\begin{aligned} T_x &= e^{ik_x}\rho_Q(X^+), \quad T_y = e^{ik_y}\rho_Q(K) \\ \rho_Q(X^+) &= \begin{pmatrix} 0 & 1 & 0 & \cdots & 0 \\ \vdots & \ddots & \ddots & \ddots & \\ \vdots & & \ddots & \ddots & 0 \\ 0 & & & \ddots & 1 \\ 1 & 0 & \cdots & \cdots & 0 \end{pmatrix}, \quad \rho_Q(K) = \mathrm{diag}(q, q^2, \cdots, q^Q) \end{aligned} \tag{A.15}$$

These operators T_x and T_y are non commutative because of the Aharonov-Bohm phase for an electron moving around the flux:

$$T_x T_y = q T_y T_x. \tag{A.16}$$

The energy spectrum consists of eigenvalues of this Hamiltonian, which is described by the Chambers relation [151]

$$\det(H(k,R) - E) = P_\phi(E,R) + h(k,R), \quad k = (k_x, k_y) \tag{A.17}$$

where $P_\phi(E,R)$ is a polynomial and $h(k,R) = 2(-1)^{Q-1}(\cos(Qk_x) + R^{2Q}\cos(Qk_y))$. The energy spectrum displayed in Fig. 42 satisfies the equation $P_\phi(E,R) = 0$ under the mid band point condition $h(k_0,R) = 0$, where $k_0 = (\pi/2Q, \pi/2Q)$. Hence the anticipated formula $P_{P/Q}(E,R) = P_{Q/P}(\widetilde{E},\widetilde{R})$ implies the equivalence of the Q-dimensional representation (A.15) of $\mathcal{U}_q(sl_2)$ and the P-dimensional representation of $\mathcal{U}_{{}^Lq}(sl_2)$, where ${}^Lq = e^{i2\pi/\phi}$ and $\mathcal{U}_{{}^Lq}(sl_2)$ is the Langlands dual quantum group of $\mathcal{U}_q(sl_2)$ [152, 153]. We write this duality map by

$$S : (\mathcal{U}_q(sl_2), H) \to (\mathcal{U}_{{}^Lq}(sl_2), \widetilde{H}), \tag{A.18}$$

where the dual Hamiltonian $\widetilde{H}$ is given by the following $P \times P$ matrix of the form

$$\widetilde{H} = \widetilde{T}_x + \widetilde{T}_x^\dagger + \widetilde{R}^2(\widetilde{T}_y + \widetilde{T}_y^\dagger), \tag{A.19}$$

where $\widetilde{T}_x = e^{i\widetilde{k}_x}\rho_P(X)$ and $\widetilde{T}_y = e^{i\widetilde{k}_y}\rho_P(Y)$. Since we expect the correspondence of the characteristic polynomials $\det(H-E) = \det(\widetilde{H} - \widetilde{E})$, we find $\widetilde{R} = R^{1/\phi}$ by comparing order of R and $\widetilde{R}$ in $h(k,R)$ and $\widetilde{h}(\widetilde{k},\widetilde{R})$.

This is consistent with the Langlands duality of quantum groups explained by the interpolating quantum group $\mathcal{U}_{q,t}(sl_2)$ [153], which is parametrized by arbitrary nonzero complex values q,t and generated by $X^\pm, K^{\pm 1}, \widetilde{K}^{\pm 1}$ such that

$$\begin{aligned} K X^\pm &= q^{\pm 2} X^\pm K, \quad \widetilde{K} X^\pm = t^{\pm 2} X^\pm \widetilde{K}, \\ [X^+, X^-] &= \frac{K\widetilde{K} - (K\widetilde{K})^{-1}}{qt - (qt)^{-1}}. \end{aligned} \tag{A.20}$$

The interpolating property of $\mathcal{U}_{q,t}(sl_2)$ appears as

$$\mathcal{U}_{q,1}(sl_2)/\{\widetilde{K} = 1\} \simeq \mathcal{U}_q(sl_2), \quad \mathcal{U}_{1,t}(sl_2)/\{K = 1\} \simeq \mathcal{U}_t(sl_2). \tag{A.21}$$

By definition, $\mathcal{U}_{q,t}(sl_2)$ is equivalent to the usual quantum group $\mathcal{U}_\varrho(sl_2)$ with generators $X^\pm, K\widetilde{K}$ and the parameter $\varrho = qt$. Taking $q = e^{i2\pi P/Q}$ and $t = {}^Lq = e^{i2\pi Q/P}$, we find $\varrho = q\ {}^Lq = e^{i2\pi(P/Q+Q/P)}$ is symmetric under exchanging P and Q. The Langlands duality of quantum groups states that any irreducible representation of $\mathcal{U}_q(sl_2)$ would be t-deformed uniquely to a representation of $\mathcal{U}_{q,t}(sl_2)$ in such a way that its specialization at $q = 1$ gives a representation of $\mathcal{U}_t(sl_2)$. The easiest case is $P = 1$ and $Q = 2$. A two-dimensional representation of $\mathcal{U}_q(sl_2)$ is dual to a one-dimensional representation of $\mathcal{U}_{{}^Lq}(sl_2)$, which is equivalent to $P_{1/2}(E,R) = P_{2/1}(\widetilde{E},\widetilde{R})$. Generically, we observe that a Q-dimensional representation of $\mathcal{U}_q(sl_2)$ and a P-dimensional representation of $\mathcal{U}_{{}^Lq}(sl_2)$ are dual. This explain the formula $P_{P/Q}(E,R) = P_{Q/P}(\widetilde{E},\widetilde{R})$.

A.8 Fractional Quantum Hall Effect

Let $G = SL_2(\mathbb{C}), {}^LG = PSL_2(\mathbb{C})$ and consider their Lie algebras $\mathfrak{g} \simeq {}^L\mathfrak{g} \simeq sl_2$. The geometric Langlands correspondence is related to the WZW models as follows [137, 154]:

$$\begin{array}{ccc} {}^LG\text{-local system} & \leftrightarrow & \text{Hecke eigensheaf on } \mathrm{Bun}_G \\ \uparrow & & \uparrow \\ \mathrm{WZW}_{\hat{k}}(sl_2) & \leftrightarrow & \mathrm{WZW}_k(sl_2) \end{array}$$

The Liouville parameter b is related to WZW models [155, 156] by

$$\hat{k} + 2 = \frac{1}{k+2} = b^2. \tag{A.22}$$

Vafa relates b^2 to ν based on M-theory and the G Chern-Simons theory [157]. In our notation it is $b^2 = 1/\nu$. The Chern-Simons theory is symmetric under $b \to 1/b$, which is the modular duality of the Liouville theory [158] and S-duality of the $SL_2(\mathbb{R})$ Chern-Simons theory [159]. Back to the WZW models and consider vertex operators $V_\alpha(z) = e^{i\alpha\phi(z)}$ of a scaler field ϕ in CFT_2. The Langlands duality is often referred to the electric/magnetic (or charge/vortex) duality [120]. Indeed physicists constructed Langlands dual groups of Lie groups in the context of electric/magnetic duality [160]. We rephrase it as the correspondence between the "electric" vertex and "magnetic" vertex [137, 161]:

$$\begin{gathered} \text{Electric vertex} \ \leftrightarrow \text{Magnetic vertex} \\ V_{\alpha_+}(z)\overline{V}_{\alpha_+}(\overline{z}) \leftrightarrow V_{\alpha_-}(z)\overline{V}_{\alpha_-}(\overline{z}) \end{gathered}$$

If we defined $\alpha_+ = \sqrt{p/q}$, $\alpha_- = -\sqrt{q/p}$ with coprimes p, q, the FQHE filling factor ν is identified with $\alpha_+ = 1/\sqrt{\nu}$. We may write $\nu = N_e/N_\phi$ as the ratio of electrons N_e to that of magnetic fluxes N_ϕ. The standard composite particle pictures associate anyon excitation modes with vortexes, which are accompanied with the statistical gauge connections [131, 133, 162]. For example, composite boson fields $\Phi(z)$ $z = (z_1, \cdots, z_n)$ obeying the Shrödinger equation $H\Phi(z) = E\Phi(z)$ generates a $\mathcal{D}$-module. Picking up vorticity would be the Hecke transformation. In this way, the charge/vortex duality plays a fundamental role for the FQHE and gives us a clear analogue of the arguments by [120].

Langlands program also sheds light on knot theory. We investigate it in terms of the FQHE. First of all, anyons with charge ν carry the fractional Hall conductance $\sigma_{xy} \propto 1/\nu$ and exchanges of their positions in the 2d system generate the braid group [163]. The KZ-equation [164], which is the differential equation of the vacuum expectation value of primary fields in the WZW model, is the corresponding integrable system. Let Conf_n be the configuration space of different n points in $\mathbb{C}$:

$$\mathrm{Conf}_n = \{(z_1, \cdots, z_n) \in \mathbb{C}^n : z_i \neq z_j \ \forall i \neq j\}.$$

Let $\{e_i\}_{i=1}^3$ be the basis of $sl_2(\mathbb{C})$ and V be a representation space of $sl_2(\mathbb{C})$. Define $\tau_{ij} \in V^{\otimes n}$ by

$$\tau_{ij} = \sum_{k=1}^{3} 1 \otimes \cdots \otimes 1 \otimes e_k \otimes 1 \otimes \cdots \otimes 1 \otimes e_k \otimes 1 \otimes \cdots \otimes 1,$$

where e_k are inserted into the i-th and the j-th positions. The KZ-equation is a differential equation of $W : \mathrm{Conf}_n \to V^{\otimes n}$

$$dW = \frac{1}{\kappa}\omega W \tag{A.23}$$

where κ is a complex parameter and $\omega = \sum_{i<j} \tau_{ij} d\log(z_i - z_j)$ is a differential one-form on Conf_n. κ is related to q-parameter of $U_q(sl_2)$ as $q = e^{2\pi i/\kappa}$. We can make contact with the WZW model by choosing $\kappa = k + 2$. Taking paths $\gamma(t) = (z_1(t), \cdots, z_n(t)) \in \mathrm{Conf}_n$ for $t \in [0, 1]$ such that $\gamma(0) = \gamma(1)$, we obtain the braid group $B_n \simeq \pi_1(\mathrm{Conf}_n/\mathfrak{S}_n)$, where $\mathfrak{S}_n$ is the permutation group of n positions. Parallel translation of $W(\gamma(t))$ along $\gamma(t)$ gives a generic monodromy representation of B_n

$$\rho_{\mathrm{KZ}} : B_n \to \mathrm{End}(V^n). \tag{A.24}$$

2d irreducible representations $T_i = \rho_{\mathrm{KZ}}(\sigma_i)$ of the generators of $B_n = \langle \sigma_1, \cdots, \sigma_{n-1} \rangle$ naturally generate the Iwahori-Hecke algebra $H_n(q)$ with $q = e^{2\pi i/\kappa}$. Take an n-tuple $(V_1, \cdots, V_n)$ of $sl_2(\mathbb{C})$ irreducible representations. A set of matrices $H = (H_1, \cdots, H_n)$ of the extended KZ-equation, where $H_i = \sum_j \rho(\tau_{ij}) d\log(z_i - z_j)$ and $\rho : V^{\otimes n} \to V_1 \otimes \cdots \otimes V_n$, defines the Gaudin model and differential equations $H\Psi = E\Psi$ $(i = 1, \cdots, n)$ gives a $\mathcal{D}$-module [116].

Finally we see how our viewpoints are consistent with several renowned works. It is possible to construct Jones polynomials by the 2d irreducible representation $\rho_{V_2} : U_q(sl_2) \to \mathrm{End}(V_2)$, which is conjugate to ρ_{KZ} [165]. We write $G = SL_2(\mathbb{C})$ and $G_c = SU(2)$. Jones polynomials can be obtained by G_c Chern-Simons action $\frac{k}{4\pi} CS(A)$ [166]. An analogue of the KZ-equation is obtained by G Chern-Simons action $S(\mathcal{A}) = \frac{k+s}{8\pi} SC(\mathcal{A}) + \frac{k-s}{8\pi} SC(\overline{\mathcal{A}})$ [167], where $k \in \mathbb{Z}$ and s is either real or pure complex. The Euler-Lagrange equation of the action $S(\mathcal{A})$ asserts that $\mathcal{A}$ is flat and thereby the moduli space of flat $SL_2(\mathbb{C})$ connections is exactly the symplectic manifold with a family of hyper Kähler structures. Tuning parameters of its complex structures leads to the Langlands duality in the context of Kapustin-Witten [120, 168]. Categorifixation of the $(U_q(sl_2), V_2)$ knot invariants (Jones polynomials) is called the Khovanov homology [169] and its Langlands duality is investigated in [168, 170]. The FQHE $\sigma_{xy} = \frac{e^2}{h}\nu$ can be explained by the Chern-Simons theory with G or G_c. The q-parameter of $U_q(sl_2)$ accommodates ν as $q = e^{2\pi i/\nu}$ and the Langlands duality of $U_q(sl_2)$ implies flipping $\nu \to 1/\nu$.

A.9 Chern-Simons Theory, S-duality and Mirror Symmetry

Quantum Hall Effect has common description based on Chern-Simons theory, therefore it is meaningful to give some comments on the relation with the Langlands duality. We consider $2+1$-dimensional system which is parametrized by $x = (x^0, x^1, x^2)$, where x^0 stands for the time-direction and x^1, x^2 represent the space-directions. We may regard our system is product of $\mathbb{R}$ and a torus T^2 since our physics on the two dimensional space we have considered so far is periodic in the x and y directions respectively.

Let A be the background gauge filed of electromagnetism. The integer Hall conductance $\sigma_{xy} = \frac{k}{2\pi}$ is described by the Chern-Simons action

$$S_{CS} = \int d^3x \frac{k}{4\pi} \epsilon^{\mu\nu\rho} A_\mu \partial_\nu A_\rho, \tag{A.25}$$

whose $U(1)$-current is

$$J^\mu = \frac{\partial S}{\partial A_\mu} = k\epsilon^{\mu\nu\rho}\partial_\nu A_\rho. \tag{A.26}$$

Especially this is nothing but the Hall current if one takes $\mu = x^1$, and the level k corresponds to the bulk Hall conductance. The duality in quantum Hall effect that acts on the filling fraction ν can be understood as S-duality that acts on the inverse level $\hbar = 1/k$, which needs to be analytically continued away from integer values in order for the quality to be meaningful. When level k is integer, the Langlands/S-duality formally maps $q = \exp(2\pi i k)$ to ${}^L q = \exp(2\pi i/k)$. Continuing q away from roots of unity is naturally accommodated in the complex Chern-Simons theory, which now indeed enjoys Langlands/S-duality [171]. This duality describes the particle vortex duality [172, 173] and the geometric Langladns correspondence is easily understood. As we discussed previously, the geometric Langlands correspondence states the duality between a Wilson loop and a Hecke operator. The Hecke operator corresponds to the vortex operator, which picks up the Chern number associated with the bulk Hall conductivity. To find the corresponding Wilson loop, we consider an anyon, which is a quasi-particle with magnetic flux.

The Landau level filling factor is defined by

$$\nu = \frac{\text{The number of electrons in the system}}{\text{The number of flux quanta passing through the system}}. \tag{A.27}$$

So ν is equivalent to the ratio of the number of electrons n_e and flux quanta ϕ per placket. If $\nu = 1/k$ there are k flux quanta per electron. We may simply regard it as $\phi = k$ and $n_e = 1$. The integer quantum Hall effect $\nu = k$ case can be regarded as $(\phi, n_e) = (1, k)$ or $(\phi, n_e) = (1/k, 1)$. If one prefers the former perspective, the duality $(\nu, \phi, n_e) \to (1/\nu, n_e, \phi)$ is similar to electric-magnetic duality as we see below soon. When one chooses the latter, the duality $\nu \to 1/\nu$ along $\phi \to 1/\phi$ makes sense. This perspective is crucial for the duality in Hofstadter's butterfly as we discuss latter.

We first investigate the case where ν is an integer (the Integer Hall effect) and will treat the fractional case latter. The modular group $SL(2,\mathbb{Z})$ acts on the complex Hall conductivity $\sigma = \sigma_{xx} + i\sigma_{xy}$ in such a way that

$$S : \sigma \to -\frac{1}{\sigma} \tag{A.28}$$

$$T : \sigma \to \sigma + 1 \tag{A.29}$$

So, with respect to $q = \exp(2\pi\sigma)$ and ${}^Lq = \exp(-2\pi/\sigma)$, the particle-vortex duality at $\sigma_{xx} = 0$ in the integer quantum Hall system ($\sigma_{xy} = \nu = k$) simply reads to $q \to {}^Lq$. Especially, on the plateau regions, where gauge connection is flat, the equation $\sigma_{xx} = 0$ holds [126, 174] and the S-duality agrees with the Langlands duality of Wilson and Hecke operators.

Let $\nu = k$, which means an unit flux ϕ_0 is attached to an electron. The corresponding Wilson loop appears as an Aharonov-Bohm (AB) phase. Namely, the vector filed α which generates imaginary and negligibly thin magnetic flux attached to each electron should satisfy $\nabla \times \alpha = 0$, however an electron moving around ϕ_0 feels the vector potential and gains the phase $\exp(i2\pi\phi_0)$. From this picture, another way to understand a Hecke operator, which is dual to the Wilson loop, is obtained as follows: the flux ϕ_0 moving around $n_e = k$ electrons picking up the dual AB phase $\exp(i2\pi k\phi_0)$. This corresponds to the Hecke operator we discussed before as the vortex operator which pics up the Chern number associated with the Berry curvature. When we consider the vorticity, the location of the vortex depends on our gauge choice, however the former perspective of the AB-phase allows us to look the system in a gauge invariant way. By the way, this S-duality can be understood as so-called the particle-vortex duality and is consistent with the physical understanding of the geometric Langlands correspondence as electric-magnetic duality. By S-duality $\nu \to 1/\nu$, the Wilson loop and the Hecke operators are exchanged and the Wilson loop has the phase $\exp(i2\pi k\phi_0)$.

Mirror symmetry and Chern-Simons theory is discussed in [171], and here we leave a short summary which connects our perspective above. A central architecture in the study of Langlands/S-duality is Hitchin's moduli space $\mathcal{M}(G,C)$, which is the classical phase space of (G) Chern-Simons theory on a 3-manifold with a boundary Riemann surface C. If one consider the complexification of G which we denote by $G_{\mathbb{C}}$ (e.g. $G = SU(2)$, $G_{\mathbb{C}} = SL(2,\mathbb{C})$), then $\mathcal{M}(G,C)$ is equivalent to the space $\mathcal{M}(G_{\mathbb{C}},C)$ of flat $G_{\mathbb{C}}$ connections on C. The S-duality maps $\mathcal{M}_{\text{flat}}(G_{\mathbb{C}},C)$ to $\mathcal{M}_{\text{flat}}({}^LG_{\mathbb{C}},C)$ and indeed they are a pair of mirror symmetry [175]. The particle-vortex duality can be described by the Landau-Ginzburg theory and, in supersymmetric situations, its analogue is referred to as mirror symmetry. Therefore, as long as we focus on the Langlands correspondence, the S-duality picture we have discussed in this work would be essentially same as the S(or T)-duality picture discussed in [120, 138] as mirror symmetry. Starting from the $\mathcal{N} = 4$ supper Yang-Mills theory,

Kapustin and Witten suggest that the geometric Langlands duality is physically understood as the mirror symmetry of A-models with the target manifold $\mathcal{M}(G, C)$ and B-models with $\mathcal{M}({}^L G, C)$, and the mirror map corresponds to the S-duality (or the electric-magnetic duality in our sense) along with the T-duality for the torus fibrations. This insight gives another evidence for the homological mirror symmetry [176].

We stress that our perspective on the relation between the quantum Hall system and the Langlands duality is exactly on the right track of this insight into the relation between the mirror symmetry and the Langlands duality. The mirror symmetry claims the duality of Calabi-Yau (CY) manifolds. The fibration of he anti-canonical bundle

$$\mathcal{O}(-K_M) \to M \tag{A.30}$$

over a Fano variety M gives a well-known prescription to obtain a CY manifold, where $-K_M = -c_1(TM)$. It is known that Fano varieties are given by polyhedra in two dimensions and in our case it corresponds to Fig. 43

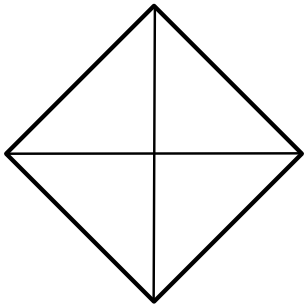

Figure 43. The polyhedron of local $\mathbb{P}^1 \times \mathbb{P}^1$.

In our case the Harper equation (A.5) corresponds to the difference equation

$$(e^x + e^{-x} - 1)\psi(x) + \psi(x - i\hbar) + \psi(x + i\hbar) = 0 \tag{A.31}$$

for the local $\mathbb{P}^1 \times \mathbb{P}^1$ model in the diagonal slice, where $\hbar = 2\pi P/Q$ for integers P, Q. And so called the mirror curve

$$e^x + e^{-x} + e^p + e^{-p} = 1 \tag{A.32}$$

corresponds to the tight-binding Hamiltonian of the quantum Hall system. The energy eigenvalues calculated from the topological string side indeed coincides with that from the quantum Hall system [99]. What is interesting and important for us is that the homological mirror symmetry can be stated as the equivalence between the enhanced triangulated category over any toric Fano variety M and the derived Fukaya-Seidel category over a Laurent polynomial W

$$D^b\mathrm{coh}(M) \simeq D^b\mathcal{F}(W). \tag{A.33}$$

This conjecture is proved for $M = \mathbb{P}^1 \times \mathbb{P}^1$ in [177]. Roughly speaking the A-models living on $D^b\mathcal{F}(W)$ are obtained by taking the limit $\hbar \to \infty$ and the B-models on $D^b\mathrm{coh}(M)$ are obtained by the classical limit $\hbar \to 0$. In this sense the mirror symmetry is understood as the strong/weak duality.

Furthermore, thanks to Nagell's algorithm (see [178] for instance), the mirror curve expression (A.32) endows us the corresponding elliptic curve of the form

$$y^2 = 4x^3 - 27x - 4347 \tag{A.34}$$

According to the classical Langlands correspondence in number theory, there is an automorphic form

$$\sum_{n=1} a_n q^n \tag{A.35}$$

such that the number defined by $b_p = p + 1 - \#$ (points of (A.34) mod p) corresponds to a_p as explained in introduction. Though the author has not found the corresponding automorphic form yet, it will be meaningful to explore in more detail.

A.10 Statistical Physics and Langlands Program

Langlands duality can be also found in statistical physics. Indeed, the correspondence of the partition functions at low and high temperature is widely known among those specialists. That's is nothing but the Langlands duality. To see this we consider two dimensional lattice models. Let q be a positive integer and $\xi_i \in \mathbb{Z}/q\mathbb{Z}$ be spin at lattice point i. The analogue of the correspondence between the L-functions is now the correspondence between the statistical partition functions:

$$Z(K) = Z(K^*), \tag{A.36}$$

where $K = J/T$ is the inverse temperature and K^* is dual to K in the sense explained later (make a quick look at Fig.44). We are mostly interested in square lattice models but the same estimation is essentially true to a generic case. The duality (A.36) of partition functions is given by the quality

$$\sum_{\xi} \prod_{<i,j>} u(\xi_i - \xi_j) = q^{-1-N} \sum_{\mu} \prod_{<\hat{i},\hat{j}>} \lambda(\mu_{\hat{i}} - \mu_{\hat{j}}), \tag{A.37}$$

where u is the Boltzmann factor $u(\xi_i - \xi_j) = \exp(K\cos(2\pi(\xi_i - \xi_j)/q))$, λ is the Fourier transformation of u, and $\{\hat{i}\}$ denotes lattice points dual to the lattice denoted by $\{i\}$ [179]. Note that this duality is in parallel with the duality of a real lattice and its reciprocal lattice. The Brillouin Zone (BZ) which is identified with torus T^2 for 2d-QHE is the Wigner-Seitz cell of the reciprocal lattice. Such a correspondence reminds us the Fourier-Mukai transformation of homomorphic bundles in terms of the Langlands duality.

Some tips to relate the Langlands program with statistical physics are proposed in [116], which works on Gaudin models, an example of $O(n)$-vector model. $n = 1$ is the Ising model, $n = 2$ is the XY model, and $n = 3$ is the Heisenberg model. In this section we consider the Ising model from a viewpoint of the Langlands program.

Duality of Ising models are classical in the following two meanings: 1) the relevant phenomena have been widely studied and many of them have been known since old times. 2) Ising model involves classical phase transition at $T > 0$. Besides physical interests, our purpose here is to explain this duality should be understood as classical Langlands duality. This is achieved when we consider a representation of the quantum group $\mathcal{U}_q(sl_2)$, where q is essentially given by the Boltzmann weight. $|q| \neq 1$ explains classicalness of the theory. This is in contrast to our previous discussions including quantum Hall effect.

The partition function of the Ising model is the $q = 2$ case. The duality (A.36) of partition functions are more precisely written as

$$\frac{Z(K)}{2^N(\cosh K)^{2N}} = \frac{Z(K^*)}{2e^{NK^*}}, \tag{A.38}$$

where $K = J/T$, N is the number of lattice points and K^* is defined by

$$K^* = -\frac{1}{2}\log(\tanh K). \tag{A.39}$$

The relation between K, K^* is not exactly the same as that between electric charge e and magnetic charge g which is $eg = 1$, but it is very close as shown in Fig. 44. Moreover taking logarithm expression

$$\frac{1}{N}\log Z(K) = \frac{1}{N}\log Z(K^*) + (\text{function without singularity}) \tag{A.40}$$

we can recover the preferable duality formula $Z(K) = Z(K^*)$ which claims the correspondence with high temperature regime K and low temperature regime K^*. Here the non-singular part is negligible since it dose not contribute to phase transition. In addition the Fourier transformation of the Boltzmann factor clearly implies the correspondence $K \leftrightarrow K^*$ between low temperature and high temperature, that is, $u(1)/u(0) = e^{-2K}$ and $\lambda(1)/\lambda(0) = e^{-2K^*}$.

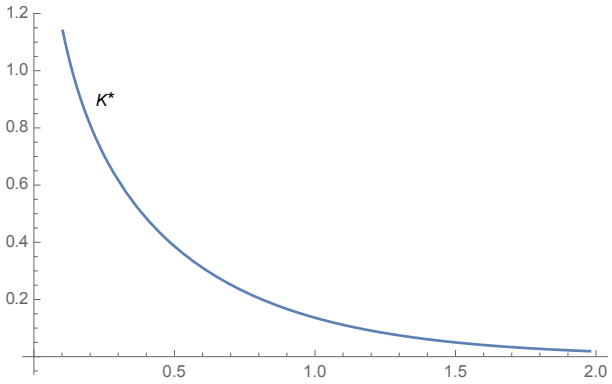

Figure 44. The plot of K^* against K.

The duality of Ising model is sometimes called the Kramers-Wannier duality[180], by which the transition temperature $K = K^* = K_c$ can be derived. We understand that the Fourier transformation of the Ising model describes this duality of the Ising models. Another way to see the duality is to consider the renormalization group. The argument is almost in parallel with the duality of Kondo effect.

A.11 Remarks on Future Directions

We have investigated the 2d QHE in terms of the Langlands program, including a geometric case, integrable systems and several algebras. The 2d IQHE is a $U(1)$ gauge theory and topological insulators with general gauge groups exhibits similar phenomena. The monopole or vortex like excitations are ubiquitous phenomena and some of them show intriguing properties. For example, the BKT transition [181–183] involves many vortexes while phase transition. Moreover it will be interesting to seek for some relations with a K-theoretic classification of topological insulators [150, 184]. Studies on topological matters would endow the Langlads program with suggestions.

As our theory unfolds, the Langlands philosophy becomes assimilated into industrial applications. First of all, braiding with anyon-like excitation modes is a powerful tool for topological quantum computation (TQC). There are two approaches to TQC from condensed matter and quantum information. Non-Abelian anyons of the FQHE are practical candidates to realize the TQC theoretically [185, 186] and experimentally [187–189]. Algorithmic braiding (a CNOT-operation) around artificial defects on surface codes is also significant [190]. Electric/magnetic duality is often referred to the Hadamard operation, which is a quantum version of the Fourier transformation. Once an Hadamard gate acts on a surface code on a graph, it is mapped to a surface code on the dual graph. This is the same as the duality of the 2d Ising model, which is realized by the Fourier transformation of Boltzmann weights assigned to vertexes [179, 180]. Indeed such duality plays a fundamental role in the VDB correspondence, which ensures universal computation using the 2d Ising model

[191]. Adiabatic quantum computation [33] or quantum annealing [32] could be such candidates. The duality of the Ising model is an excellent example to understand the Langlands duality, since a partition function Z is an analogue of a number theoretical L-function and it exhibits the exact high/low temperature duality $\frac{Z(K)}{g^N(K)} = \frac{Z(K^*)}{g^N(K^*)}$, where $K = J/T, K^* = -\frac{1}{2}\log(\tanh K)$ and g is a certain function. The number theoretical Langlands correspondence asserts the equality $L_H = L_F$ between a Hecke L_H-function and a Frobenius L_F-function, whose analogue is defined for local systems in our case.

We have discussed the simplest case, and it should be natural to explore a generic case. One of the key ingredients is the topological terms (the Wess-Zumino-Witten (WZW) terms) associated with the non linear sigma models [150]. And the geometric Langlands correspondence manifests power for investigating the WZW model [137]. This suggests that mathematical background of topological insulators would be much more fruitful than what it had been believed. It is interesting to build another connection to the work done by Kapustin and Witten [120], where $\mathcal{N} = 4$ super Yang-Mills theory is essential to explain the geometric Langlands correspondence via mirror symmetry and S-duality. We can seek for a likely scenario in string theoretical approaches to the quantum Hall effect (and topological insulators) [192, 193], in which the two-dimensional quantum Hall effect is described by using the $D3$-brane, on which the $\mathcal{N} = 4$ supper symmetry does live [194]. Moreover a generic topological insulator can be explained by the corresponding D-brane configuration, hence it may attract a general interest to build more strong connections among the geometric Langlands, topological insulators, and the supper symmetric theory.

Moreover 3-dimensional understanding on Jones polynomials, which describes knots, is given by the Chern-Simons theory [166]. Categorufication of the Jones polynomial is known as Khovanov homology [195–198]. Its physical interpretation is also proposed by Gukov, Vafa, and Schwarz [199] in the context of topological string theory. More recently its connection with gauge theory has been considered [168, 170, 200] and it is predicted that the Langlands correspondence based on the $\mathcal{N} = 4$ super Yang-Mills theory plays a fundamental role to understand Khovanov homology. It is a challenging open problem to find a physically realistic explanation about the conjecture, since knot theory and Jones polynomial endow the FQHE with fundamental description of anyons.

Duality is universally crucial in physics. As we have discussed, electric/magnetic duality, strong/weak duality, and high/low duality can be explained by the Langlands duality. In this sense, the Langlands program is a grand unified theory of mathematics and physics.

Acknowledgements

The author thanks collaborators, especially Travis Humble, Viktor Jahnke, Keun-Young Kim, Mikito Koshino, Yoshiyuki Matsuki and Yuma Nakamura for useful discussion. He also thanks Koji Hashimoto, Norihiro Iizuka, Keisuke Fujii, and Kin-ya Oda for comments on this thesis. D-Wave 2000Q at Oak Ridge National Laboratory was used for results in Sec 3.

References

[1] K. Ikeda, V. Jahnke, K. Y. Kim and K. B. Huh*to appear* (2019) .

[2] K. Ikeda, Y. Nakamura and T. S. Humble, *Application of quantum annealing to nurse scheduling problem*, *Scientific Reports* **9** (2019) 12837.

[3] K. Ikeda, *Universal Computation with Quantum Fields*, 1910.02833.

[4] Y. Matsuki, K. Ikeda and M. Koshino*to appear* (2019) .

[5] Y. Matsuki and K. Ikeda, *Comments on the fractal energy spectrum of honeycomb lattice with defects*, *Journal of Physics Communications* **3** (2019) 055003.

[6] K. Ikeda, *Hofstadter's butterfly and langlands duality*, *Journal of Mathematical Physics* **59** (2018) 061704 [https://doi.org/10.1063/1.4998635].

[7] K. Ikeda, *Quantum Hall Effect and Langlands Program*, *Annals Phys.* **397** (2018) 136 [1708.00419].

[8] K. Ikeda, *Topological Aspects of Matters and Langlands Program*, 1812.11879.

[9] P. Roushan, C. Neill, J. Tangpanitanon, V. M. Bastidas, A. Megrant, R. Barends et al., *Spectroscopic signatures of localization with interacting photons in superconducting qubits*, *Science* **358** (2017) 1175 [http://science.sciencemag.org/content/358/6367/1175.full.pdf].

[10] R. P. Feynman, *Quantum mechanical computers*, *Foundations of Physics* **16** (1986) 507.

[11] D. Deutsch, *Quantum theory, the church-turing principle and the universal quantum computer*, *Proceedings of the Royal Society of London. A. Mathematical and Physical Sciences* **400** (1985) 97 [https://royalsocietypublishing.org/doi/pdf/10.1098/rspa.1985.0070].

[12] A. Church, *An unsolvable problem of elementary number theory*, *American journal of mathematics* **58** (1936) 345.

[13] A. M. Turing, *On computable numbers, with an application to the entscheidungsproblem*, *Proceedings of the London Mathematical Society* **s2-42** (1937) 230.

[14] D. S. Abrams and S. Lloyd, *Simulation of many-body fermi systems on a universal quantum computer*, *Phys. Rev. Lett.* **79** (1997) 2586.

[15] D. W. Berry, G. Ahokas, R. Cleve and B. C. Sanders, *Efficient quantum algorithms for simulating sparse hamiltonians*, *Communications in Mathematical Physics* **270** (2007) 359.

[16] C. Zalka, *Simulating quantum systems on a quantum computer*, *Proceedings of the Royal Society of London Series A* **454** (1998) 313 [quant-ph/9603026].

[17] S. P. Jordan, K. S. M. Lee and J. Preskill, *Quantum Algorithms for Quantum Field Theories*, *Science* **336** (2012) 1130 [1111.3633].

[18] S. P. Jordan, H. Krovi, K. S. M. Lee and J. Preskill, *BQP-completeness of scattering in scalar quantum field theory*, *Quantum* **2** (2018) 44.

[19] S. H. Adachi and M. P. Henderson, *Application of Quantum Annealing to Training of Deep Neural Networks*, *arXiv e-prints* (2015) arXiv:1510.06356 [1510.06356].

[20] T. Albash and D. A. Lidar, *Adiabatic quantum computation*, *Rev. Mod. Phys.* **90** (2018) 015002.

[21] R. P. Feynman, *Quantum mechanical computers*, *Optics News* **11** (1985) 11.

[22] J. D. Biamonte and P. J. Love, *Realizable hamiltonians for universal adiabatic quantum computers*, *Phys. Rev. A* **78** (2008) 012352.

[23] R. Jozsa and A. Miyake, *Matchgates and classical simulation of quantum circuits*, *Proceedings of the Royal Society of London Series A* **464** (2008) 3089 [0804.4050].

[24] P. Jordan and E. Wigner, *Über das paulische äquivalenzverbot*, *Zeitschrift für Physik* **47** (1928) 631.

[25] F. Arute, K. Arya, R. Babbush, D. Bacon, J. C. Bardin, R. Barends et al., *Quantum supremacy using a programmable superconducting processor*, *Nature* **574** (2019) 505.

[26] A. Lucas, *Ising formulations of many np problems*, *Frontiers in Physics* **2** (2014) 5.

[27] A. M. Childs, E. Farhi and S. Gutmann, *An example of the difference between quantum and classical random walks*, *Quantum Information Processing* **1** (2002) 35.

[28] R. D. Somma, D. Nagaj and M. Kieferová, *Quantum speedup by quantum annealing*, *Phys. Rev. Lett.* **109** (2012) 050501.

[29] S. Kirkpatrick, C. D. Gelatt and M. P. Vecchi, *Optimization by simulated annealing*, *Science* **220** (1983) 671 [https://science.sciencemag.org/content/220/4598/671.full.pdf].

[30] M. Suzuki, *Generalized trotter's formula and systematic approximants of exponential operators and inner derivations with applications to many-body problems*, *Communications in Mathematical Physics* **51** (1976) 183.

[31] H. F. Trotter, *On the product of semi-groups of operators*, *Proc. Amer. Math. Soc.* **10** (1959) 545.

[32] T. Kadowaki and H. Nishimori, *Quantum annealing in the transverse ising model*, *Phys. Rev. E* **58** (1998) 5355.

[33] E. Farhi, J. Goldstone, S. Gutmann and M. Sipser, *Quantum Computation by Adiabatic Evolution*, *ArXiv e-prints* (2000) quant [quant-ph/0001106].

[34] Y. Seki and H. Nishimori, *Quantum annealing with antiferromagnetic fluctuations*, *Phys. Rev. E* **85** (2012) 051112 [1203.2418].

[35] K. Fujii, *Quantum speedup in stoquastic adiabatic quantum computation*, *arXiv e-prints* (2018) arXiv:1803.09954 [1803.09954].

[36] S. Bravyi, D. P. DiVincenzo, R. I. Oliveira and B. M. Terhal, *The Complexity of Stoquastic Local Hamiltonian Problems*, *arXiv e-prints* (2006) quant [quant-ph/0606140].

[37] B. Damski and M. M. Rams, *Exact results for fidelity susceptibility of the quantum ising model: the interplay between parity, system size, and magnetic field*, *Journal of Physics A: Mathematical and Theoretical* **47** (2013) 025303.

[38] S. Dusuel and J. Vidal, *Continuous unitary transformations and finite-size scaling exponents in the lipkin-meshkov-glick model*, *Phys. Rev. B* **71** (2005) 224420.

[39] P. Pfeuty, *The one-dimensional ising model with a transverse field*, *Annals of Physics* **57** (1970) 79 .

[40] C. R. Laumann, R. Moessner, A. Scardicchio and S. L. Sondhi, *Quantum adiabatic algorithm and scaling of gaps at first-order quantum phase transitions*, *Phys. Rev. Lett.* **109** (2012) 030502.

[41] J. Tsuda, Y. Yamanaka and H. Nishimori, *Energy gap at first-order quantum phase transitions: An anomalous case*, *Journal of the Physical Society of Japan* **82** (2013) 114004 [https://doi.org/10.7566/JPSJ.82.114004].

[42] S. Muthukrishnan, T. Albash and D. A. Lidar, *Tunneling and speedup in quantum optimization for permutation-symmetric problems*, *Phys. Rev. X* **6** (2016) 031010.

[43] A. Larkin and Y. N. Ovchinnikov, *Quasiclassical method in the theory of superconductivity*, *Sov Phys JETP* **28** (1969) 1200.

[44] J. Maldacena, S. H. Shenker and D. Stanford, *A bound on chaos*, *JHEP* **08** (2016) 106 [1503.01409].

[45] A. Kitaev, "Hidden correlations in the hawking radiation and thermal noise."

[46] M. Gärttner, J. G. Bohnet, A. Safavi-Naini, M. L. Wall, J. J. Bollinger and A. M. Rey, *Measuring out-of-time-order correlations and multiple quantum spectra in a trapped-ion quantum magnet*, *Nature Physics* **13** (2017) 781 [1608.08938].

[47] J. Li, R. Fan, H. Wang, B. Ye, B. Zeng, H. Zhai et al., *Measuring Out-of-Time-Order Correlators on a Nuclear Magnetic Resonance Quantum Simulator*, *Physical Review X* **7** (2017) 031011 [1609.01246].

[48] R. J. Lewis-Swan, A. Safavi-Naini, J. J. Bollinger and A. M. Rey, *Unifying scrambling, thermalization and entanglement through measurement of fidelity*

out-of-time-order correlators in the Dicke model, *Nature Communications* **10** (2019) 1581 [1808.07134].

[49] B. Yoshida and N. Y. Yao, *Disentangling Scrambling and Decoherence via Quantum Teleportation*, *Physical Review X* **9** (2019) 011006 [1803.10772].

[50] C. B. DaÄ§, K. Sun and L. M. Duan, *Detection of Quantum Phases via Out-of-Time-Order Correlators*, *Phys. Rev. Lett.* **123** (2019) 140602 [1902.05041].

[51] Z.-H. Sun, J.-Q. Cai, Q.-C. Tang, Y. Hu and H. Fan, *Out-of-time-order correlators and quantum phase transitions in the Rabi and Dicke model*, *arXiv e-prints* (2018) arXiv:1811.11191 [1811.11191].

[52] Q. Wang and F. Pérez-Bernal, *Probing excited-state quantum phase transition in a quantum many body system via out-of-time-ordered correlator*, *arXiv e-prints* (2018) arXiv:1812.01920 [1812.01920].

[53] M. Heyl, F. Pollmann and B. DÃşra, *Detecting equilibrium and dynamical quantum phase transitions in ising chains via out-of-time-ordered correlators*, *Physical Review Letters* **121** (2018) .

[54] H. Shen, P. Zhang, R. Fan and H. Zhai, *Out-of-time-order correlation at a quantum phase transition*, *Phys. Rev. B* **96** (2017) 054503 [1608.02438].

[55] C. B. Dağ, K. Sun and L.-M. Duan, *Detection of quantum phases via out-of-time-order correlators*, *Phys. Rev. Lett.* **123** (2019) 140602.

[56] Y. Huang, F. G. S. L. BrandÃčo and Y.-L. Zhang, *Finite-size scaling of out-of-time-ordered correlators at late times*, *Phys. Rev. Lett.* **123** (2019) 010601 [1705.07597].

[57] V. Jahnke, *Recent developments in the holographic description of quantum chaos*, *Adv. High Energy Phys.* **2019** (2019) 9632708 [1811.06949].

[58] V. Khemani, D. A. Huse and A. Nahum, *Velocity-dependent Lyapunov exponents in many-body quantum, semiclassical, and classical chaos*, *Phys. Rev.* **B98** (2018) 144304 [1803.05902].

[59] B. Craps, M. D. Clerck, D. Janssens, V. Luyten and C. Rabideau, *Lyapunov growth in quantum spin chains*, 1908.08059.

[60] H. Gharibyan, M. Hanada, B. Swingle and M. Tezuka, *Quantum Lyapunov Spectrum*, *JHEP* **04** (2019) 082 [1809.01671].

[61] T. Jörg, F. Krzakala, J. Kurchan, A. C. Maggs and J. Pujos, *Energy gaps in quantum first-order mean-field–like transitions: The problems that quantum annealing cannot solve*, *EPL (Europhysics Letters)* **89** (2010) 40004.

[62] Y. Susa, J. F. Jadebeck and H. Nishimori, *Relation between quantum fluctuations and the performance enhancement of quantum annealing in a nonstoquastic hamiltonian*, *Phys. Rev. A* **95** (2017) 042321.

[63] A. Perdomo-Ortiz, S. E. Venegas-Andraca and A. Aspuru-Guzik, *A study of*

heuristic guesses for adiabatic quantum computation, *Quantum Information Processing* **10** (2011) 33.

[64] D. Venturelli and A. Kondratyev, *Reverse quantum annealing approach to portfolio optimization problems*, *Quantum Machine Intelligence* **1** (2019) 17.

[65] A. D. King, J. Carrasquilla, J. Raymond, I. Ozfidan, E. Andriyash, A. Berkley et al., *Observation of topological phenomena in a programmable lattice of 1,800 qubits*, *Nature* **560** (2018) 456.

[66] M. Ohkuwa, H. Nishimori and D. A. Lidar, *Reverse annealing for the fully connected p-spin model*, *Phys. Rev. A* **98** (2018) 022314.

[67] Y. Yamashiro, M. Ohkuwa, H. Nishimori and D. A. Lidar, *Dynamics of reverse annealing for the fully connected p-spin model*, *Phys. Rev. A* **100** (2019) 052321.

[68] S. den Hartog, *On the complexity of nurse scheduling problems*, Master's thesis, 2016.

[69] F. Della Croce and F. Salassa, *A variable neighborhood search based matheuristic for nurse rostering problems*, *Annals of Operations Research* **218** (2014) 185.

[70] Z. Bäumelt, J. Dvořák, P. Šůcha and Z. Hanzálek, *A novel approach for nurse rerostering based on a parallel algorithm*, *European Journal of Operational Research* **251** (2016) 624 .

[71] T. Osogami and H. Imai, *Classification of various neighborhood operations for the nurse scheduling problem*, in *Algorithms and Computation*, G. Goos, J. Hartmanis, J. van Leeuwen, D. T. Lee and S.-H. Teng, eds., (Berlin, Heidelberg), pp. 72–83, Springer Berlin Heidelberg, 2000.

[72] E. K. Burke, P. De Causmaecker, G. V. Berghe and H. Van Landeghem, *The state of the art of nurse rostering*, *Journal of Scheduling* **7** (2004) 441.

[73] E. Farhi, J. Goldstone, S. Gutmann, J. Lapan, A. Lundgren and D. Preda, *A quantum adiabatic evolution algorithm applied to random instances of an np-complete problem*, *Science* **292** (2001) 472 [http://science.sciencemag.org/content/292/5516/472.full.pdf].

[74] D. Aharonov, W. van Dam, J. Kempe, Z. Landau, S. Lloyd and O. Regev, *Adiabatic quantum computation is equivalent to standard quantum computation*, *SIAM Review* **50** (2008) 755 [https://doi.org/10.1137/080734479].

[75] M. W. Johnson, M. H. S. Amin, S. Gildert, T. Lanting, F. Hamze, N. Dickson et al., *Quantum annealing with manufactured spins*, *Nature* **473** (2011) 194 EP .

[76] D. Venturelli, S. Mandra, S. Knysh, B. OâĂŹGorman, R. Biswas and V. Smelyanskiy, *Quantum optimization of fully connected spin glasses*, *Physical Review X* **5** (2015) 031040.

[77] Z. Bian, F. Chudak, W. Macready, A. Roy, R. Sebastiani and S. Varotti, *Solving SAT and MaxSAT with a Quantum Annealer: Foundations, Encodings, and Preliminary Results*, *arXiv e-prints* (2018) arXiv:1811.02524 [1811.02524].

[78] F. Neukart, G. Compostella, C. Seidel, D. von Dollen, S. Yarkoni and B. Parney, *Traffic flow optimization using a quantum annealer*, *arXiv e-prints* (2017) arXiv:1708.01625 [1708.01625].

[79] T. Stollenwerk, B. O'Gorman, D. Venturelli, S. Mandrà, O. Rodionova, H. K. Ng et al., *Quantum Annealing Applied to De-Conflicting Optimal Trajectories for Air Traffic Management*, *arXiv e-prints* (2017) arXiv:1711.04889 [1711.04889].

[80] G. Rosenberg, P. Haghnegahdar, P. Goddard, P. Carr, K. Wu and M. L. de Prado, *Solving the Optimal Trading Trajectory Problem Using a Quantum Annealer*, *IEEE Journal of Selected Topics in Signal Processing* **10** (2016) 1053 [1508.06182].

[81] F. Neukart, G. Compostella, C. Seidel, D. von Dollen, S. Yarkoni and B. Parney, *Traffic flow optimization using a quantum annealer*, *Frontiers in ICT* **4** (2017) 29.

[82] A. D. King, J. Carrasquilla, J. Raymond, I. Ozfidan, E. Andriyash, A. Berkley et al., *Observation of topological phenomena in a programmable lattice of 1,800 qubits*, *Nature* **560** (2018) 456.

[83] D. O'Malley, *An approach to quantum-computational hydrologic inverse analysis*, *Scientific Reports* **8** (2018) 6919.

[84] D. Venturelli, D. J. J. Marchand and G. Rojo, *Quantum Annealing Implementation of Job-Shop Scheduling*, *arXiv e-prints* (2015) arXiv:1506.08479 [1506.08479].

[85] T. B. Cooper and J. H. Kingston, *The complexity of timetable construction problems*, in *International Conference on the Practice and Theory of Automated Timetabling*, pp. 281–295, Springer, 1995.

[86] J. Preskill, *Quantum Computing in the NISQ era and beyond*, *arXiv e-prints* (2018) arXiv:1801.00862 [1801.00862].

[87] I. Ozfidan, C. Deng, A. Y. Smirnov, T. Lanting, R. Harris, L. Swenson et al., *Demonstration of nonstoquastic Hamiltonian in coupled superconducting flux qubits*, *arXiv e-prints* (2019) arXiv:1903.06139 [1903.06139].

[88] T. S. Humble, A. J. McCaskey, R. S. Bennink, J. J. Billings, E. DÊijAzevedo, B. D. Sullivan et al., *An integrated programming and development environment for adiabatic quantum optimization*, *Computational Science & Discovery* **7** (2014) 015006.

[89] C. Klymko, B. D. Sullivan and T. S. Humble, *Adiabatic quantum programming: minor embedding with hard faults*, *Quantum information processing* **13** (2014) 709.

[90] K. E. Hamilton and T. S. Humble, *Identifying the minor set cover of dense connected bipartite graphs via random matching edge sets*, *Quantum Information Processing* **16** (2017) 94.

[91] E. F. Dumitrescu, A. L. Fisher, T. D. Goodrich, T. S. Humble, B. D. Sullivan and A. L. Wright, *Benchmarking treewidth as a practical component of tensor network simulations*, *PLOS ONE* **13** (2018) 1.

[92] J. Cai, W. G. Macready and A. Roy, *A practical heuristic for finding graph minors*, *arXiv preprint arXiv:1406.2741* (2014) .

[93] S. Okada, M. Ohzeki, M. Terabe and S. Taguchi, *Improving solutions by embedding larger subproblems in a d-wave quantum annealer*, *Scientific reports* **9** (2019) 2098.

[94] T. Kadowaki and M. Ohzeki, *Experimental and Theoretical Study of Thermodynamic Effects in a Quantum Annealer*, *arXiv e-prints* (2019) arXiv:1902.04709 [1902.04709].

[95] P. Ray, B. K. Chakrabarti and A. Chakrabarti, *Sherrington-kirkpatrick model in a transverse field: Absence of replica symmetry breaking due to quantum fluctuations*, *Phys. Rev. B* **39** (1989) 11828.

[96] D. R. Hofstadter, *Energy levels and wave functions of Bloch electrons in rational and irrational magnetic fields*, **14** (1976) 2239.

[97] M. Aidelsburger, M. Atala, M. Lohse, J. T. Barreiro, B. Paredes and I. Bloch, *Realization of the hofstadter hamiltonian with ultracold atoms in optical lattices*, *Phys. Rev. Lett.* **111** (2013) 185301.

[98] H. Miyake, G. A. Siviloglou, C. J. Kennedy, W. C. Burton and W. Ketterle, *Realizing the harper hamiltonian with laser-assisted tunneling in optical lattices*, *Phys. Rev. Lett.* **111** (2013) 185302.

[99] Y. Hatsuda, H. Katsura and Y. Tachikawa, *Hofstadter's butterfly in quantum geometry*, *New J. Phys.* **18** (2016) 103023 [1606.01894].

[100] Z. Duan, J. Gu, Y. Hatsuda and T. Sulejmanpasic, *Instantons in the Hofstadter butterfly: difference equation, resurgence and quantum mirror curves*, *ArXiv e-prints* (2018) [1806.11092].

[101] J. G. Pedersen and T. G. Pedersen, *Hofstadter butterflies and magnetically induced band-gap quenching in graphene antidot lattices*, *Phys. Rev. B* **87** (2013) 235404.

[102] S. İslamoğlu, M. O. Oktel and O. b. u. Gülseren, *Hofstadter butterfly of graphene with point defects*, *Phys. Rev. B* **85** (2012) 235414.

[103] K. S. Novoselov, Z. Jiang, Y. Zhang, S. Morozov, H. L. Stormer, U. Zeitler et al., *Room-temperature quantum hall effect in graphene*, *Science* **315** (2007) 1379.

[104] Z. Jiang, Y. Zhang, Y.-W. Tan, H. Stormer and P. Kim, *Quantum hall effect in graphene*, *Solid State Communications* **143** (2007) 14 .

[105] R. Peierls, *Zur theorie des diamagnetismus von leitungselektronen*, *Zeitschrift für Physik* **80** (1933) 763.

[106] D. Xiao, M.-C. Chang and Q. Niu, *Berry phase effects on electronic properties*, *Rev. Mod. Phys.* **82** (2010) 1959.

[107] A. Widom, *Thermodynamic derivation of the Hall effect current*, *Physics Letters A* **90** (1982) 474.

[108] P. Streda, *Theory of quantised hall conductivity in two dimensions*, *Journal of Physics C: Solid State Physics* **15** (1982) L717.

[109] D. J. Thouless, M. Kohmoto, M. P. Nightingale and M. den Nijs, *Quantized hall conductance in a two-dimensional periodic potential*, *Phys. Rev. Lett.* **49** (1982) 405.

[110] N. Nemec and G. Cuniberti, *Hofstadter butterflies of bilayer graphene*, **75** (2007) 201404 [cond-mat/0612369].

[111] P. Moon and M. Koshino, *Energy spectrum and quantum hall effect in twisted bilayer graphene*, *Phys. Rev. B* **85** (2012) 195458.

[112] M. C. Geisler, J. H. Smet, V. Umansky, K. von Klitzing, B. Naundorf, R. Ketzmerick et al., *Detection of a landau band-coupling-induced rearrangement of the hofstadter butterfly*, *Phys. Rev. Lett.* **92** (2004) 256801.

[113] C. Albrecht, J. H. Smet, K. von Klitzing, D. Weiss, V. Umansky and H. Schweizer, *Evidence of hofstadter's fractal energy spectrum in the quantized hall conductance*, *Phys. Rev. Lett.* **86** (2001) 147.

[114] R. P. Langlands, *Problems in the theory of automorphic forms to salomon bochner in gratitude*, in *Lectures in Modern Analysis and Applications III*, C. T. Taam, ed., (Berlin, Heidelberg), pp. 18–61, Springer Berlin Heidelberg, 1970.

[115] D. Gaitsgory, *On a vanishing conjecture appearing in the geometric langlands correspondence*, *Annals of mathematics* **160** (2004) 617.

[116] E. Frenkel, *Affine algebras, Langlands duality and Bethe ansatz*, in *Mathematical physics. Proceedings, 11th International Congress, Paris, France, July 18-22, 1994*, 1995, q-alg/9506003.

[117] G. Laumon, *La correspondance de langlands sur les corps de fonctions*, in *Séminaire Bourbaki*, vol. 1999/2000 of *Astérisque*, pp. 207–265, Société mathématique de France, (2002), http://http://www.numdam.org/item/SB$_1$999 – 2000$_{42_{207_0}}$.

[118] T. Hausel and M. Thaddeus, *Mirror symmetry, Langlands duality, and the Hitchin system*, *Invent. Math.* **153** (2003) 197 [math/0205236].

[119] E. Frenkel, D. Gaitsgory and K. Vilonen, *On the geometric Langlands conjecture*, *arXiv Mathematics e-prints* (2000) math/0012255 [math/0012255].

[120] A. Kapustin and E. Witten, *Electric-Magnetic Duality And The Geometric Langlands Program*, *Commun. Num. Theor. Phys.* **1** (2007) 1 [hep-th/0604151].

[121] Gukov, Sergei and Witten, Edward, *Gauge theory, ramification, and the geometric langlands program*, *Current Developments in Mathematics* **2006** (2008) 35.

[122] M. Aganagic, E. Frenkel and A. Okounkov, *Quantum q-langlands correspondence*, *Transactions of the Moscow Mathematical Society* **79** (2018) 1.

[123] T. Ando, Y. Matsumoto, and Y. Uemura, *Theory of hall effect in a two-dimensional electron system*, *Journal of the Physical Society of Japan* **39** (1975) 279 [https://doi.org/10.1143/JPSJ.39.279].

[124] R. B. Laughlin, *Quantized hall conductivity in two dimensions*, *Phys. Rev. B* **23** (1981) 5632.

[125] D J Thouless, *Localisation and the two-dimensional hall effect*, *Journal of Physics C: Solid State Physics* **14** (1981) 3475.

[126] K. v. Klitzing, G. Dorda and M. Pepper, *New method for high-accuracy determination of the fine-structure constant based on quantized hall resistance*, *Phys. Rev. Lett.* **45** (1980) 494.

[127] R. Kubo, *Statistical-mechanical theory of irreversible processes. i. general theory and simple applications to magnetic and conduction problems*, *Journal of the Physical Society of Japan* **12** (1957) 570 [https://doi.org/10.1143/JPSJ.12.570].

[128] P. W. Anderson, *Absence of diffusion in certain random lattices*, *Phys. Rev.* **109** (1958) 1492.

[129] A. Pruisken, *On localization in the theory of the quantized hall effect: A two-dimensional realization of the Îÿ-vacuum*, *Nuclear Physics B* **235** (1984) 277 .

[130] Laughlin, R. B., *Anomalous quantum hall effect: An incompressible quantum fluid with fractionally charged excitations*, *Phys. Rev. Lett.* **50** (1983) 1395.

[131] ZHANG, SHOU CHENG, *The chernâĂŞsimonsâĂŞlandauâĂŞginzburg theory of the fractional quantum hall effect*, *International Journal of Modern Physics B* **06** (1992) 25 [https://doi.org/10.1142/S0217979292000037].

[132] J. K. Jain, *Composite-fermion approach for the fractional quantum hall effect*, *Phys. Rev. Lett.* **63** (1989) 199.

[133] N. Read, *Order parameter and ginzburg-landau theory for the fractional quantum hall effect*, *Phys. Rev. Lett.* **62** (1989) 86.

[134] P. Deligne, *Les Constantes des Equations Fonctionnelles des Fonctions L*, pp. 501–597. Springer Berlin Heidelberg, Berlin, Heidelberg, 1973. 10.1007/978-3-540-37855-6-7.

[135] V. G. Drinfel'd, *Two-dimensional l-adic representations of the galois group of a global field of characteristic p and automorphic forms on gl(2)*, *Journal of Soviet Mathematics* **36** (1987) 93.

[136] L. Lafforgue, *Chtoucas de drinfeld et correspondance de langlands*, *Inventiones mathematicae* **147** (2002) 1.

[137] Frenkel, Edward, *Lectures on the Langlands program and conformal field theory*, in *Proceedings, Les Houches School of Physics: Frontiers in Number Theory, Physics and Geometry II: On Conformal Field Theories, Discrete Groups and Renormalization: Les Houches, France, March 9-21, 2003*, pp. 387–533, 2007, DOI.

[138] E. Witten, *More On Gauge Theory And Geometric Langlands*, 1506.04293.

[139] D. Gaiotto, *S-duality of boundary conditions and the Geometric Langlands program*, 1609.09030.

[140] S. Gukov and E. Witten, *Gauge theory, ramification, and the geometric langlands program*, *Current Developments in Mathematics, 2006* (2008) 35 [hep-th/0612073].

[141] E. Witten, *Geometric Langlands From Six Dimensions*, 0905.2720.

[142] P. Goddard, J. Nuyts and D. Olive, *Gauge theories and magnetic charge*, *Nuclear Physics B* **125** (1977) 1 .

[143] M. Kohmoto, *Topological invariant and the quantization of the hall conductance*, *Annals of Physics* **160** (1985) 343.

[144] Y. Hatsugai, *Chern number and edge states in the integer quantum hall effect*, *Phys. Rev. Lett.* **71** (1993) 3697.

[145] M. Rothstein, *Connections on the total picard sheaf and the kp hierarchy*, *Acta Applicandae Mathematica* **42** (1996) 297.

[146] S. Mukai, *Duality between $d(x)$ and $d(\hat{x})$ with its application to picard sheaves*, *Nagoya Math. J.* **81** (1981) 153.

[147] P. B. Wiegmann and A. V. Zabrodin, *Bethe-ansatz for the bloch electron in magnetic field*, *Phys. Rev. Lett.* **72** (1994) 1890.

[148] M. Koshino and H. Aoki, *Integer quantum hall effect in isotropic three-dimensional crystals*, *Phys. Rev. B* **67** (2003) 195336.

[149] Y. Hatsugai, *Edge states in the integer quantum hall effect and the riemann surface of the bloch function*, *Phys. Rev. B* **48** (1993) 11851.

[150] A. P. Schnyder, S. Ryu, A. Furusaki and A. W. W. Ludwig, *Classification of topological insulators and superconductors in three spatial dimensions*, *Phys. Rev. B* **78** (2008) 195125.

[151] W. G. Chambers, *Linear-network model for magnetic breakdown in two dimensions*, *Phys. Rev.* **140** (1965) A135.

[152] L. D. Faddeev, *Modular double of quantum group*, *Math. Phys. Stud.* **21** (2000) 149 [math/9912078].

[153] E. Frenkel and D. Hernandez, *Langlands duality for representations of quantum groups*, *Mathematische Annalen* **349** (2011) 705.

[154] J. Teschner, *Quantization of the Hitchin moduli spaces, Liouville theory, and the geometric Langlands correspondence I*, *Adv. Theor. Math. Phys.* **15** (2011) 471 [1005.2846].

[155] J. Wess and B. Zumino, *Consequences of anomalous ward identities*, *Physics Letters B* **37** (1971) 95 .

[156] E. Witten, *Global aspects of current algebra*, *Nuclear Physics B* **223** (1983) 422 .

[157] C. Vafa, *Fractional Quantum Hall Effect and M-Theory*, 1511.03372.

[158] L. D. Faddeev, R. M. Kashaev and A. Y. Volkov, *Strongly coupled quantum discrete*

liouville theory.i: Algebraic approach and duality, Communications in Mathematical Physics **219** (2001) 199.

[159] Y. Terashima and M. Yamazaki, *SL(2,R) Chern-Simons, Liouville, and gauge theory on duality walls*, Journal of High Energy Physics **2011** (2011) 135.

[160] P. Goddard and D. I. Olive, *Magnetic monopoles in gauge field theories*, Reports on Progress in Physics **41** (1978) 1357.

[161] E. Frenkel, *Vertex algebras and algebraic curves*, in *Séminaire Bourbaki*, no. 276 in Astérisque, pp. 299–339, Société mathématique de France, (2002), http://http://www.numdam.org/item/SB$_1$999 – 2000$_{4}$2$_{2}$99$_0$.

[162] R. RAJARAMAN and S. L. SONDHI, *A field theory for the read operator*, International Journal of Modern Physics B **10** (1996) 793 [https://doi.org/10.1142/S0217979296000337].

[163] G. Moore and N. Read, *Nonabelions in the fractional quantum hall effect*, Nuclear Physics B **360** (1991) 362 .

[164] V. Knizhnik and A. Zamolodchikov, *Current algebra and wess-zumino model in two dimensions*, Nuclear Physics B **247** (1984) 83 .

[165] T. Kohno, *Monodromy representations of braid groups and yang-baxter equations*, Annales de l'Institut Fourier **37** (1987) 139.

[166] E. Witten, *Quantum field theory and the jones polynomial*, Comm. Math. Phys. **121** (1989) 351.

[167] E. Witten, *Quantization of chern-simons gauge theory with complex gauge group*, Comm. Math. Phys. **137** (1991) 29.

[168] E. Witten, *Two Lectures on Gauge Theory and Khovanov Homology*, 1603.03854.

[169] M. Khovanov, *A categorification of the jones polynomial*, Duke Math. J. **101** (2000) 359.

[170] E. Witten, *Khovanov Homology And Gauge Theory*, 1108.3103.

[171] T. Dimofte and S. Gukov, *Chern-Simons Theory and S-duality*, JHEP **05** (2013) 109 [1106.4550].

[172] C. P. Burgess and B. P. Dolan, *Particle vortex duality and the modular group: Applications to the quantum Hall effect and other 2-D systems*, Phys. Rev. **B63** (2001) 155309 [hep-th/0010246].

[173] M. A. Metlitski and A. Vishwanath, *Particle-vortex duality of two-dimensional dirac fermion from electric-magnetic duality of three-dimensional topological insulators*, Phys. Rev. B **93** (2016) 245151.

[174] J.-I. Wakabayashi and S. Kawaji, *Hall effect in silicon MOS inversion layers under strong magnetic fields*, Journal of the Physical Society of Japan **44** (1978) 1839.

[175] T. Hausel and M. Thaddeus, *Mirror symmetry, Langlands duality, and the Hitchin system*, Inventiones Mathematicae **153** (2003) 197 [math/0205236].

[176] M. Kontsevich, *Homological algebra of mirror symmetry*, in *in Proceedings of the International Congress of Mathematicians*, pp. 120–139, 1994.

[177] P. Seidel, *Vanishing cycles and mutation*, in *European Congress of Mathematics*, C. Casacuberta, R. M. Miró-Roig, J. Verdera and S. Xambó-Descamps, eds., (Basel), pp. 65–85, Birkhäuser Basel, 2001.

[178] M.-X. Huang, A. Klemm and M. Poretschkin, *Refined stable pair invariants for E-, M- and $[p, q]$-strings*, *JHEP* **11** (2013) 112 [1308.0619].

[179] F. Y. Wu and Y. K. Wang, *Duality transformation in a manyâĂŘcomponent spin model*, *Journal of Mathematical Physics* **17** (1976) 439 [https://aip.scitation.org/doi/pdf/10.1063/1.522914].

[180] H. A. Kramers and G. H. Wannier, *Statistics of the two-dimensional ferromagnet. part i*, *Phys. Rev.* **60** (1941) 252.

[181] J M Kosterlitz and D J Thouless, *Ordering, metastability and phase transitions in two-dimensional systems*, *Journal of Physics C: Solid State Physics* **6** (1973) 1181.

[182] D. J. Bishop and J. D. Reppy, *Study of the superfluid transition in two-dimensional ^{4}He films*, *Phys. Rev. Lett.* **40** (1978) 1727.

[183] D. J. Resnick, J. C. Garland, J. T. Boyd, S. Shoemaker and R. S. Newrock, *Kosterlitz-thouless transition in proximity-coupled superconducting arrays*, *Phys. Rev. Lett.* **47** (1981) 1542.

[184] K. Shiozaki and M. Sato, *Topology of crystalline insulators and superconductors*, *Physical Review B* **90** (2014) 165114.

[185] M. Freedman, A. Kitaev, M. Larsen and Z. Wang, *Topological quantum computation*, *Bulletin of the American Mathematical Society* **40** (2003) 31.

[186] D. Aharonov, V. Jones and Z. Landau, *A polynomial quantum algorithm for approximating the jones polynomial*, *Algorithmica* **55** (2009) 395.

[187] Y. Kasahara, T. Ohnishi, Y. Mizukami, O. Tanaka, S. Ma, K. Sugii et al., *Majorana quantization and half-integer thermal quantum hall effect in a kitaev spin liquid*, *Nature* **559** (2018) 227.

[188] Q. L. He, L. Pan, A. L. Stern, E. C. Burks, X. Che, G. Yin et al., *Chiral majorana fermion modes in a quantum anomalous hall insulator–superconductor structure*, *Science* **357** (2017) 294 [http://science.sciencemag.org/content/357/6348/294.full.pdf].

[189] D. Takane, S. Souma, K. Nakayama, T. Nakamura, H. Oinuma, K. Hori et al., *Observation of a dirac nodal line in* alb_2, *Phys. Rev. B* **98** (2018) 041105.

[190] A. Kitaev, *Fault-tolerant quantum computation by anyons*, *Annals of Physics* **303** (2003) 2 .

[191] M. Van den Nest, W. Dür and H. J. Briegel, *Completeness of the classical 2d ising model and universal quantum computation*, *Phys. Rev. Lett.* **100** (2008) 110501.

[192] S. Ryu and T. Takayanagi, *Topological Insulators and Superconductors from D-branes*, *Phys. Lett.* **B693** (2010) 175 [1001.0763].

[193] S. Ryu and T. Takayanagi, *Topological Insulators and Superconductors from String Theory*, *Phys. Rev.* **D82** (2010) 086014 [1007.4234].

[194] E. Witten, *Bound states of strings and p-branes*, *Nucl. Phys.* **B460** (1996) 335 [hep-th/9510135].

[195] M. Khovanov, *A categorification of the Jones polynomial*, *ArXiv Mathematics e-prints* (1999) [math/9908171].

[196] M. Khovanov, *A functor-valued invariant of tangles*, *ArXiv Mathematics e-prints* (2001) [math/0103190].

[197] M. Khovanov, *Categorifications of the colored Jones polynomial*, *ArXiv Mathematics e-prints* (2003) [math/0302060].

[198] M. Khovanov, *Link homology and Frobenius extensions*, *ArXiv Mathematics e-prints* (2004) [math/0411447].

[199] S. Gukov, A. S. Schwarz and C. Vafa, *Khovanov-Rozansky homology and topological strings*, *Lett. Math. Phys.* **74** (2005) 53 [hep-th/0412243].

[200] R. Mazzeo and E. Witten, *The Nahm Pole Boundary Condition*, 1311.3167.